

Supplementary Information

Contents

| | |
|---|----|
| Appendix S1. Site Details | 3 |
| Appendix S2. Methods for reconstruction of <i>DBH</i> | 4 |
| Appendix S3. Methods for climate data evaluation and correction | 5 |
| Appendix S4. Methods for comparing our approach with traditional methods | 6 |
| Appendix S5. Dealing with rapidly changing climate and tree growth | 8 |
| Table S1. Site Details. | 9 |
| Table S2. Species analyzed, their characteristics, and bark allometries applied. | 10 |
| Table S3. Sampling details for species by site. | 11 |
| Table S4. Allometric equations for bark thickness. | 13 |
| Table S5. Qualitative comparison of results from this study with previous studies employing conventional methods. | 14 |
| Figure S1. Density plot of core record start years by species for Barro Colorado Nature Monument (Panama). | 17 |
| Figure S2. Density plot of core record start years by species for Huai Kha Khaeng (Thailand). | 18 |
| Figure S3. Density plot of core record start years by species for the Smithsonian Conservation Biology Institute (Virginia, USA). | 19 |
| Figure S4. Density plot of core record start years by species for Lilley Dickey Woods (Indiana, USA). | 20 |
| Figure S5. Density plot of core record start years by species for Harvard Forest (Massachusetts, USA). | 21 |
| Figure S6. Density plot of core record start years by species for Zofin Forest (Czech Republic). | 22 |
| Figure S7. Density plot of core record start years by species for Niobrara (Nebraska, USA). | 23 |
| Figure S8. Density plot of core record start years by species for Little Tesuque (New Mexico, USA). | 24 |
| Figure S9. Density plot of core record start years by species for Cedar Breaks (Utah, USA). | 25 |
| Figure S10. Density plot of core record start years by species for Scotty Creek (Northwest Territory, Canada). | 26 |
| Figure S11. Comparison of our approach with traditional methods of identifying climate signals: LITU at SCBI. | 27 |
| Figure S12. Comparison of our approach with traditional methods of identifying climate signals: ABAL at Zofin. | 28 |
| Figure S13. Comparison of our approach with traditional methods of identifying climate signals: PSME at Cedar Breaks. | 29 |
| Figure S14. Comparison of our approach with traditional methods of identifying climate signals: PIMA at Scotty Creek. | 30 |
| Figure S15. (PRE at SCBI) | 31 |
| Figure S16. (PET at SCBI) | 32 |
| Figure S17. (TMX/TMP at HKK) | 33 |
| Figure S18. Best GLS models including climate and DBH for Barro Colorado Nature Monument (Panama) | 34 |
| Figure S19. Best GLS models including climate, DBH, and year for Barro Colorado Nature Monument (Panama) | 35 |
| Figure S20. Best GLS models including climate and DBH for Huai Kha Khaeng (Thailand) | 36 |
| Figure S21. Best GLS models including climate, DBH, and year for Huai Kha Khaeng (Thailand) | 37 |
| Figure S22. Best GLS models including climate and DBH for the Smithsonian Conservation Biology Institute (Virginia, USA) | 38 |

| | |
|---|----|
| Figure S23. Best GLS models including climate, DBH, and year for the Smithsonian Conservation Biology Institute (Virginia, USA) | 39 |
| Figure S24. Best GLS models including climate and DBH for Lilley Dickey Woods (Indiana, USA) | 40 |
| Figure S25. Best GLS models including climate, DBH, and year for Lilley Dickey Woods (Indiana, USA) | 41 |
| Figure S26. Best GLS models including climate and DBH for Harvard Forest (Massachusetts, USA) | 42 |
| Figure S27. Best GLS models including climate, DBH, and year for Harvard Forest (Massachusetts, USA) | 43 |
| Figure S28. Best GLS models including climate and DBH for Zofin Forest (Czech Republic) | 44 |
| Figure S29. Best GLS models including climate, DBH, and year for Zofin Forest (Czech Republic) | 45 |
| Figure S30. Best GLS models including climate and DBH for Niobrara (Nebraska, USA) | 46 |
| Figure S31. Best GLS models including climate, DBH, and year for Niobrara (Nebraska, USA) | 47 |
| Figure S32. Best GLS models including climate and DBH for Little Tesuque (New Mexico, USA) | 48 |
| Figure S33. Best GLS models including climate, DBH, and year for Little Tesuque (New Mexico, USA) | 49 |
| Figure S34. Best GLS models including climate and DBH for Cedar Breaks (Utah, USA) | 50 |
| Figure S35. Best GLS models including climate, DBH, and year for Cedar Breaks (Utah, USA) | 51 |
| Figure S36. Best GLS models including climate and DBH for Scotty Creek (Northwest Territory, Canada) | 52 |
| Figure S37. Best GLS models including climate, DBH, and year for Scotty Creek (Northwest Territory, Canada) | 53 |
| Figure S38. Climate responses at Scotty Creek (Northwest Territory, Canada) before and after 1970. | 54 |
| Figure S39. (RW_interactions_all) | 55 |
| Figure S40. (BAI_interactions_all) | 56 |
| Figure S41. (Decadal BCNM) | 57 |
| Figure S42. (Decadal HKK) | 58 |
| Figure S43. (Decadal SCBI) | 59 |
| Figure S45. (Decadal HF) | 61 |
| Figure S46. (Decadal ZOF) | 62 |
| Figure S47. (Decadal NIO) | 63 |
| Figure S48. (Decadal LT) | 64 |
| Figure S49. (Decadal CB) | 65 |
| Figure S50. (Decadal SC) | 66 |
| SI References | 67 |

Appendix S1. Site Details

(include descriptions of stand history, global change dynamics)

Barro Colorado Nature Monument, Panama

We note that the secondary forest status of much of BCNM differs from ForestGEO's 50-ha plot on Barro Colorado Island (within BCNM), which is old-growth, and shows little directional trend in tree growth (Rutishauser et al., 2020).

Huai Kha Khaeng, Thailand

Melia azedarach – a highly shade-intolerant species that establishes in the open (Baker & Bunyavejchewin, 2006) and was sampled opportunistically outside the ForestGEO plot at HKK (Vlam et al., 2014), where it presumably established under open conditions (Baker et al., 2005).

The site underwent a widespread, catastrophic disturbance in the mid-1800s and several smaller, more localized disturbances in the 1910s, 1940s, and 1960s (Baker et al., 2005)

Smithsonian Conservation Biology Institute, Virginia, USA

Lilly Dickey Woods, Indiana, USA

Harvard Forest, USA

Žofín Forest Dynamics Plot, Czech Republic

Niobrara, Nebraska, USA

Riparian site BEPA are growing on N facing slopes near stream

Little Tesuque, New Mexico, USA

Cedar Breaks, Utah, USA

Scotty Creek, Northwest Territories, Canada

melting permafrost

Appendix S2. Methods for reconstruction of DBH

This is still rough/ mostly notes.

In most cases, when a recent *DBH* measurement was available, *DBH* was reconstructed from the outside in. In cases where *DBH* was not available, but when we knew that the core hit pith or could reasonably estimate how far off it was based on the curvature of the rings (Applequist, 1958; Duncan, 1989), *DBH* was reconstructed from the inside out.

For each core, *DBH* can be reconstructed outside-in (based on recent *DBH*, subtracting growth recorded in tree rings) or inside-out (summing *RW* from the inside out,—only when core hit pith or distance to pith can be reliably estimated). We generally gave precedence to the outside-in approach. Specifically, when *DBH* was taken at the time of coring,

At some of our sites where *DBH* was not taken at the time of coring (*SCBI*), *DBH* measurements taken before or slightly after the time of coring could be used. (see issue #19 in *ForestGEO_dendro*) If before, ... If after... For all outside-in reconstructions, if a negative *DBH* was predicted...

When there were more than one cores for a tree, the *DBH* reconstructions from each core were averaged to produce a single estimate of the tree's *DBH* through time. When the start or end dates of the records from the cores differed, we extrapolated growth of the shorter core to match the years covered by the longer core. Specifically, to fill in years at the more recent end, we assumed that the average growth rate of the ten years prior to the missing records applied to the missing years. To fill in years at the beginning of the tree's lifespan, we likewise assumed that the ten years adjacent to the missing record applied to the missing years; however, if this yielded a negative *DBH* estimate for the earliest year in the reconstruction, we divided the existing minimum *DBH* by number of years missing and applied that value to each year. We note that these reconstructed growth records were used only for the reconstruction of *DBH* and were not included as response variables in any of our analyses.

In either case we need bark thickness—ideally allometries describing the relationship between *DBH* and bark thickness (Table S4). This is especially critical for thick-barked species. When bark thickness data were available, we generated allometries (issue #8 in *ForestGEO_dendro*)... lognormal model with intercept forced to zero: `lm(bark_depth.mm ~ -1 + log(dbh_no_bark.cm+1):bark_species, data = bark)`. When bark thickness data were not available, we used published bark allometries from other sources (Table S4)

Appendix S3. Methods for climate data evaluation and correction

For BCNM, we calculated monthly PPT and PDF from daily precipitation readings made on BCNM starting in 1929 (Paton, 2019).

Appendix S4. Methods for comparing our approach with traditional methods

To test whether our methods gave similar results to traditional methods, we conducted qualitative comparisons of our results to previous studies based on the same cores (Table S5) and conducted a formal quantitative comparison for four species (Figs. S11-S14), as detailed below.

Qualitative comparison

For all species-site combinations, we reviewed previous studies characterizing the climate sensitivity of growth using conventional methods. In most cases, we were able to compare with previous studies from the same sites and sets of cores. When these were not available, we reviewed regional-level analyses believed to be representative of the site.

Results from previous studies were compiled alongside results from the climate-only model in this study (Table S5). Where previous studies examined numerous climate variables or time windows (e.g., Helcoski et al., 2019), we focus on those most relevant to our findings.

Beyond the methodological differences, original studies based on the same sets of cores varied from this one and from one another in factors including the exact set of cores analyzed, climate data sources, time frame of analysis, approaches to identifying candidate climate variables and windows (including whether this is done on a site or species level), methods for detrending and standardizing to build chronologies, and whether the effects of temperature and precipitation are considered separately (original studies) or additively (this study). To standardize for such differences, we selected a subset of species for a standardized quantitative comparison, as detailed below.

Quantitative comparison

We also conducted a formal comparison of our approach to conventional methods using identical tree-ring and climate data for four species: PSME (Cedar Breaks, Utah), ABAL (*Žofín*), PIMA (Scotty Creek), and LITU (SCBI; Figs. S11-S14). These species were selected for analysis because they have been well-studied in the past. For each species, we compared climate sensitivities for the top precipitation- and temperature-group variables, as identified in the main analysis.

Prior to analysis, data were prepared and cleaned as described in the Methods section, resulting in an identical set of records for input into each analysis. For the approach developed here, analysis was conducted as described in the Methods section, but with the *climwin* climate variable selection process limited to just the species of interest (as opposed to all species at the site), climate variables considered individually rather than additively, analysis of only first-order linear relationships, and with start date adjusted to match the conventional method (see below). *Climwin* is a useful analytical tool that automates the process of running and comparing numerous regressions, but its use does not alter results relative to what would be obtained via a more conventional approach; numerous climate drivers and time windows can be compared without *climwin* (e.g., REFS), and *climwin* can also be used on residual chronologies. Following the *climwin* analysis step, we extracted *beta* coefficients describing the slope of the relationship between climate and *RW*. *Beta* coefficients, along with their standard error, were obtained for each month within the analysis time frame (Table S1) and for the time window identified as optimal by *climwin*.

For the analysis using conventional methods, the ring-width series from each core was standardized via ARSTAN using a 2/3rds n spline, where n is the number of years in the series (Cook, 1985; Cook & Kairiukstis, 1990). (*The following italic text is self-plagiarized from Helcoski and needs to be reworded:*) *The influence of outliers in all series was reduced using the adaptive power transformation, which also stabilises the variance over time (Cook & Peters, 1997). Next, each series was stabilised using either the average correlation between raw ring-width series (*rbar*) method or a 1/3rds spline method to adjust changes in variance as series replication decreased towards the earlier portion of each chronology (Jones et al., 1997). The 1/3rds spline method was chosen when replication in the inner portion of each chronology (c. the inner 30–50 yr of each record depending on full chronology length) dropped below three trees. Once that step was complete, a robust biweight mean chronology for each species was calculated from the ring-width indices (Cook, 1985). We chose to use residual chronologies because the autoregressive standardisation process in creating them removes much of the tree-level autocorrelation in growth and these chronologies would most likely contain the most*

conservative information on drivers of interannual growth (Cook, 1985).

We defined chronology start dates according to the subsample signal strength (SSS), using a cutoff of SSS = 0.80 (or 80% of the population signal). Thus, for this analysis only, we defined chronology start dates as the year the SSS exceeded 0.80 or two years after the start of the climate record, whichever came later. SSS exceeded 0.80 well before the start of the 1901 start of climate records for PSME (1800s), ABAL (1700), and PIMA (1850s). For LITU, SSS reached 0.8 with 11 trees in 1919, which we used as the start date for this series. We note that these start date criteria differ from those used in the main analysis (Table S3), which had earlier start dates because the analysis was not constrained by a need to represent the full population signal. End dates were defined as the last full year prior to sampling (Table S3), or 2007 for CB.

Beta (slope) coefficients for the relationship between tree growth and the monthly climate variable were derived as in Helcoski et al. (2019): (*SELF-PLAGIARIZED CONTENT:*) *Analyses of climate-growth relationships were conducted using ‘dplR’ (Bunn, 2008) and ‘bootRes’ (Zang & Biondi, 2013), which correlated functions and bootstrapped confidence intervals for the relationships between annual growth and monthly climate variables following Biondi & Waikul (2004).* Pearson correlations between climate variables and tree-ring chronologies were converted to linear slopes using the method of Charney et al. (2016).

Finally, we generated plots comparing month-by-month *beta* coefficients describing climate sensitivity, and also comparing *beta* coefficients for the window identified as optimal by *climwin* Figs. S11-S14).

The result is that our approach yields climate correlations with greater variance but lower standard error of slope estimates (Figs. S11-S14).

We note that despite designing the analyses to be as comparable as possible, one-to-one correspondence of *beta* coefficients is not necessarily expected for several reasons. First, although the analysis time frame is standardized between the two approaches, the relative influence of each year will generally vary between the two approaches. The traditional approach, which all cores into a single residual chronology with one value per year, gives equal weighting to each year. In contrast, under the approach developed here, the number records per year will vary across the analysis time frame, generally increasing over time as the younger trees enter the analysis. Thus, where many younger trees are included in the analysis, the two approaches will effectively give different weights to the years included in the analysis period. In cases where climate-sensitivity differs between old and young trees, or where the climate and/or climate response changed substantially over the analysis time frame (e.g., at Scotty Creek; Fig. S14; Sniderhan & Baltzer, 2016), this may lead to divergence of the climate sensitivities estimated by the two methods.

Second, traditional analysis methods (using ARSTAN) were primarily designed to distill population-level variation to obtain the strongest possible climate signal for the reconstruction of past climate (**Cook & Kariustis**), not to characterize climate responses on the individual level, where variation is inherently higher. While conversion of Pearson correlations to linear slopes *sensu* Charney et al. (2016) approximates climate responses, it does not provide an exact slope describing the relationship between individual-level or population mean growth and climate. This is because standardization of variance and averaging of individual-level residuals prior to the climate analysis fundamentally alters and obfuscates individual-level responses.

We suspect that both of these factors may underlie the tendency for the traditional method to estimate stronger climate sensitivity than the approach developed here for Scotty Creek (Fig. S14), a comprehensively sampled black spruce forest (i.e., including young trees) on melting permafrost. We note, however, that there are no statistically significant differences in the *beta* coefficients of the two approaches at this site.

Appendix S5. Dealing with rapidly changing climate and tree growth

ISSUE #25 in ForestGEO-climate-sensitivity

Our analysis included two sites where climate change has had pronounced effects on tree growth: Scotty Creek, NW Territories, Canada (SC) and Little Tesuque, New Mexico, USA (LT). At SC, rapidly rising temperatures are causing melting permafrost, summer moisture stress, resulting in negative growth trends in basal area index (*BAI*) starting around 1950 and significant growth declines since 1970 in 56% of trees (Sniderhan & Baltzer, 2016). At LT, increasingly warm drought has dramatically reduced growth (Williams et al., 2013), resulting in many missing rings in recent years.

Problematically, correlating tree growth residuals from which climate-driven trends had been removed against the climate signal with a strong directional trend would not necessarily identify the most relevant climate drivers.

For these sites, we experimented with three approaches to identifying the most important climate drivers (1) the method described above, (2) detrending the climate variables (**AT:prewhitening?**) prior to the climwin step, and (3) splitting analyses into decades before and after 1970 (*sensu* Sniderhan & Baltzer, 2016).

Table S1. Site Details.

| site code | site name | latitude | longitude | elevation (m.a.s.l.) | cores within ForestGEO plot? | canopy positions | tree statuses | date range | dormant season* | months in climwin |
|-----------|--|----------|-----------|-------------------------|------------------------------------|----------------------------|---------------|------------|-----------------|-------------------|
| BCNM | Barro Colorado Nature Monument | 9.15430 | -79.8461 | 120-160 | no | canopy | live, dead | 1931-2014 | Nov-Apr | pOct-cDec |
| HKK | Huai Kha Khaeng | 15.63240 | 99.2170 | 549-638 | no | all | live | 1903-2011 | Nov-Apr | pOct-cDec |
| SCBI | Smithsonian Conservation Biology Institute | 38.89350 | -78.1454 | 273-338 | yes | all | live, dead | 1903-2017 | Oct-Apr | pMay-cAug |
| LDW | Lilly Dickey Woods | 39.23590 | -86.2181 | 230-303 | | canopy | live, dead | 1903-2019 | | pMay-cAug |
| HF | Harvard Forest | 42.53880 | -72.1755 | 340-368 | yes | all | live, dead | 1903-2014 | | pMay-cAug |
| ZOF | Zofin Forest Dynamics Plot | 48.66380 | 14.7073 | 736-829 | some | all | live, dead | 1903-2013 | Oct-Mar | pMay-cAug |
| NIO | Niobrara | 42.78000 | -100.0210 | 644-702 | ??? | canopy | live | | Oct-Apr | pMay-cAug |
| LT | Little Tesuque | 35.73838 | -105.8382 | 2684 - 2702 | n.a. | canopy / sub- canopy | live | 1903-2018 | Oct-Apr | pMay-cAug |
| CB | Utah Forest Dynamics Plot | 37.66150 | -112.8525 | 3020-3169 | yes | | live | 1903-2007 | | pMay-cAug |
| SC | Scotty Creek | 61.30000 | -121.3000 | 280 | no | all | live, dead | 1903-2013 | Sept-Apr | pMay-cAug |

*Refers to approximate period during which woody growth ceases (dry season in the tropics, winter for temperate and boreal sites).

Table S2. Species analyzed, their characteristics, and bark allometries applied.

| species code | family | latin name | sites sampled | leaf type | leaf phenology | light requirements* | bark allometry** |
|--------------|--------------|--------------------------------|---------------|------------|---------------------------|---------------------|------------------|
| ABAL | Pinaceae | <i>Abies alba</i> | ZOF | needleleaf | evergreen | shade-tolerant | 2 |
| ABBI | Pinaceae | <i>Abies bifolia</i> | CB | needleleaf | evergreen | shade-tolerant | 2 |
| ACRU | Sapindaceae | <i>Acer rubrum</i> | HF | broadleaf | deciduous (cold) | intermediate | 3 |
| ACSA | Sapindaceae | <i>Acer saccharum</i> | LDW | broadleaf | deciduous (cold) | shade-tolerant | 3 |
| AFXY | Fabaceae | <i>Afzelia xylocarpa</i> | HKK | broadleaf | deciduous (drought) | light-demanding | neglected |
| BEAL | Betulaceae | <i>Betula alleghaniensis</i> | HF | broadleaf | deciduous (cold) | intermediate | 4 |
| BEPA | Betulaceae | <i>Betula papyrifera</i> | NIO | broadleaf | deciduous (cold) | light-demanding | 5 |
| CACO | Juglandaceae | <i>Carya cordiformis</i> | SCBI | broadleaf | deciduous (cold) | light-demanding | 6 |
| CAGL | Juglandaceae | <i>Carya glabra</i> | SCBI | broadleaf | deciduous (cold) | intermediate | 7 |
| CAOV | Juglandaceae | <i>Carya ovata</i> | LDW | broadleaf | deciduous (cold) | intermediate | 7 |
| CAOVL | Juglandaceae | <i>Carya ovalis</i> | SCBI | broadleaf | deciduous (cold) | intermediate | 8 |
| CATO | Juglandaceae | <i>Carya tomentosa</i> | SCBI | broadleaf | deciduous (cold) | light-demanding | 9 |
| CHTA | Meliaceae | <i>Chukrasia tabularis</i> | HKK | broadleaf | brevi-deciduous (drought) | intermediate | neglected |
| FAGR | Fagaceae | <i>Fagus grandifolia</i> | HF, SCBI | broadleaf | deciduous (cold) | shade-tolerant | neglected |
| FASY | Fagaceae | <i>Fagus sylvatica</i> | ZOF | broadleaf | deciduous (cold) | shade-tolerant | neglected |
| FRAM | Oleaceae | <i>Fraxinus americana</i> | LDW, SCBI | broadleaf | deciduous (cold) | intermediate | 10 |
| FRNI | Oleaceae | <i>Fraxinus nigra</i> | SCBI | broadleaf | deciduous (cold) | intermediate | 10 |
| JACO | Bignoniaceae | <i>Jacaranda copaia</i> | BCNM | broadleaf | deciduous (drought) | light-demanding | 11 |
| JUNI | Juglandaceae | <i>Juglans nigra</i> | SCBI | broadleaf | deciduous (cold) | light-demanding | 12 |
| LITU | Magnoliaceae | <i>Liriodendron tulipifera</i> | LDW, SCBI | broadleaf | deciduous (cold) | light-demanding | 13 |
| MEAZ | Meliaceae | <i>Melia azedarach</i> | HKK | broadleaf | deciduous (drought) | light-demanding | neglected |
| PIAB | Pinaceae | <i>Picea abies</i> | HF | needleleaf | evergreen | shade-tolerant | 14 |
| PIEN | Pinaceae | <i>Picea engelmannii</i> | CB | needleleaf | evergreen | shade-tolerant | 14 |
| PIFL | Pinaceae | <i>Pinus flexilis</i> | CB | needleleaf | evergreen | light-demanding | 17 |
| PILO | Pinaceae | <i>Pinus longaeva</i> | CB | needleleaf | evergreen | light-demanding | neglected |
| PIMA | Pinaceae | <i>Pincea mariana</i> | SC | needleleaf | evergreen | shade-tolerant | 15 |
| PIPO | Pinaceae | <i>Pinus ponderosa</i> | LT | needleleaf | evergreen | light-demanding | 16 |
| PIPU | Pinaceae | <i>Pincea pungens</i> | CB | needleleaf | evergreen | intermediate | 14 |
| PIST | Pinaceae | <i>Pinus strobus</i> | HF, SCBI | needleleaf | evergreen | intermediate | 18 |
| PIST3 | Pinaceae | <i>Pinus strobiformis</i> | LT | needleleaf | evergreen | light-demanding | 17 |
| POTR | Salicaceae | <i>Populus tremuloides</i> | CB | broadleaf | deciduous (cold) | light-demanding | 19 |
| PSME | Pinaceae | <i>Pseudotsuga menziesii</i> | CB | needleleaf | evergreen | intermediate | 20 |
| QUAL | Fagaceae | <i>Quercus alba</i> | LDW, SCBI | broadleaf | deciduous (cold) | intermediate | 21 |
| QUMO | Fagaceae | <i>Quercus montana</i> | LDW, SCBI | broadleaf | deciduous (cold) | intermediate | 22 |
| QURU | Fagaceae | <i>Quercus rubra</i> | HF, LDW, SCBI | broadleaf | deciduous (cold) | intermediate | 23 |
| QUVE | Fagaceae | <i>Quercus velutina</i> | LDW, SCBI | broadleaf | deciduous (cold) | intermediate | 24 |
| TEPA | Burseraceae | <i>Tetragastris panamensis</i> | BCNM | broadleaf | evergreen | shade-tolerant | 25 |
| TOCI | Meliaceae | <i>Toona ciliata</i> | HKK | broadleaf | deciduous (drought) | intermediate | neglected |
| TRTU | Meliaceae | <i>Trichilia tuberculata</i> | BCNM | broadleaf | evergreen | shade-tolerant | 26 |
| TSCA | Pinaceae | <i>Tsuga canadensis</i> | HF | needleleaf | evergreen | shade-tolerant | 27 |

*For extratropical species, light requirements are classified based on the database of Niinemets & Valladares (2006). For tropical species, categorization is based on Alfaro-Sánchez et al. (2017) for BCNM and Vlam et al. (2014) for HKK.

**Bark allometry field indicates the species and site sampled to construct the bark allometry. When neither raw data nor an allometric equation for the study species was available, we selected the most appropriate equation that could be located for similar species. Equations are given in Table S4.

Table S3. Sampling details for species by site.

| site | species code | all | | with DBH | | DBH range | | date range |
|------|--------------|---------|---------|----------|---------|-------------|----------------|------------|
| | | n trees | n cores | n trees | n cores | sampled | reconstructed* | |
| BCNM | JACO | 12 | 18 | 11 | 17 | 30.2-63.5 | 2.6-56.4 | 1931-2014 |
| BCNM | TEPA | 18 | 29 | 17 | 26 | 22.1-59.5 | 2.7-49.4 | 1931-2014 |
| BCNM | TRTU | 23 | 37 | 20 | 31 | 20.7-43.6 | 4.8-41.5 | 1931-2014 |
| CB | ABBI | 22 | 41 | 20 | 39 | 13.9-54.2 | 0-50.4 | 1903-2019 |
| CB | PIEN | 14 | 23 | 12 | 20 | 14-54.9 | 2.2-43.4 | 1903-2019 |
| CB | PIFL | 13 | 21 | 12 | 20 | 17.6-64.1 | 4.5-58.5 | 1903-2018 |
| CB | PILO | 17 | 25 | 7 | 11 | 45.8-63.6 | 35.4-57.5 | 1903-2019 |
| CB | PIPU | 16 | 29 | 15 | 28 | 22.4-50.8 | 8.6-50.5 | 1903-2019 |
| CB | POTR | 17 | 27 | 17 | 27 | 23.6-47.6 | 7.7-44.5 | 1903-2019 |
| CB | PSME | 11 | 21 | 11 | 21 | 10.6-64.2 | 2.6-63.3 | 1903-2019 |
| HF | ACRU | 18 | 59 | 18 | 59 | 10.1-22.1 | 0.9-20.4 | 1903-2013 |
| HF | BEAL | 13 | 44 | 13 | 44 | 10.2-37.9 | 1.6-20.5 | 1904-2013 |
| HF | QURU | 74 | 180 | 73 | 177 | 19.5-53 | 1.1-48.3 | 1903-2014 |
| HF | TSCA | 32 | 83 | 32 | 83 | 10.6-37 | 0.6-33.5 | 1923-2014 |
| HKK | AFXY | 39 | 127 | 39 | 127 | 20.1-98.7 | 0.1-81.4 | 1903-2011 |
| HKK | CHTA | 28 | 70 | 28 | 70 | 16-64.6 | 0.2-59.5 | 1904-2010 |
| HKK | MEAZ | 46 | 130 | 46 | 130 | 25.6-98.1 | 3.8-80.3 | 1914-2011 |
| HKK | TOCI | 45 | 143 | 45 | 143 | 16.6-116.4 | 1.7-80.5 | 1903-2011 |
| LDW | ACSA | 35 | 66 | 34 | 64 | 9-64.6 | 0-52.4 | 1903-2019 |
| LDW | CAOV | 9 | 18 | 8 | 16 | unknown | 0.6-37.4 | 1903-2013 |
| LDW | LITU | 15 | 28 | 14 | 26 | unknown | 1.2-69.4 | 1903-2019 |
| LDW | QUAL | 10 | 20 | 0 | 0 | NA | NA | 1903-2013 |
| LDW | QUMO | 10 | 20 | 8 | 16 | unknown | 1.1-52.4 | 1903-2013 |
| LDW | QUVE | 9 | 18 | 0 | 0 | NA | NA | 1903-2013 |
| LT | PIPO | 10 | 20 | 10 | 20 | 23.2-52.8 | 14.6-48.4 | 1903-2018 |
| LT | PIST3 | 7 | 14 | 7 | 14 | 25.7-39.8 | 4.2-34.4 | 1903-2018 |
| NIO | BEPA | 28 | 84 | 28 | 84 | unknown | 0.4-30.5 | 1948-1995 |
| SCBI | CACO | 15 | 15 | 15 | 15 | 10.62-38.52 | 1.6-32.2 | 1903-2015 |
| SCBI | CAGL | 39 | 39 | 36 | 36 | 10.28-52.31 | 1.6-49.3 | 1903-2015 |
| SCBI | CAOVL | 25 | 25 | 24 | 24 | 15.11-60.32 | 2.6-47.2 | 1903-2015 |
| SCBI | CATO | 15 | 15 | 14 | 14 | 12.86-35.95 | 3.7-28.4 | 1903-2015 |
| SCBI | FAGR | 76 | 76 | 76 | 76 | 10.05-41.02 | 0.1-41.2 | 1920-2009 |
| SCBI | FRAM | 66 | 66 | 63 | 63 | 6.85-94.73 | 0.1-84.4 | 1903-2016 |
| SCBI | FRNI | 12 | 12 | 12 | 12 | 11.04-39.2 | 0.5-27.3 | 1903-1996 |
| SCBI | JUNI | 30 | 30 | 29 | 29 | 20.4-76.19 | 4.6-59.5 | 1903-2010 |

(continued)

| site | species code | all | | with DBH | | DBH range | | date range |
|------|--------------|---------|---------|----------|---------|-------------|----------------|------------|
| | | n trees | n cores | n trees | n cores | sampled | reconstructed* | |
| SCBI | LITU | 106 | 106 | 105 | 105 | 10-91.42 | 0.1-81.1 | 1903-2010 |
| SCBI | PIST | 36 | 36 | 36 | 36 | 13.92-50.96 | 0.5-44.3 | 1931-2010 |
| SCBI | QUAL | 66 | 66 | 66 | 66 | 11.4-76.73 | 0.3-70.4 | 1903-2009 |
| SCBI | QUMO | 67 | 67 | 67 | 67 | 10.22-84.59 | 0.3-69.5 | 1903-2017 |
| SCBI | QURU | 70 | 70 | 70 | 70 | 11.07-87.65 | 2.5-79.2 | 1903-2016 |
| SCBI | QUVE | 81 | 81 | 81 | 81 | 16.02-82.33 | 0.5-78.4 | 1903-2009 |
| SC | PIMA | 443 | 443 | 395 | 395 | 7-24 | 0-16.4 | 1903-2013 |
| ZOF | ABAL | 46 | 46 | 46 | 46 | 50-121 | 21.1-107.4 | 1903-2010 |
| ZOF | FASY | 1369 | 1369 | 1369 | 1369 | unknown | 0.1-115.3 | 1903-2013 |
| ZOF | PCAB | 644 | 644 | 642 | 642 | unknown | 0-126.4 | 1903-2011 |

*Maximum reconstructed DBH's analyzed are less than maximum sampled DBH's because we discard size ranges with < 3 conspecific trees.

Table S4. Allometric equations for bark thickness.

| species | equation | source | n | DBH.range.cm | site | source.1 |
|--------------------------------|--|----------|----|--------------|------------------------------|---|
| <i>Abies alba</i> | $bark.mm = ((0.05 + 0.06 * (dbh.cm/2.54))/2) * 2.54$ | equation | NA | | North America | Miles, Patrick D.; Smith, W. Brad. 2009. |
| <i>Acer pseudoplatanus</i> | $bark.mm = 0.619 * \log(dbh.cm + 1)$ | data | 10 | 8.2-39.6 | SCBI | Anderson-Teixeira et al. (2015) |
| <i>Betula alleghaniensis</i> | $bark.mm = ((0.15 + 0.03 * (dbh.cm/2.54))/2) * 2.54$ | equation | NA | | North America | Miles, Patrick D.; Smith, W. Brad. 2009. |
| <i>Betula papyrifera</i> | $bark.mm = ((0.13 + 0.05 * (dbh.cm/2.54))/2) * 2.54$ | equation | NA | | North America | Miles, Patrick D.; Smith, W. Brad. 2009. |
| <i>Carya cordiformis</i> | $bark.mm = 0.793 * \log(dbh.cm + 1)$ | data | 9 | 5.9-68.2 | SCBI | Anderson-Teixeira et al. (2015) |
| <i>Carya glabra</i> | $bark.mm = 1.035 * \log(dbh.cm + 1)$ | data | 8 | 19.1-78 | SCBI | Anderson-Teixeira et al. (2015) |
| <i>Carya ovalis</i> | $bark.mm = 1.531 * \log(dbh.cm + 1)$ | data | 8 | 6.4-63.1 | SCBI | Anderson-Teixeira et al. (2015) |
| <i>Carya tomentosa</i> | $bark.mm = 1.105 * \log(dbh.cm + 1)$ | data | 8 | 5-57.3 | SCBI | Anderson-Teixeira et al. (2015) |
| <i>Fraxinus americana</i> | $bark.mm = 2.223 * \log(dbh.cm + 1)$ | data | 9 | 6.1-94.2 | SCBI | Anderson-Teixeira et al. (2015) |
| <i>Jacaranda copaia</i> | $bark.mm = 2.993 * \log(dbh.cm + 1)$ | data | 5 | 45.6-75 | Panama | Raquel Alfaro-Sánchez (unpublished data) |
| <i>Juglans nigra</i> | $bark.mm = 2.107 * \log(dbh.cm + 1)$ | data | 9 | 13.6-85.4 | SCBI | Anderson-Teixeira et al. (2015) |
| <i>Liriodendron tulipifera</i> | $bark.mm = 1.637 * \log(dbh.cm + 1)$ | data | 9 | 27.5-136.5 | SCBI | Anderson-Teixeira et al. (2015) |
| <i>Picea abies</i> | $bark.mm = ((0.15 + 0.04 * (dbh.cm/2.54))/2) * 2.54$ | equation | NA | | North America | Miles, Patrick D.; Smith, W. Brad. 2009. |
| <i>Picea mariana</i> | $bark.mm = 3.726 * \log(dbh.cm + 1)$ | data | 12 | 6.9-7.9 | Scotty Creek | Rajit Patankar and Jennifer Baltzer (unpublished data) |
| <i>Pinus flexilis</i> | $bark.mm = (1.299 * \sqrt{(dbh.cm)^{0.609}})^2$ | equation | 29 | 10-130 | California (3 montane sites) | Zeibig-Kichas et al. (2016) |
| <i>Pinus ponderosa</i> | $bark.mm = (1.298 * \sqrt{(dbh.cm)^{0.802}})^2$ | equation | 81 | 5-160 | California (4 montane sites) | Zeibig-Kichas et al. (2016) |
| <i>Pinus strobus</i> | $bark.mm = ((0.02 + 0.10 * (dbh.cm/2.54))/2) * 2.54$ | equation | NA | | North America | Miles, Patrick D.; Smith, W. Brad. 2009. |
| <i>Populus tremuloides</i> | $bark.mm = ((0.10 + 0.07 * (dbh.cm/2.54))/2) * 2.54$ | equation | NA | | North America | Miles, Patrick D.; Smith, W. Brad. 2009. |
| <i>Pseudotsuga menziesii</i> | $bark.mm = (0.785 * \sqrt{(dbh.cm)})^2$ | equation | 30 | 10-200 | California (3 montane sites) | Zeibig-Kichas et al. (2016) |
| <i>Quercus alba</i> | $bark.mm = 1.828 * \log(dbh.cm + 1)$ | data | 10 | 9.3-101.8 | SCBI | Anderson-Teixeira et al. (2015) |
| <i>Quercus montana</i> | $bark.mm = 2.083 * \log(dbh.cm + 1)$ | data | 8 | 5.8-99.1 | SCBI | Anderson-Teixeira et al. (2015) |
| <i>Quercus rubra</i> | $bark.mm = 0.98 * \log(dbh.cm + 1)$ | data | 10 | 24.1-143.2 | SCBI | Anderson-Teixeira et al. (2015) |
| <i>Quercus velutina</i> | $bark.mm = 1.394 * \log(dbh.cm + 1)$ | data | 8 | 16.2-110.7 | SCBI | Anderson-Teixeira et al. (2015) |
| <i>Tetragastris panamensis</i> | $bark.mm = 1.672 * \log(dbh.cm + 1)$ | data | 4 | 22.7-48.8 | Panama | Raquel Alfaro-Sánchez (unpublished data) |
| <i>Trichilia tuberculata</i> | $bark.mm = 1.367 * \log(dbh.cm + 1)$ | data | 12 | 21-40.5 | Panama | Raquel Alfaro-Sánchez (unpublished data), Pete Kerby-Miller and Helene Muller-Landau (unpublished data) |
| <i>Tsuga canadensis</i> | $bark.mm = ((0.18 + 0.08 * (dbh.cm/2.54))/2) * 2.54$ | equation | NA | | North America | Miles, Patrick D.; Smith, W. Brad. 2009. |

For assignments of species as proxies for those with out available bark allometries, see Table S2.

Table S5. Qualitative comparison of results from this study with previous studies employing conventional methods.

| species | Precipitation response | | Temperature response | | reference |
|--|---|---|---|--|----------------------------|
| | previously observed | observed here | previously observed | observed here | |
| Barro Colorado Nature Monument, Panama | | | | | |
| JACO | pos. correlation to Apr-Dec <i>PPT</i> (strongest of the 3 species) | pos. correlation to Mar-Dec <i>PPT</i> (strongest of the 3 species) | no sig. correlation to annual T_{mean} or T_{min} | neg. response to Feb-Mar T_{min} | Alfaro-Sánchez et al. 2017 |
| TEPA | pos. correlation to Apr-Dec <i>PPT</i> (response weaker than JACO, similar to TRTU) | pos. correlation to Mar-Dec <i>PPT</i> (response weaker than JACO, similar to TRTU) | no sig. correlation to annual T_{mean} or T_{min} | no sig. correlation to Feb-Mar T_{min} | Alfaro-Sánchez et al. 2017 |
| TRTU | pos. correlation to Apr-Dec <i>PPT</i> (response weaker than JACO, similar to TEPA) | pos. correlation to Mar-Dec <i>PPT</i> (response weaker than JACO, similar to TEPA) | no sig. correlation to annual T_{mean} or T_{min} | non-sig. slight pos. response to Feb-Mar T_{min} | Alfaro-Sánchez et al. 2017 |
| Huai Kha Khaeng, Thailand | | | | | |
| AFXY | sig. pos. correlation with June <i>PPT</i> , otherwise n.s. | slight concave-down response to p.Sept-June <i>PPT</i> frequency | sig. neg. correlation with T_{max} in Aug and Dec; T_{min} in p.Oct., Jul, Aug | slight concave-down response to Apr-Oct T_{max} | Vlam et al. 2013 |
| CHTA | sig. pos. correlation with April <i>PPT</i> , otherwise n.s. | slight concave-down response to p.Sept-June <i>PPT</i> frequency | sig. neg. correlation with T_{max} in May, Aug-Sept; T_{min} in Feb, May, Aug | slight neg. response to Apr-Oct T_{max} | Vlam et al. 2013 |
| MEAZ | sig. pos. correlation with April <i>PPT</i> , otherwise n.s. | concave-down response to p.Sept-June <i>PPT</i> frequency | sig. neg. correlation with T_{max} in May-Aug; T_{min} in May-Aug | neg. response to Apr-Oct T_{max} | Vlam et al. 2013 |
| TOCI | sig. pos. correlation with p.Oct-p.Nov and April-May <i>PPT</i> | concave-down /increasing response to p.Sept-June <i>PPT</i> frequency | sig. neg. correlation with T_{max} every month from pOct-June (excluding March); T_{min} in Jan and Mar-Aug | neg. response to Apr-Oct T_{max} | Vlam et al. 2013 |
| Smithsonian Conservation Biology Institute, Virginia, USA | | | | | |
| CACO | pos. correlations with May-Aug <i>PPT</i> (sig. May, July) | neg. correlations with May-Aug <i>PET</i> (sig. May-July) | **(sig or ns)** neg. response to May-July <i>PET</i> | Helcoski et al. 2019 | |
| CAGL | pos. correlations with May-Aug <i>PPT</i> (sig. May) | neg. correlations with May-Aug <i>PET</i> (n.s.) | **(sig or ns)** neg. response to May-July <i>PET</i> | Helcoski et al. 2019 | |
| CAOVL | pos. correlations with May-Aug <i>PPT</i> (sig. Aug) | neg. correlations with May-Aug <i>PET</i> (sig. all months) | **(sig or ns)** neg. response to May-July <i>PET</i> | Helcoski et al. 2019 | |
| CATO | pos. correlations with May-Aug <i>PPT</i> (n.s.) | neg. correlations with May-Aug <i>PET</i> (sig. June) | **(sig or ns)** neg. response to May-July <i>PET</i> | Helcoski et al. 2019 | |
| FAGR | pos. correlations with May-Aug <i>PPT</i> (sig. July-Aug) | neg. correlations with May-Aug <i>PET</i> (sig. July-Aug) | **(sig or ns)** neg. response to May-July <i>PET</i> | Helcoski et al. 2019 | |
| FRAM | pos. correlations with May-Aug <i>PPT</i> (sig. May-June) | neg. correlations with May-Aug <i>PET</i> (sig. May-June) | **(sig or ns)** neg. response to May-July <i>PET</i> | Helcoski et al. 2019 | |
| FRNI | no sig. correlations with peak growing season <i>PPT</i> | no sig. correlations with peak growing season <i>PET</i> | **(sig or ns)** neg. response to May-July <i>PET</i> | Helcoski et al. 2019 | |
| JUNI | pos. correlations with May-Aug <i>PPT</i> (sig. Jun-Aug) | neg. correlations with May-Aug <i>PET</i> (sig. July-Aug) | non-sig. neg. response to May-July <i>PET</i> | Helcoski et al. 2019 | |

S5, cont.

| species | Precipitation response | | Temperature response | | reference |
|--|---|-------------------------------------|---|---|---|
| | previously observed | observed here | previously observed | observed here | |
| Smithsonian Conservation Biology Institute, Virginia, USA (cont.) | | | | | |
| LITU | pos. correlations with May-Aug <i>PPT</i> (sig. May-July) | | neg. correlations with May-Aug <i>PET</i> (sig. all months) | **(sig or ns)** neg. response to May-July <i>PET</i> | Helcoski et al. 2019 |
| PIST | pos. correlations with May-Aug <i>PPT</i> (n.s.) | | neg. correlations with May-Aug <i>PET</i> (n.s.) | **(sig or ns)** neg. response to May-July <i>PET</i> | Helcoski et al. 2019 |
| QUAL | pos. correlations with May-Aug <i>PPT</i> (sig. May) | | neg. correlations with May-Aug <i>PET</i> (sig. all months) | **(sig or ns)** neg. response to May-July <i>PET</i> | Helcoski et al. 2019 |
| QUMO | pos. correlations with May-Aug <i>PPT</i> (sig. May) | | neg. correlations with May-Aug <i>PET</i> (sig. May-June, Aug) | **(sig or ns)** neg. response to May-July <i>PET</i> | Helcoski et al. 2019 |
| QURU | pos. correlations with May-Aug <i>PPT</i> (n.s.) | | neg. correlations with May-Aug <i>PET</i> (sig. May, July-Aug) | **(sig or ns)** neg. response to May-July <i>PET</i> | Helcoski et al. 2019 |
| QUVE | pos. correlations with May-Aug <i>PPT</i> (sig. May-July) | | neg. correlations with May-Aug <i>PET</i> (sig. all months) | **(sig or ns)** neg. response to May-July <i>PET</i> | Helcoski et al. 2019 |
| Lilly Dickey Woods, Indiana, USA | | | | | |
| LITU | pos. correlations with Jun-Aug PDSI | pos. response to June <i>PPT</i> | neg. response to Jun-Aug <i>T_{max}</i> | neg. response to June <i>PET</i> | Maxwell, Harley, and Robeson 2016 |
| QUAL | pos. correlations with Jun-Aug PDSI | pos. response to June <i>PPT</i> | neg. response to Jun-Aug <i>T_{max}</i> | neg. response to June <i>PET</i> | Maxwell, Harley, and Robeson 2016 |
| QUMO | pos. correlations with Jun-Aug PDSI | pos. response to June <i>PPT</i> | neg. response to Jun-Aug <i>T_{max}</i> | neg. response to June <i>PET</i> | Maxwell, Harley, and Robeson 2016 |
| QUVE | pos. correlations with Jun-Aug PDSI | pos. response to June <i>PPT</i> | neg. response to Jun-Aug <i>T_{max}</i> | neg. response to June <i>PET</i> | Maxwell, Harley, and Robeson 2016 |
| Harvard Forest, Massachusetts, USA | | | | | |
| ACRU | | | no response to Jan- April <i>T_{min}</i> * | neg. correlation to Mar <i>PET</i> | Alexander et al. 2019 |
| BEAL | | | no response to Jan- April <i>T_{min}</i> * | ns neg correlation with Mar <i>PET</i> | Alexander et al. 2019 |
| QURU | | | no response to Jan- April <i>T_{min}</i> * | slight concave-down decreasing response to Mar <i>PET</i> | Alexander et al. 2019 |
| TSCA | | | pos. response to Jan- April <i>T_{min}</i> * | pos. response to March <i>PET</i> | Alexander et al. 2019 |

S5, cont.

| species | Precipitation response | | Temperature response | | reference |
|---|--|---|--|--------------------------------------|---|
| | previously observed | observed here | previously observed | observed here | |
| Žofín Forest Dynamics Plot, Czech Republic | | | | | |
| ABAL | no sig. correlations with June-July <i>PPT</i> | slight concave-down response to p.Jun-p.July <i>PPT</i> frequency | sig. pos. correlation to April T (strongest T correlation) | pos. response to Jan-March T_{max} | Kašpar, Tumajer, Vašíčková, and Šamonil, in review |
| FASY | no sig. correlations with June-July <i>PPT</i> | pos. response to p.Jun-p.July <i>PPT</i> frequency | sig. pos. correlation to Jan T (strongest T correlation) | pos. response to Jan-March T_{max} | Kašpar, Tumajer, Vašíčková, and Šamonil, in review |
| PIAB | modest pos. correlations (n.s) with June-July <i>PPT</i> >700m elev. sites moisture limited June-Aug | pos. response to p.Jun-p.July <i>PPT</i> frequency | sig. pos. correlation to March T (strongest current-year T correlation) >700m elev. sites temperature limited except June-Aug | pos. response to Jan-March T_{max} | Kašpar, Tumajer, Vašíčková, and Šamonil, in review Tumajer et al. 2017 |
| Niobrara, Nebraska, USA | | | | | |
| BEPA | little relationship to ppt within analysis timeframe (exception: pos. corr. with pAug pre); stronger relationship to streamflow and PDSI | | little relationship to T_{mean} within analysis timeframe (exception: neg. corr. with pJune and cJan T_{mean}) | | Bumann et al. 2019 |
| Little Tesuque, New Mexico, USA | | | | | |
| PIPO | | | | | Touchan et al., 2011 and Williams et al., 2013 |
| PIST2 | | | | | Touchan et al., 2011 and Williams et al., 2013 |
| Cedar Breaks, Utah, USA | | | | | |
| Scotty Creek, NW Territories, Canada | | | | | |
| | | | | | Sniderhan and Baltzer 2016 |

*Indicates results from a regional study including but not limited to cores from the focal site.

**Indicates results from a regional study not including the focal site, but believed to be representative.

Figure S1. Density plot of core record start years by species for Barro Colorado Nature Monument (Panama).

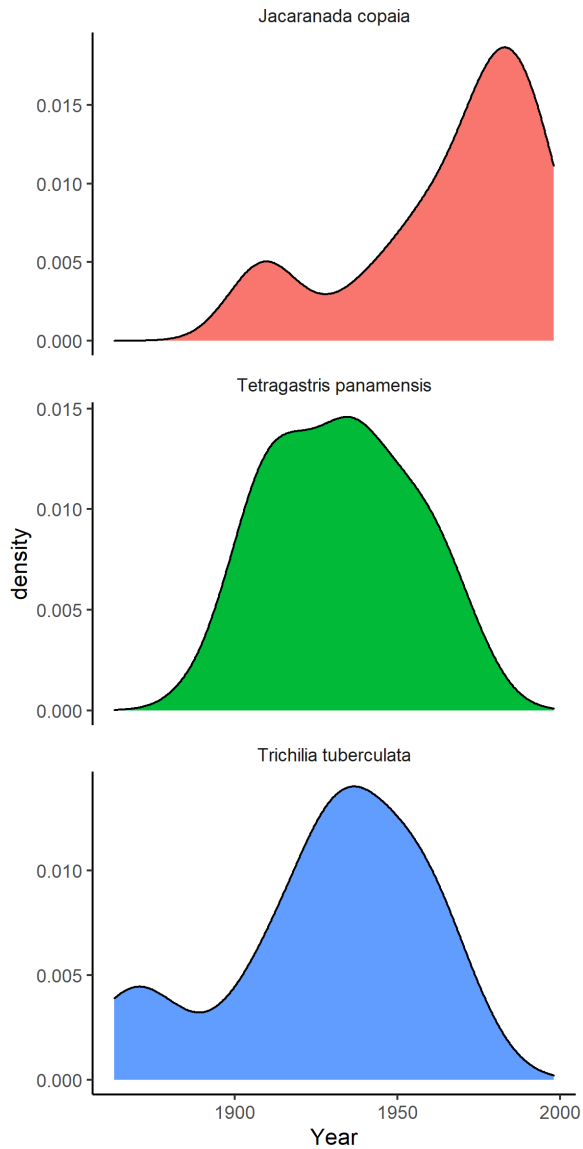


Figure S1. Density plot of core record start years by species for Barro Colorado Nature Monument (Panama). This distribution approximates—but does not entirely match—the age distribution of trees cored. The core record start year can occur after a tree's recruitment year (i.e., year when the tree reached coring height) if the core fails to hit center or if the tree's center is lost to heartrot. “Heartrot was common at this site, implying that recruitment years are overestimated for some trees.”

Figure S2. Density plot of core record start years by species for Huai Kha Khaeng (Thailand).

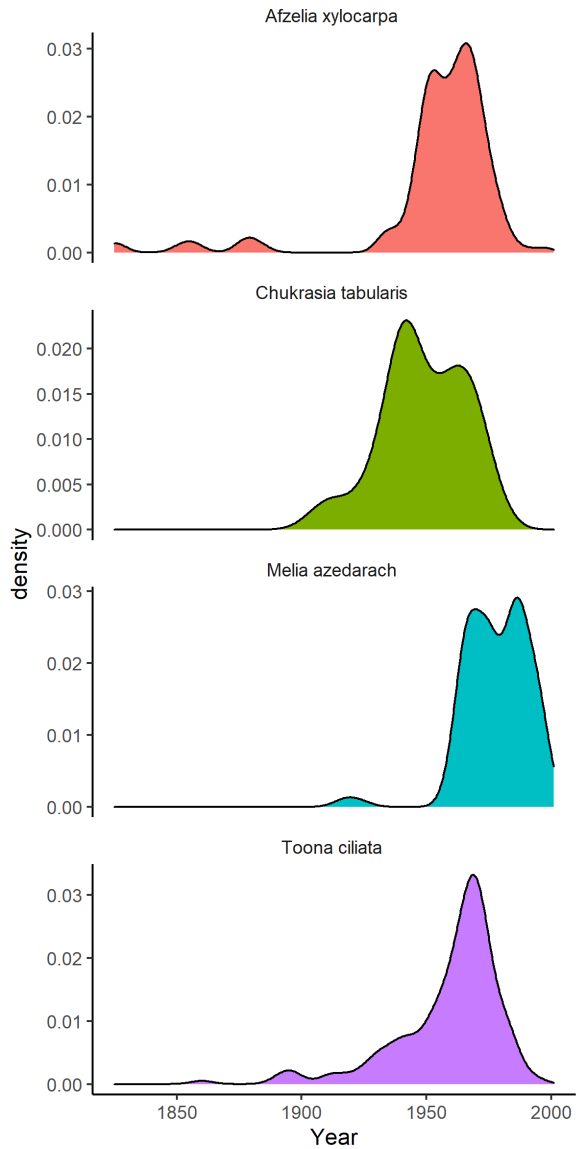


Figure S2. Density plot of core record start years by species for Huai Kha Khaeng (Thailand). This distribution approximates—but does not entirely match—the age distribution of trees cored. The core record start year can occur after a tree's recruitment year (i.e., year when the tree reached coring height) if the core fails to hit center or if the tree's center is lost to heartrot.

Figure S3. Density plot of core record start years by species for the Smithsonian Conservation Biology Institute (Virginia, USA).

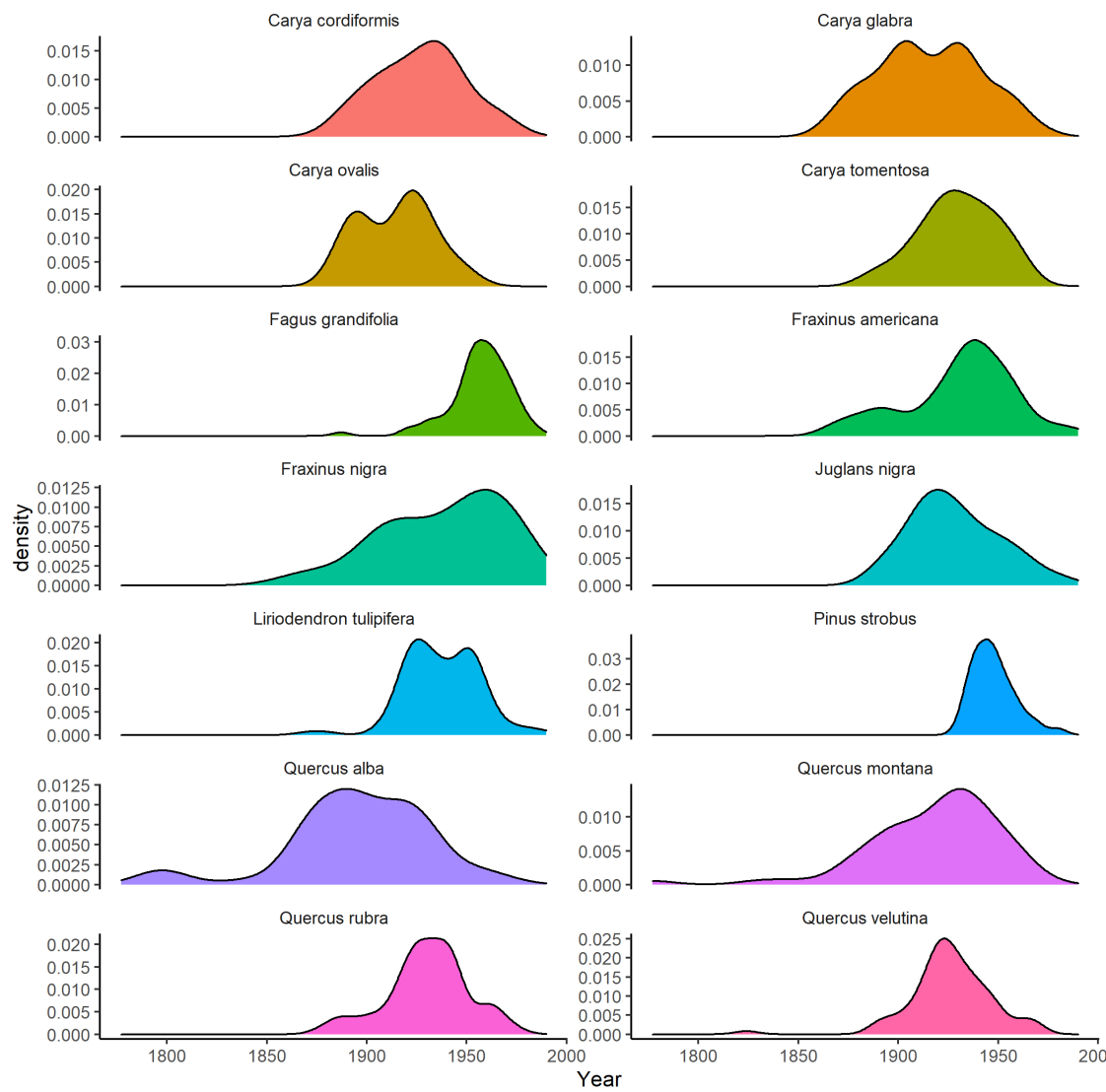


Figure S3. Density plot of core record start years by species for the Smithsonian Conservation Biology Institute (Virginia, USA). This distribution approximates—but does not entirely match—the age distribution of trees cored. The core record start year can occur after a tree's recruitment year (i.e., year when the tree reached coring height) if the core fails to hit center or if the tree's center is lost to heartrot.

Figure S4. Density plot of core record start years by species for Lilley Dickey Woods (Indiana, USA).

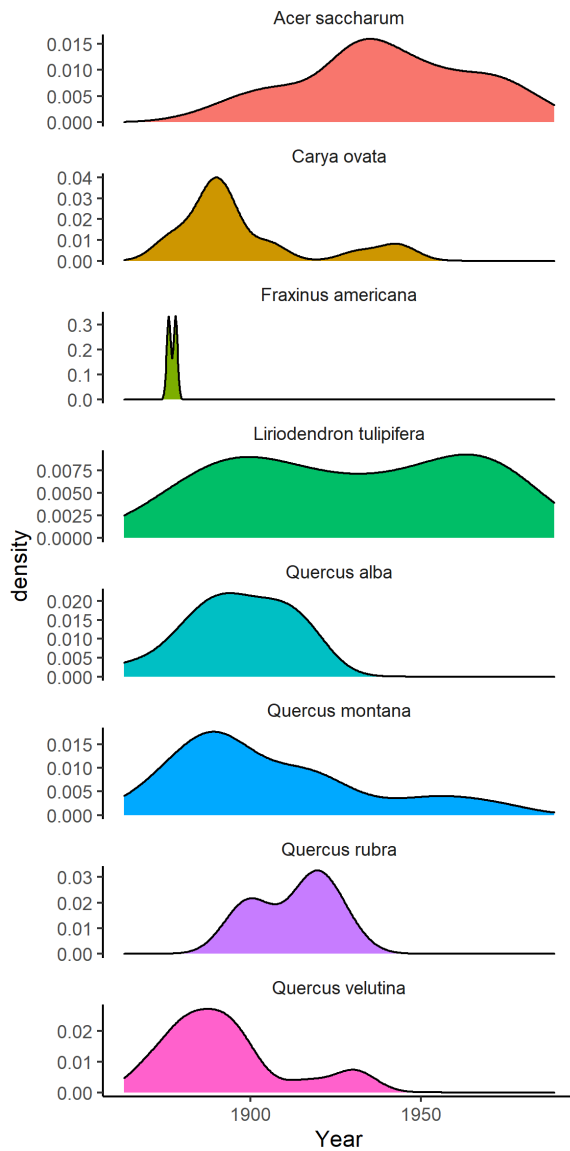


Figure S4. Density plot of core record start years by species for Lilley Woods (Indiana, USA). This distribution approximates—but does not entirely match—the age distribution of trees cored. The core record start year can occur after a tree's recruitment year (i.e., year when the tree reached coring height) if the core fails to hit center or if the tree's center is lost to heartrot.

Figure S5. Density plot of core record start years by species for Harvard Forest (Massachusetts, USA).

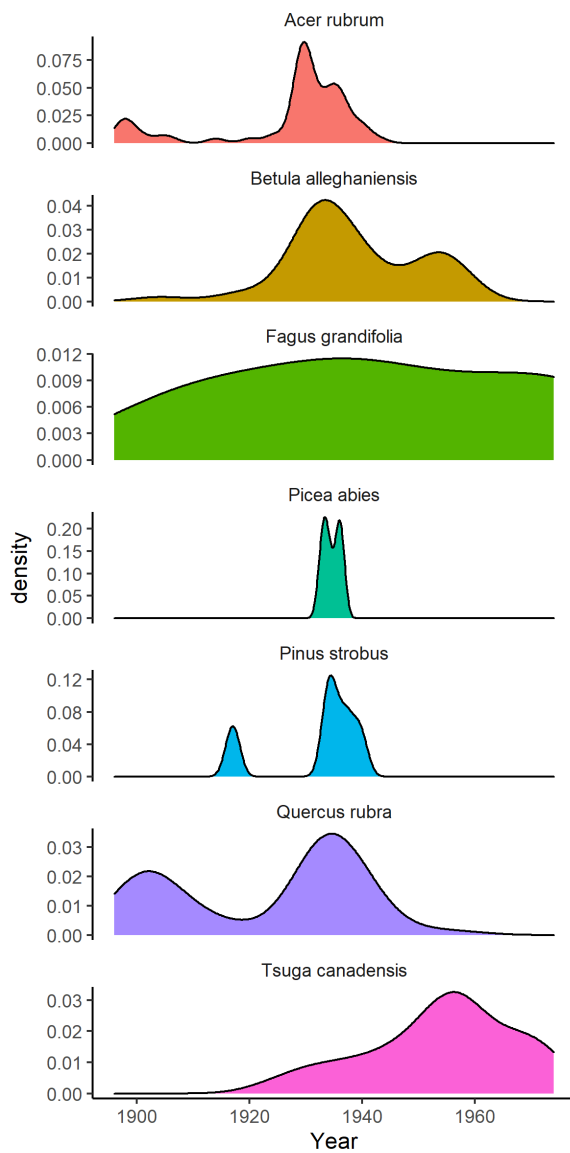


Figure S5. Density plot of core record start years by species for Harvard Forest (Massachusetts, USA). This distribution approximates—but does not entirely match—the age distribution of trees cored. The core record start year can occur after a tree's recruitment year (i.e., year when the tree reached coring height) if the core fails to hit center or if the tree's center is lost to heartrot.

Figure S6. Density plot of core record start years by species for Zofin Forest (Czech Republic).

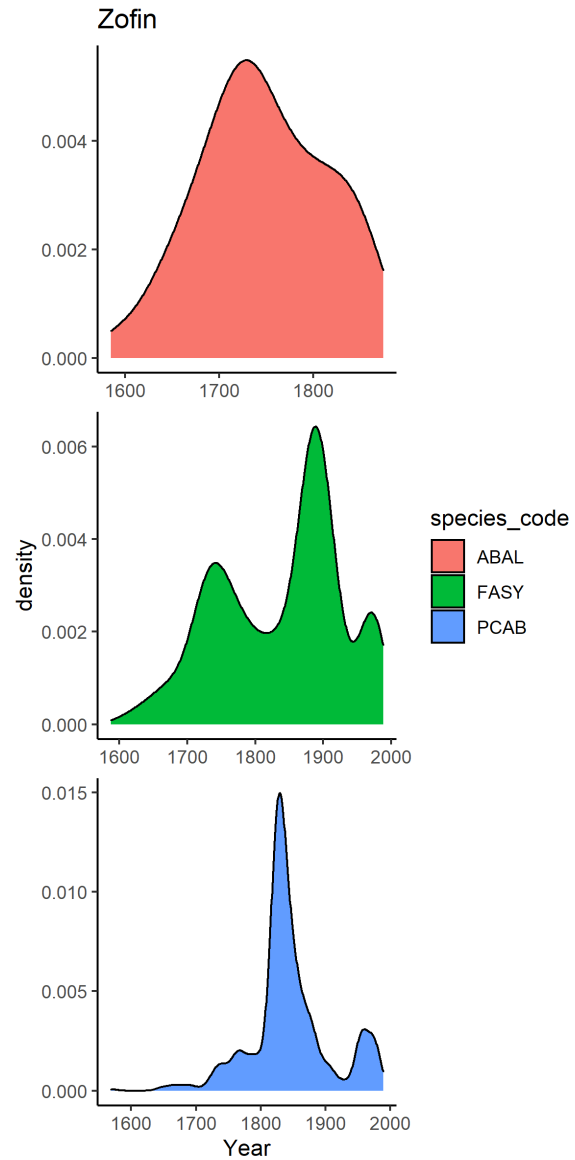


Figure S6. Density plot of core record start years by species for Zofin Forest (Czech Republic). This distribution approximates—but does not entirely match—the age distribution of trees cored. The core record start year can occur after a tree's recruitment year (i.e., year when the tree reached coring height) if the core fails to hit center or if the tree's center is lost to heartrot.

Figure S7. Density plot of core record start years by species for Niobrara (Nebraska, USA).

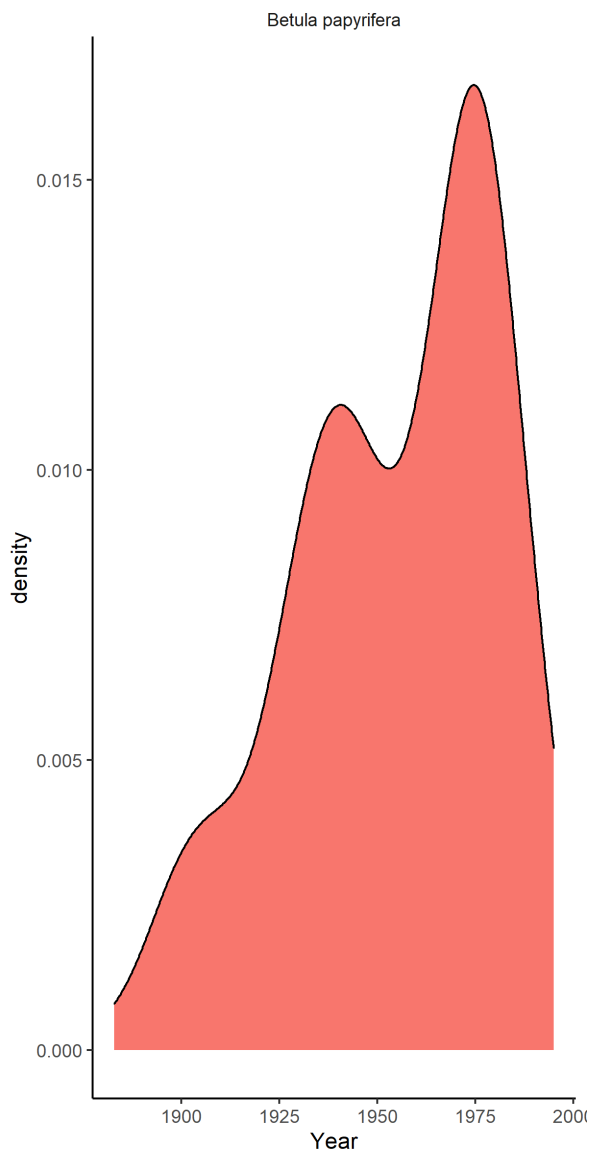


Figure S7. Density plot of core record start years for Niobrara (Nebraska, USA). This distribution approximates—but does not entirely match—the age distribution of trees cored. The core record start year can occur after a tree's recruitment year (i.e., year when the tree reached coring height) if the core fails to hit center or if the tree's center is lost to heartrot.

Figure S8. Density plot of core record start years by species for Little Tesuque (New Mexico, USA).

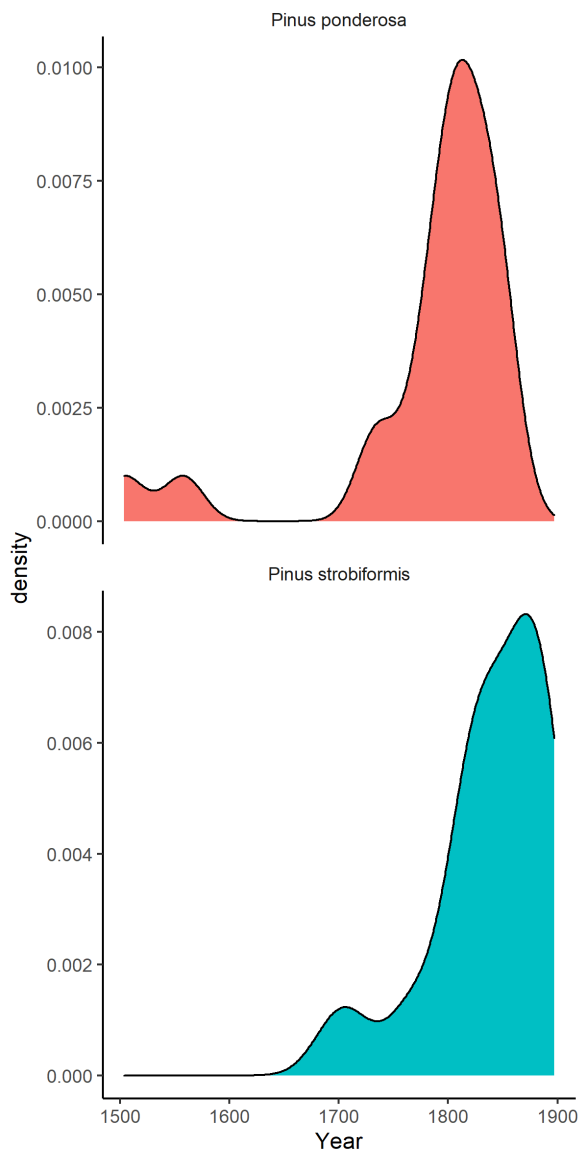


Figure S8. Density plot of core record start years by species for Little Tesuque (New Mexico, USA). This distribution approximates—but does not entirely match—the age distribution of trees cored. The core record start year can occur after a tree's recruitment year (i.e., year when the tree reached coring height) if the core fails to hit center or if the tree's center is lost to heartrot.

Figure S9. Density plot of core record start years by species for Cedar Breaks (Utah, USA).

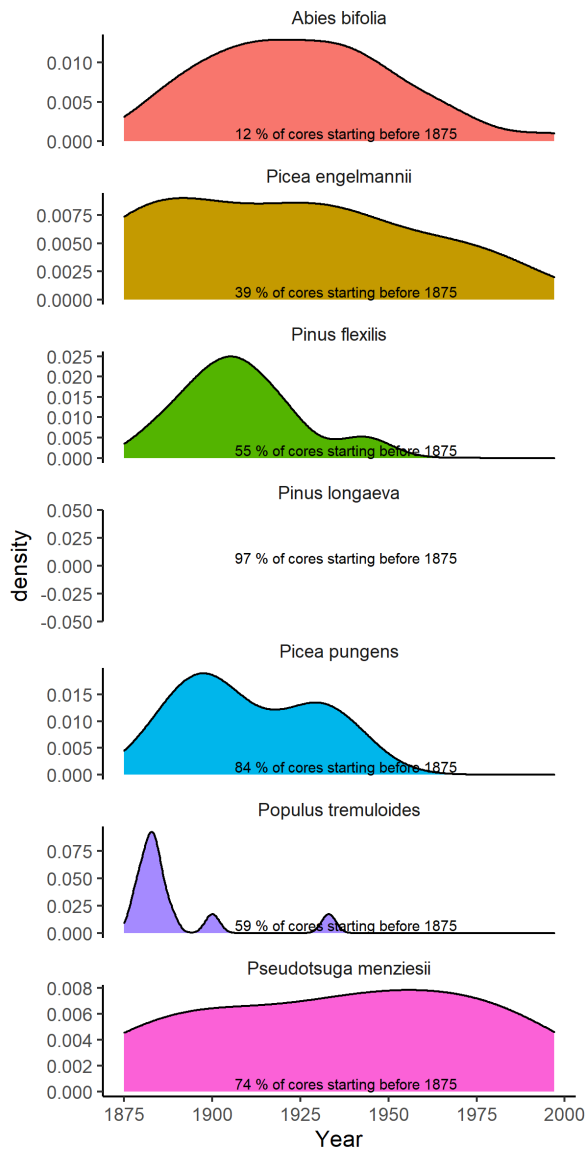


Figure S9. Density plot of core record start years by species for Cedar Breaks (Utah, USA). This distribution approximates—but does not entirely match—the age distribution of trees cored. The core record start year can occur after a tree's recruitment year (i.e., year when the tree reached coring height) if the core fails to hit center or if the tree's center is lost to heartrot. “Species with low density of record start years within the plotted time-frame established primarily prior to 1850.”

Figure S10. Density plot of core record start years by species for Scotty Creek (Northwest Territory, Canada).

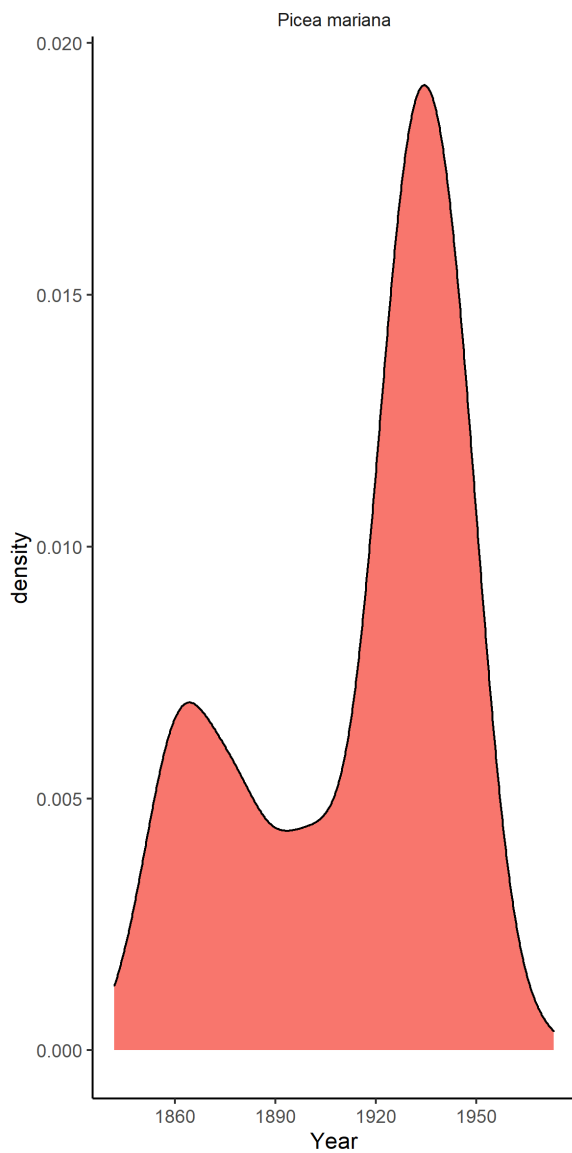
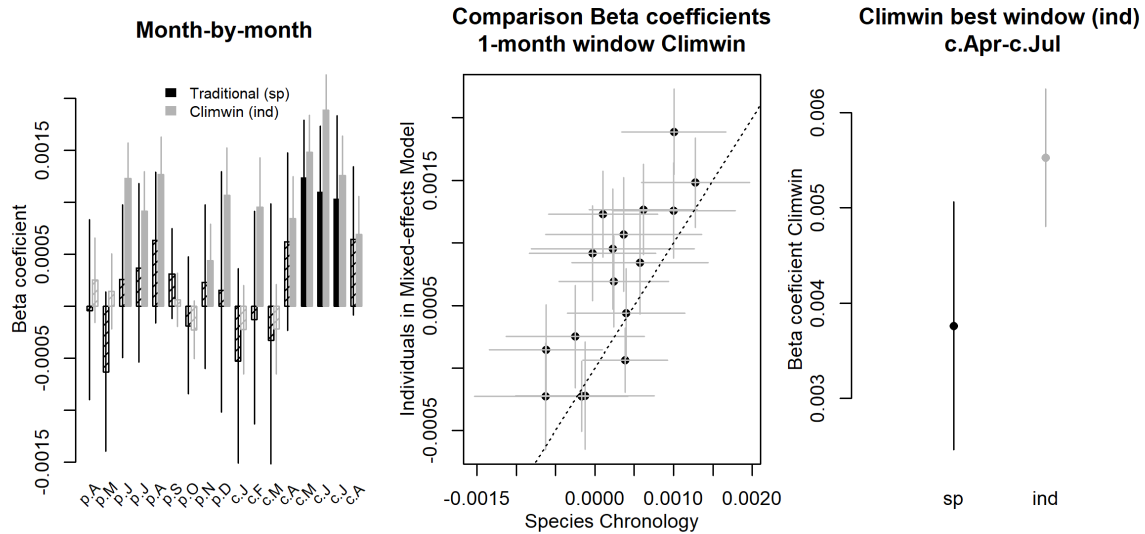


Figure S10. Density plot of core record start years for Scotty Creek (Northwest Territory, Canada). This distribution approximates—but does not entirely match—the age distribution of trees cored. The core record start year can occur after a tree's recruitment year (i.e., year when the tree reached coring height) if the core fails to hit center or if the tree's center is lost to heartrot.

Figure S11. Comparison of our approach with traditional methods of identifying climate signals: LITU at SCBI.

Precipitation



Potential Evapotranspiration

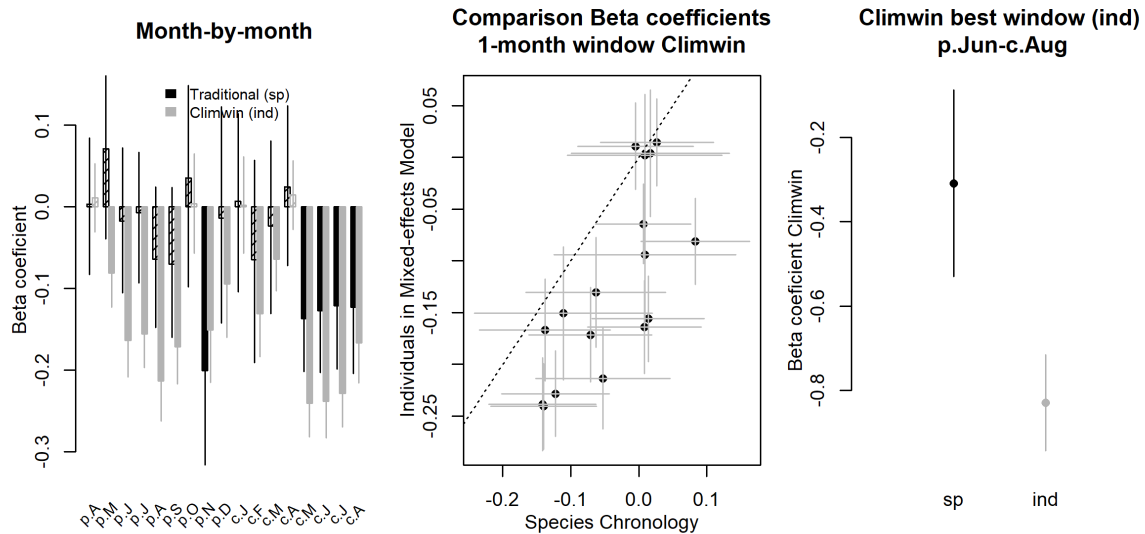
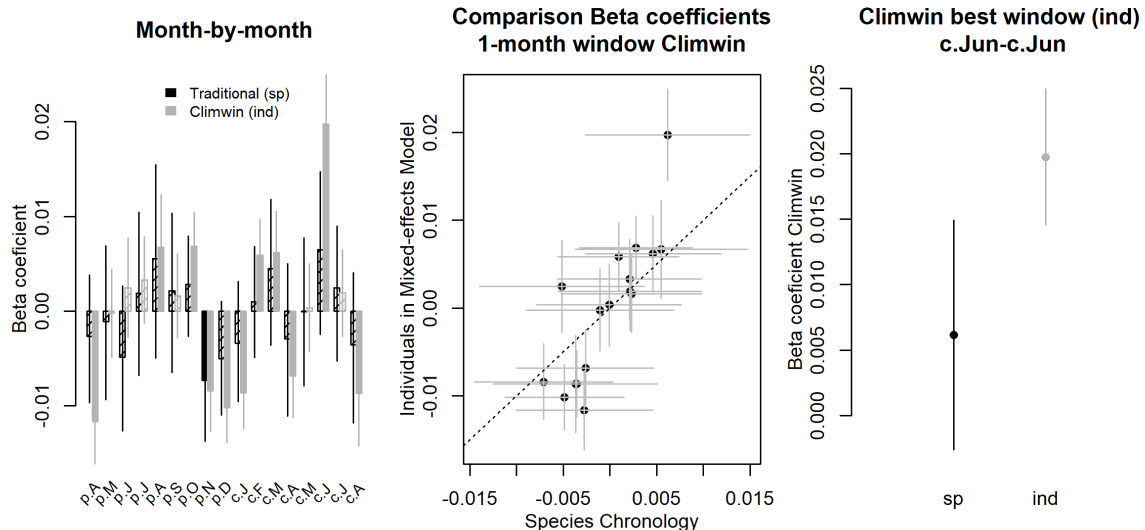


Figure S11. Comparison of our approach with traditional methods of identifying climate signals: LITU at SCBI. Shown are responses to the precipitation- and temperature-group variables selected as most influential by the *climwin* analysis. Left panels show a month-by-month comparison of *beta* (slope) coefficients for the relationship between tree growth and the monthly climate variable from species-level residual chronologies (traditional approach) and from individual-level analysis in *climwin* (approach presented here). Center panels compare the monthly *beta* coefficient estimates, with the dotted line indicating 1:1 correspondence. Finally, the right panels compare *beta* coefficients for the optimal window selected by *climwin*. Error bars indicate standard error of slope estimates. Note that 1:1 correspondence is not necessarily expected. See Appendix 5 for analysis methods and discussion of expected correspondence.

Figure S12. Comparison of our approach with traditional methods of identifying climate signals: ABAL at Zofin.

Precipitation Day Frequency



Maximum temperature

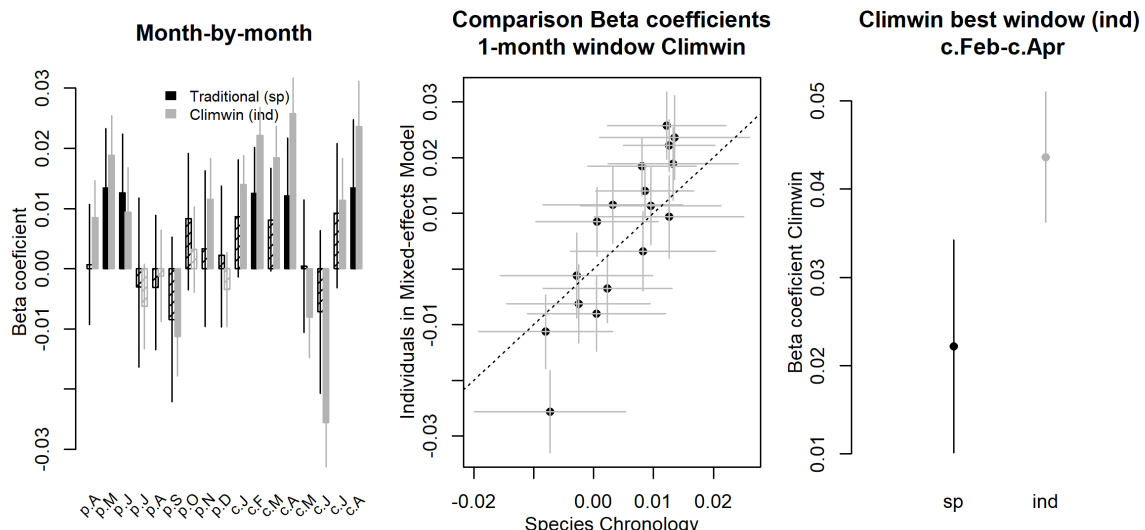
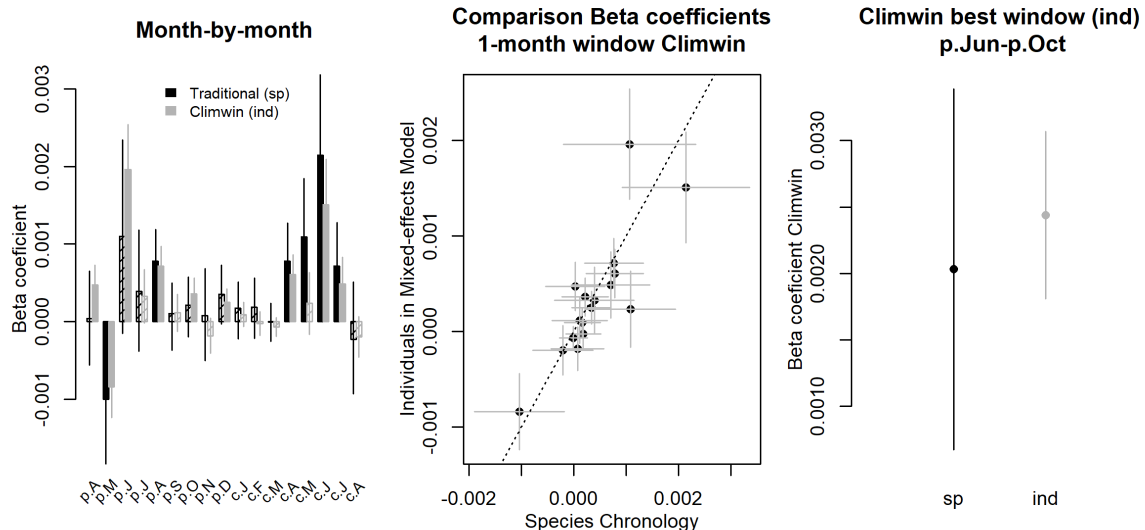


Figure S12. Comparison of our approach with traditional methods of identifying climate signals: ABAL at Zofin. Shown are responses to the precipitation- and temperature-group variables selected as most influential by the *climwin* analysis. Left panels show a month-by-month comparison of *beta* (slope) coefficients for the relationship between tree growth and the monthly climate variable from species-level residual chronologies (traditional approach) and from individual-level analysis in *climwin* (approach presented here). Center panels compare the monthly *beta* coefficient estimates, with the dotted line indicating 1:1 correspondence. Finally, the right panels compare *beta* coefficients for the optimal window selected by *climwin*. Error bars indicate standard error of slope estimates. Note that 1:1 correspondence is not necessarily expected. See Appendix 5 for analysis methods and discussion of expected correspondence.

Figure S13. Comparison of our approach with traditional methods of identifying climate signals: PSME at Cedar Breaks.

Precipitation



Maximum temperature

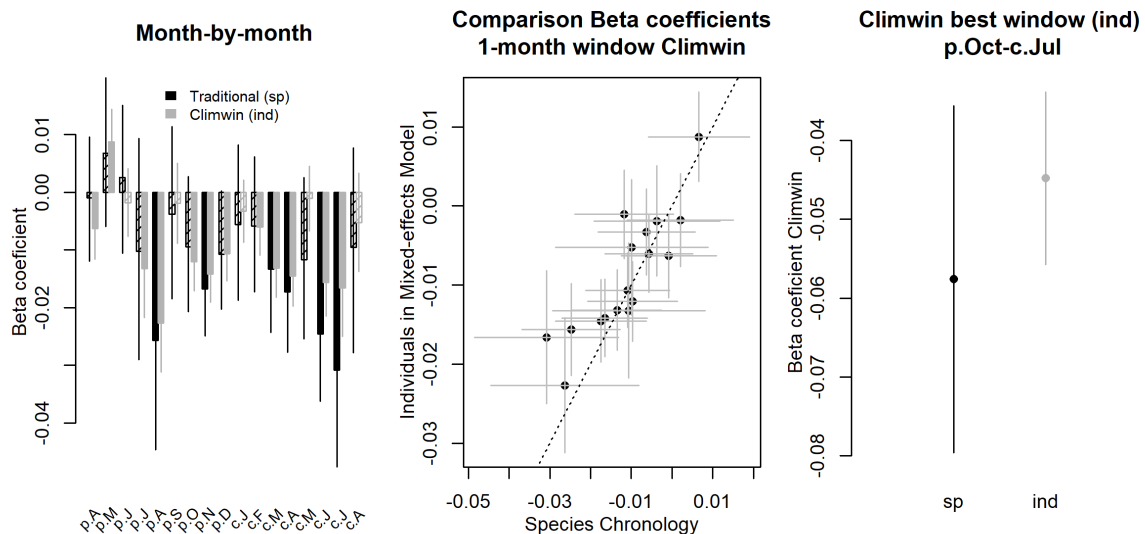
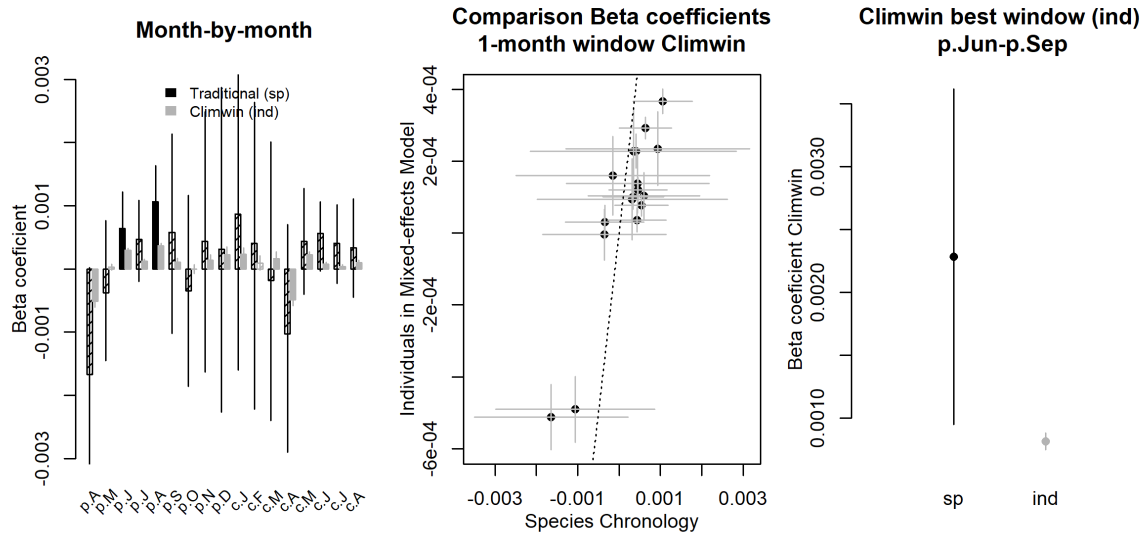


Figure S13. Comparison of our approach with traditional methods of identifying climate signals: PSME at Cedar Breaks. Shown are responses to the precipitation- and temperature-group variables selected as most influential by the *climwin* analysis. Left panels show a month-by-month comparison of *beta* (slope) coefficients for the relationship between tree growth and the monthly climate variable from species-level residual chronologies (traditional approach) and from individual-level analysis in *climwin* (approach presented here). Center panels compare the monthly *beta* coefficient estimates, with the dotted line indicating 1:1 correspondence. Finally, the right panels compare *beta* coefficients for the optimal window selected by *climwin*. Error bars indicate standard error of slope estimates. Note that 1:1 correspondence is not necessarily expected. See Appendix 5 for analysis methods and discussion of expected correspondence.

Figure S14. Comparison of our approach with traditional methods of identifying climate signals: PIMA at Scotty Creek.

Precipitation



Maximum temperature

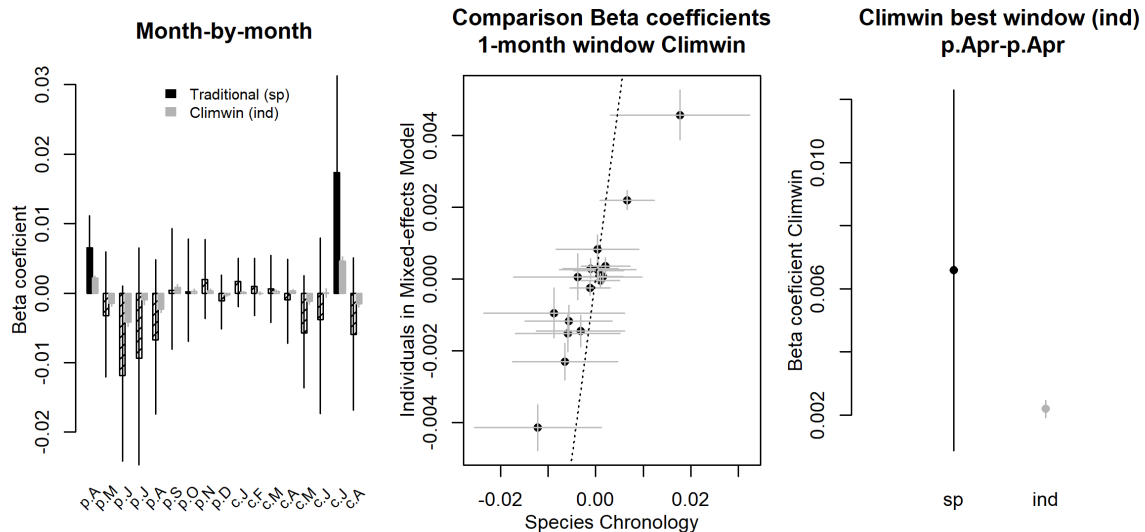


Figure S14. Comparison of our approach with traditional methods of identifying climate signals: PIMA at Scotty Creek. Shown are responses to the precipitation- and temperature-group variables selected as most influential by the *climwin* analysis. Left panels show a month-by-month comparison of *beta* (slope) coefficients for the relationship between tree growth and the monthly climate variable from species-level residual chronologies (traditional approach) and from individual-level analysis in *climwin* (approach presented here). Center panels compare the monthly *beta* coefficient estimates, with the dotted line indicating 1:1 correspondence. Finally, the right panels compare *beta* coefficients for the optimal window selected by *climwin*. Error bars indicate standard error of slope estimates. Note that 1:1 correspondence is not necessarily expected. See Appendix 5 for analysis methods and discussion of expected correspondence.

Figure S15. (PRE at SCBI)

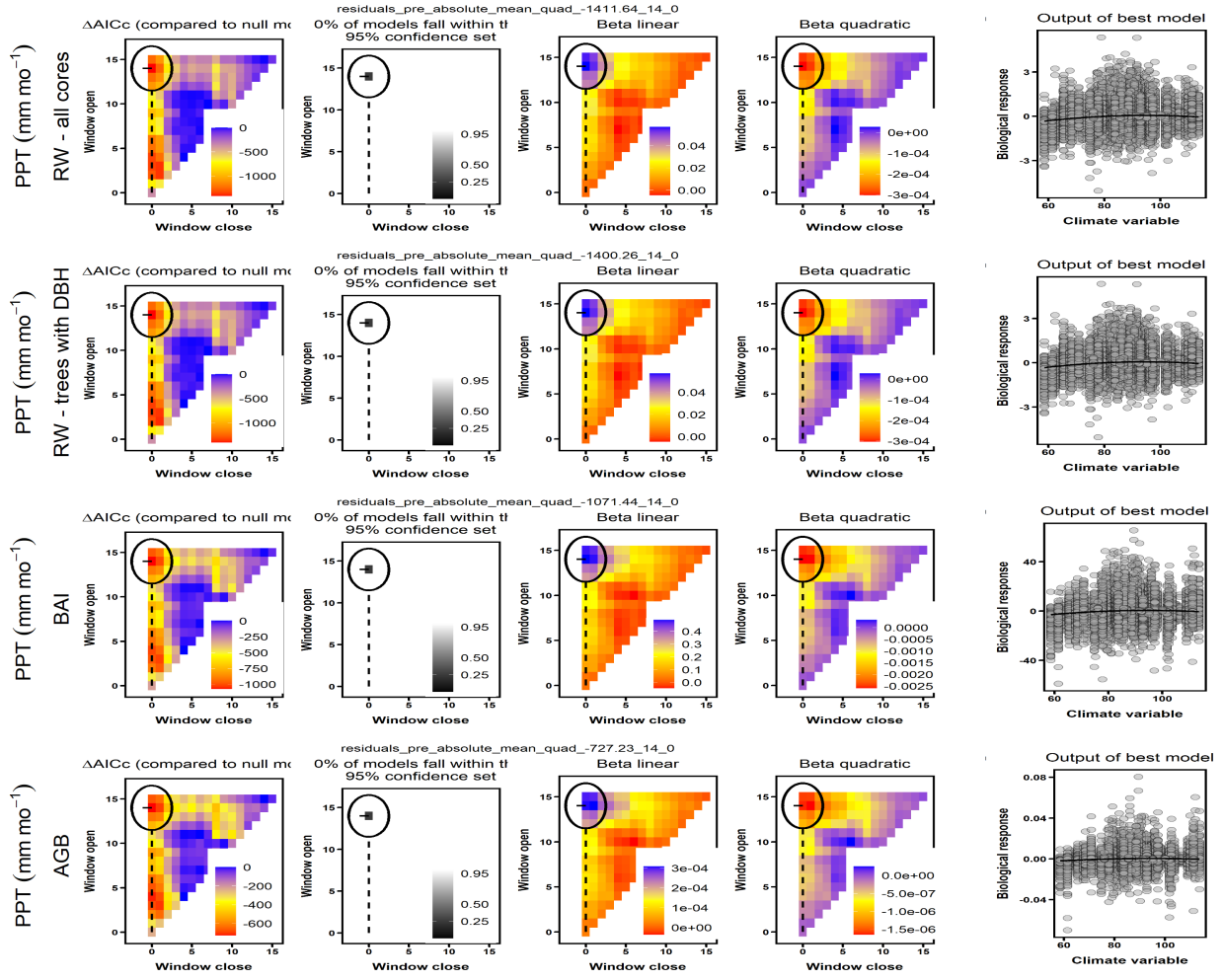


Figure S15. (PRE at SCBI) Here, *climwin* identified **GIVE WINDOW** precipitation (*PPT*) as the strongest climate variable across all four analyses (*RW* with and without trees for which *DBH* could not be reconstructed, *BAI*, ΔAGB).

Figure S16. (PET at SCBI)

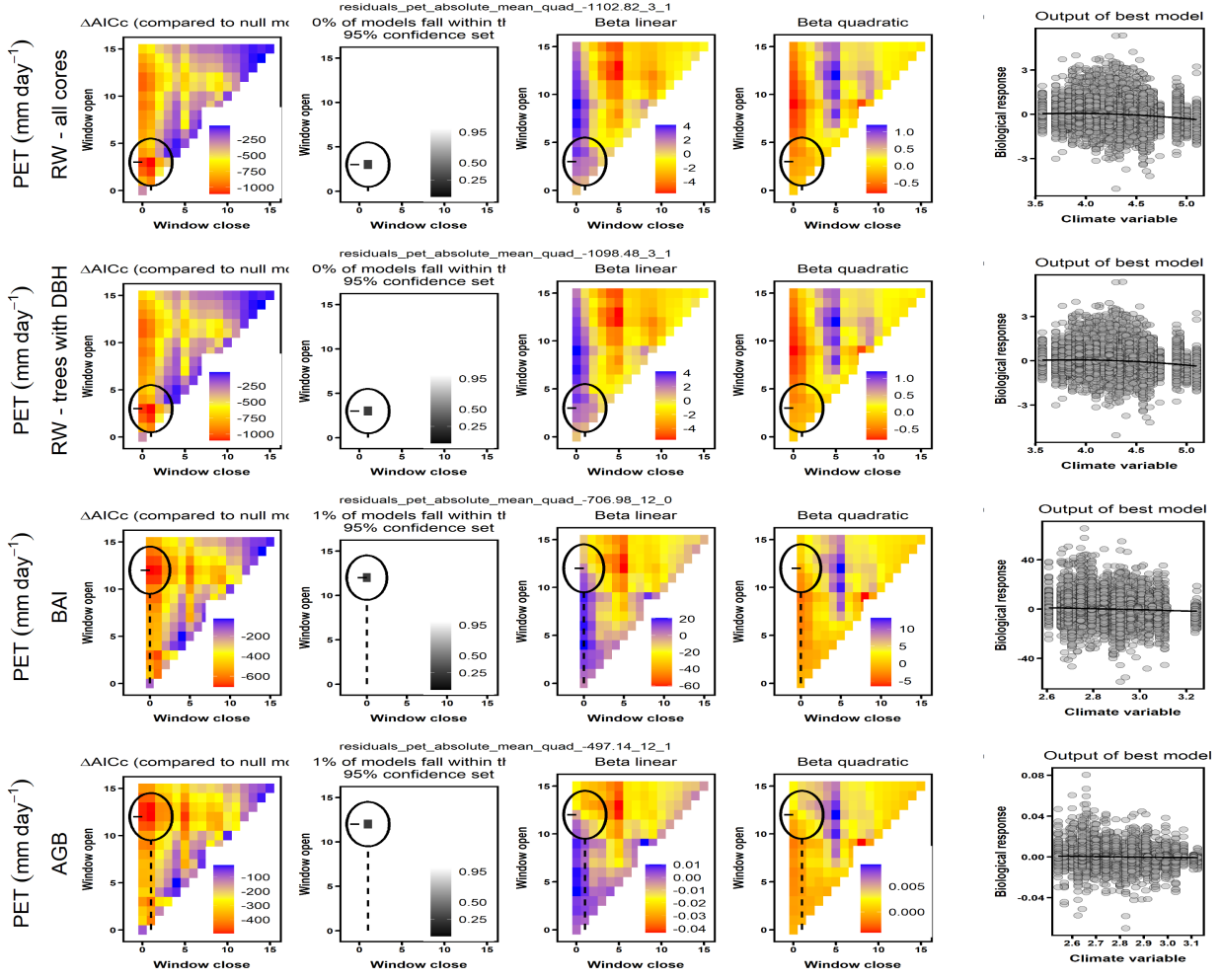


Figure S16. (PET at SCBI) Here, *climwin* identified potential evapotranspiration (*PET*) as the strongest climate variable across all four analyses (*RW* with and without trees for which *DBH* could not be reconstructed, *BAI*, ΔAGB), but a different window (**GIVE WINDOW**) was chosen for *BAI* and ΔAGB than for *RW* (**GIVE WINDOW**).

Figure S17. (TMX/TMP at HKK)

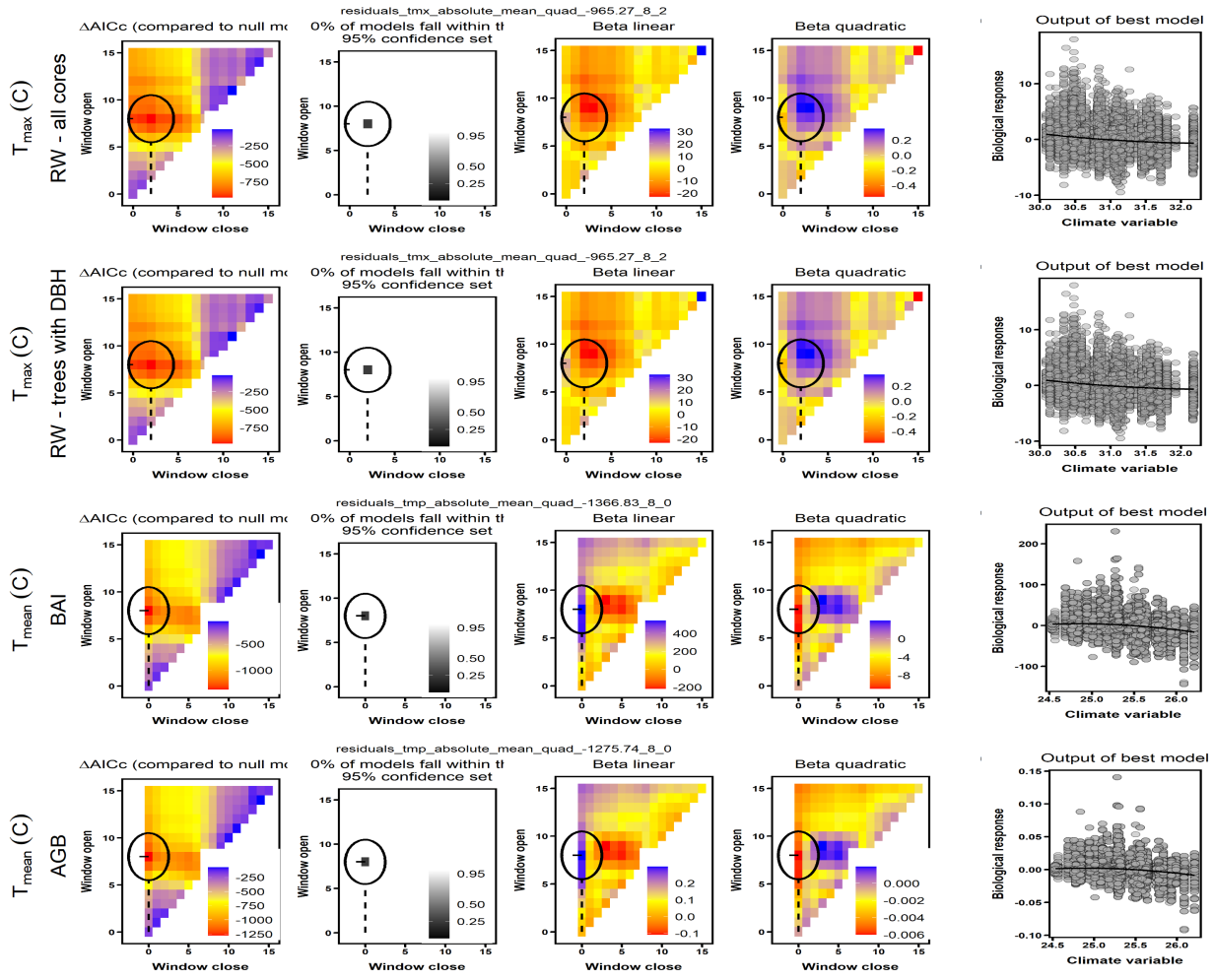


Figure S17. (TMX/TMP at HKK) Here....

Figure S18. Best GLS models including climate and DBH for Barro Colorado Nature Monument (Panama)

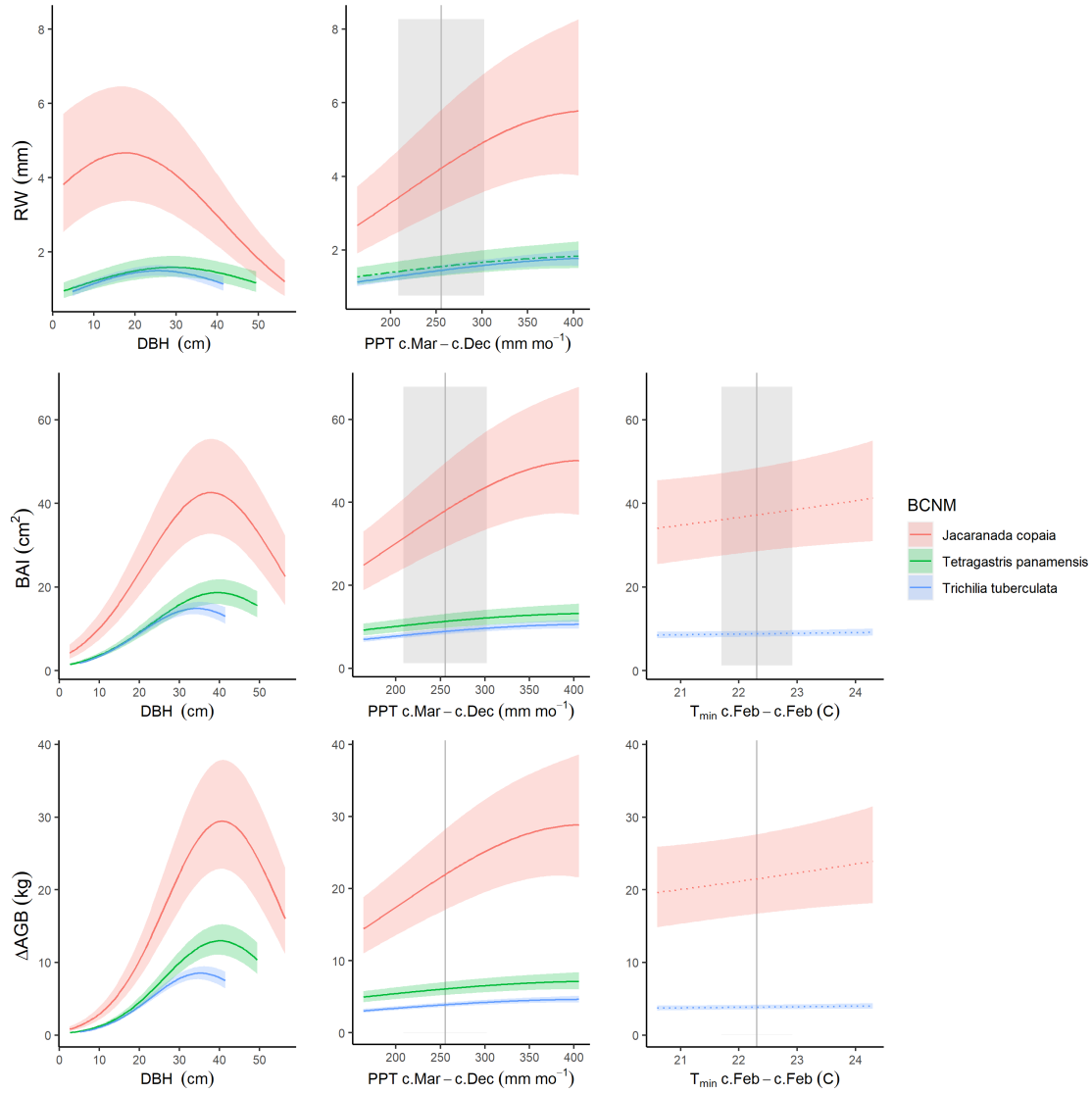


Figure S18. Best GLS models including climate and DBH for Barro Colorado Nature Monument (Panama) for all three growth metrics examined here. Precipitation and temperature group variables are as selected by *climwin* (p=previous year, c=current year). For each species, relationships are plotted if included in top model, with best-fit polynomials plotted with solid lines when both first- and second-order terms are significant, dashed lines when only one term is significant, and dotted lines when neither is significant. Transparent ribbons indicate 95% confidence intervals. Vertical grey lines indicate the long-term mean for the climate variable, shading indicates 1 SD.

Figure S19. Best GLS models including climate, DBH, and year for Barro Colorado Nature Monument (Panama)

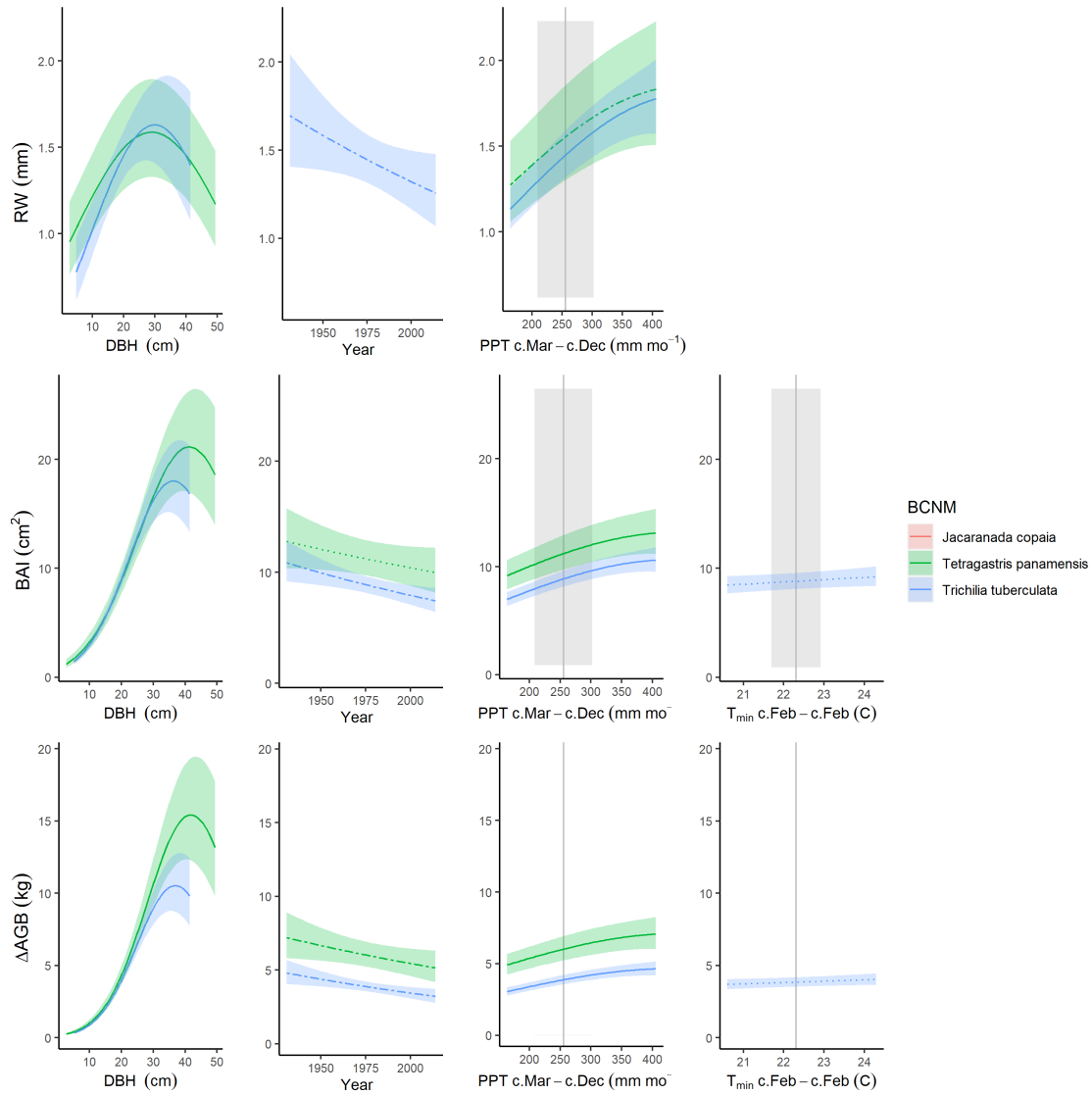


Figure S19. Best GLS models including climate, DBH, and year for Barro Colorado Nature Monument (Panama) for all three growth metrics examined here. Precipitation and temperature group variables are as selected by *climwin* ($p=p$ revious year, $c=c$ urrent year). For each species, relationships are plotted if included in top model, with best-fit polynomials plotted with solid lines when both first- and second-order terms are significant, dashed lines when only one term is significant, and dotted lines when neither is significant. Transparent ribbons indicate 95% confidence intervals. Vertical grey lines indicate the long-term mean for the climate variable, shading indicates 1 SD.

Figure S20. Best GLS models including climate and DBH for Huai Kha Khaeng (Thailand)

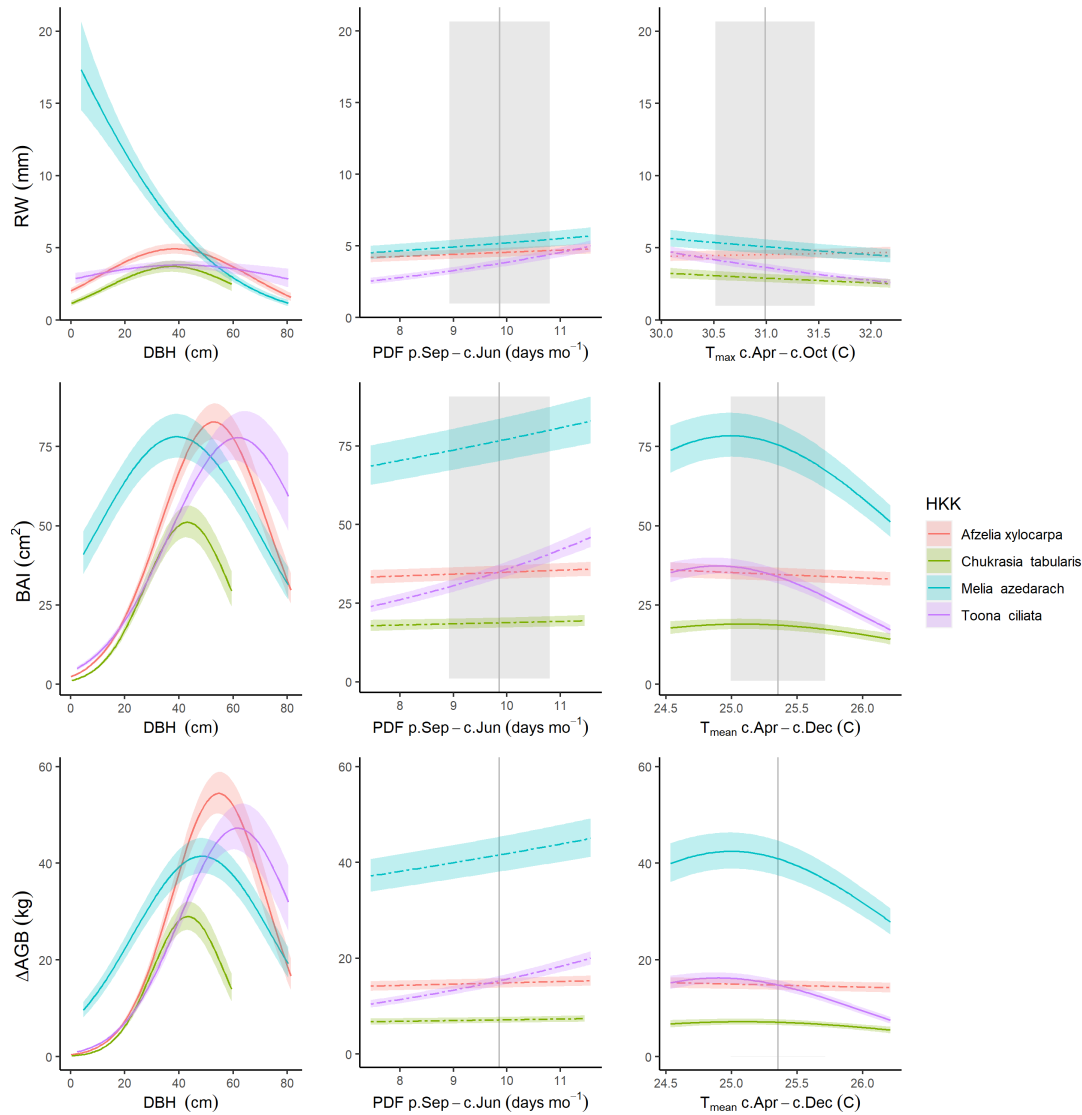


Figure S20. Best GLS models including climate and DBH for Huai Kha Khaeng (Thailand) for all three growth metrics examined here. Precipitation and temperature group variables are as selected by *climwin* (*p*=previous year, *c*=current year). For each species, relationships are plotted if included in top model, with best-fit polynomials plotted with solid lines when both first- and second-order terms are significant, dashed lines when only one term is significant, and dotted lines when neither is significant. Transparent ribbons indicate 95% confidence intervals. Vertical grey lines indicate the long-term mean for the climate variable, shading indicates 1 SD.

Figure S21. Best GLS models including climate, DBH, and year for Huai Kha Khaeng (Thailand)

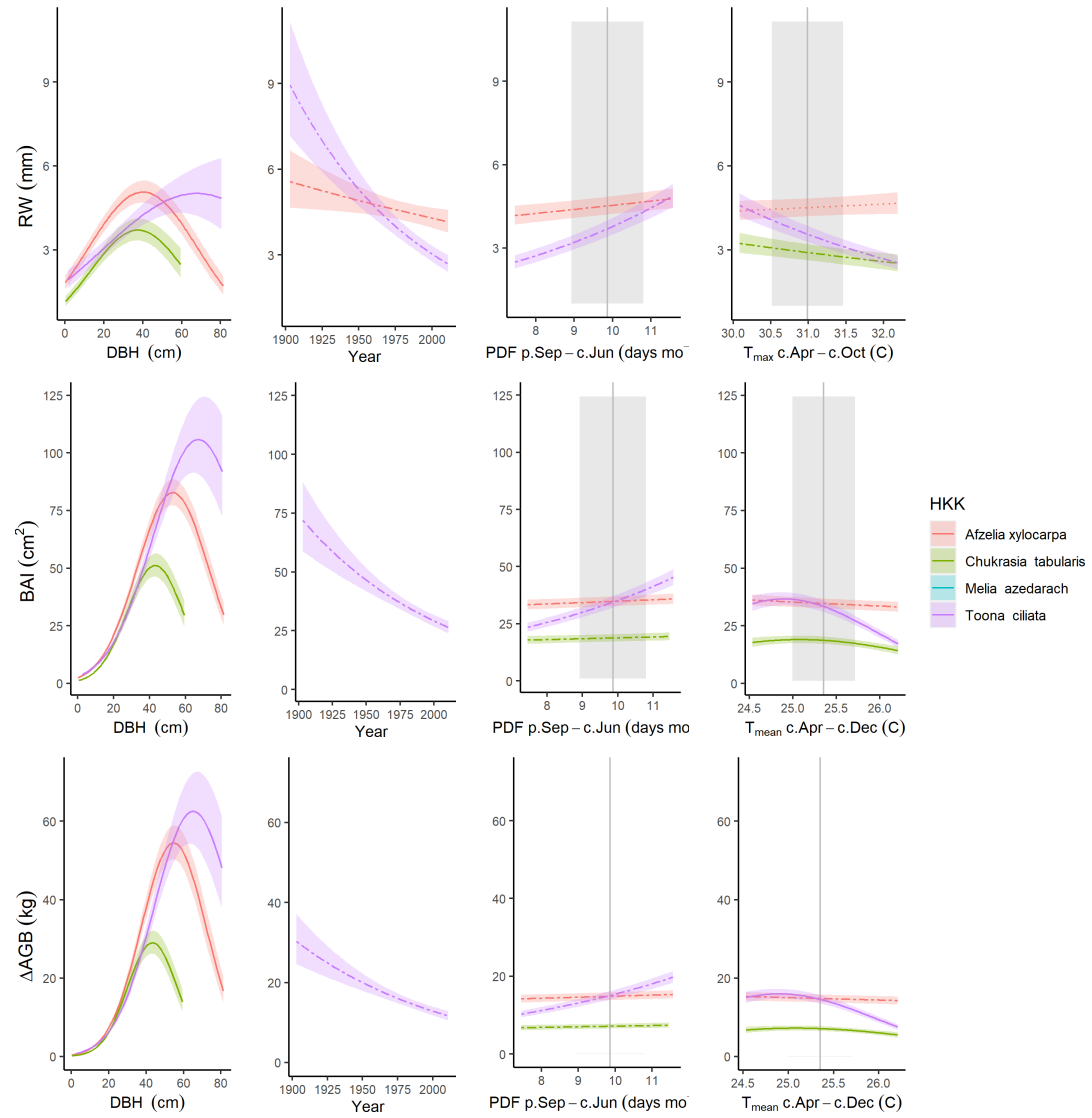


Figure S21. Best GLS models including climate, DBH, and year for Huai Kha Khaeng (Thailand) for all three growth metrics examined here. Precipitation and temperature group variables are as selected by *climwin* (p=previous year, c=current year). For each species, relationships are plotted if included in top model, with best-fit polynomials plotted with solid lines when both first- and second-order terms are significant, dashed lines when only one term is significant, and dotted lines when neither is significant. Transparent ribbons indicate 95% confidence intervals. Vertical grey lines indicate the long-term mean for the climate variable, shading indicates 1 SD.

Figure S22. Best GLS models including climate and DBH for the Smithsonian Conservation Biology Institute (Virginia, USA)

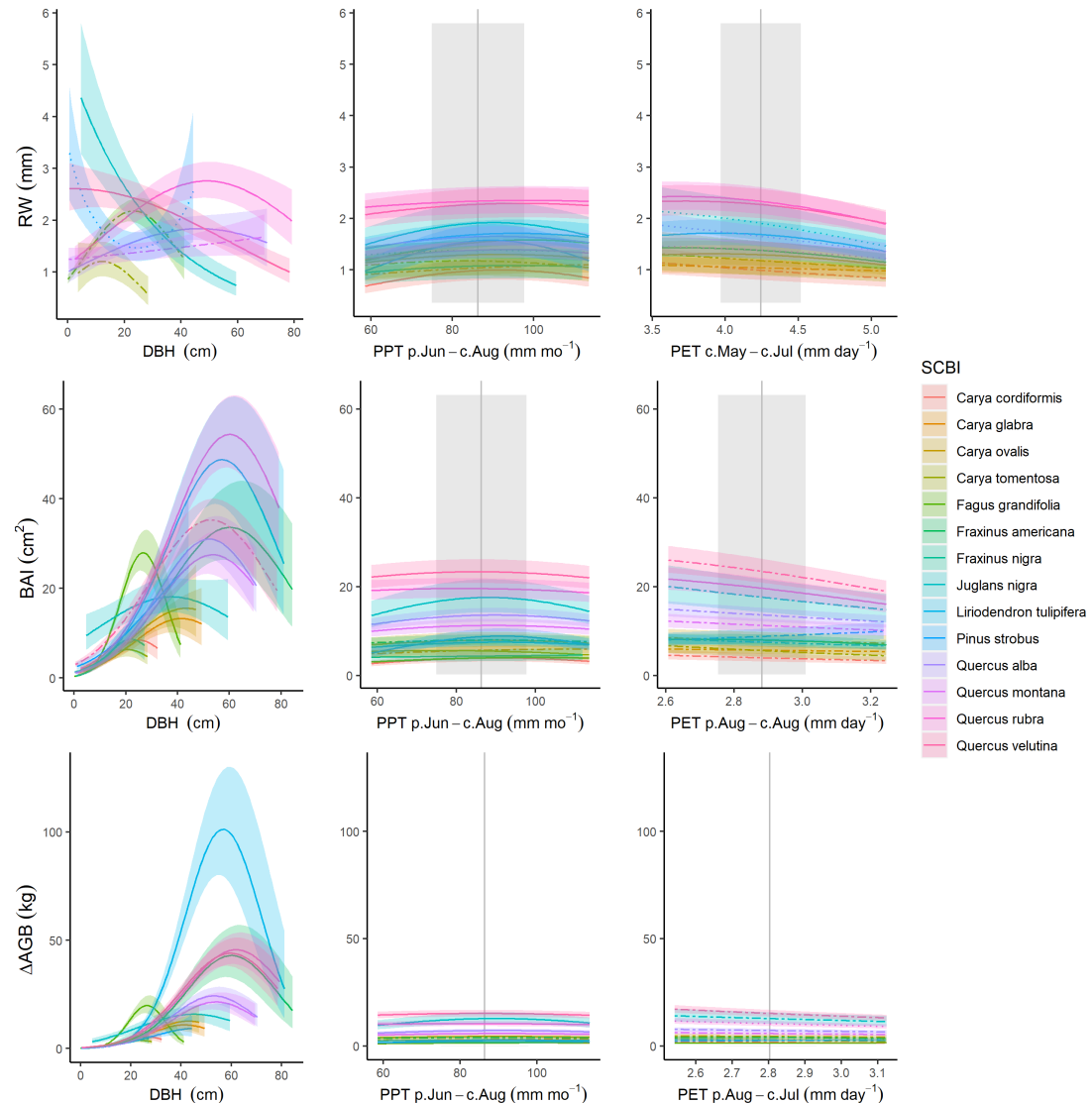


Figure S22. Best GLS models including climate and DBH for the Smithsonian Conservation Biology Institute (Virginia, USA) for all three growth metrics examined here. Precipitation and temperature group variables are as selected by *climwin* (p=previous year, c=current year). For each species, relationships are plotted if included in top model, with best-fit polynomials plotted with solid lines when both first- and second-order terms are significant, dashed lines when only one term is significant, and dotted lines when neither is significant. Transparent ribbons indicate 95% confidence intervals. Vertical grey lines indicate the long-term mean for the climate variable, shading indicates 1 SD.

Figure S23. Best GLS models including climate, DBH, and year for the Smithsonian Conservation Biology Institute (Virginia, USA)

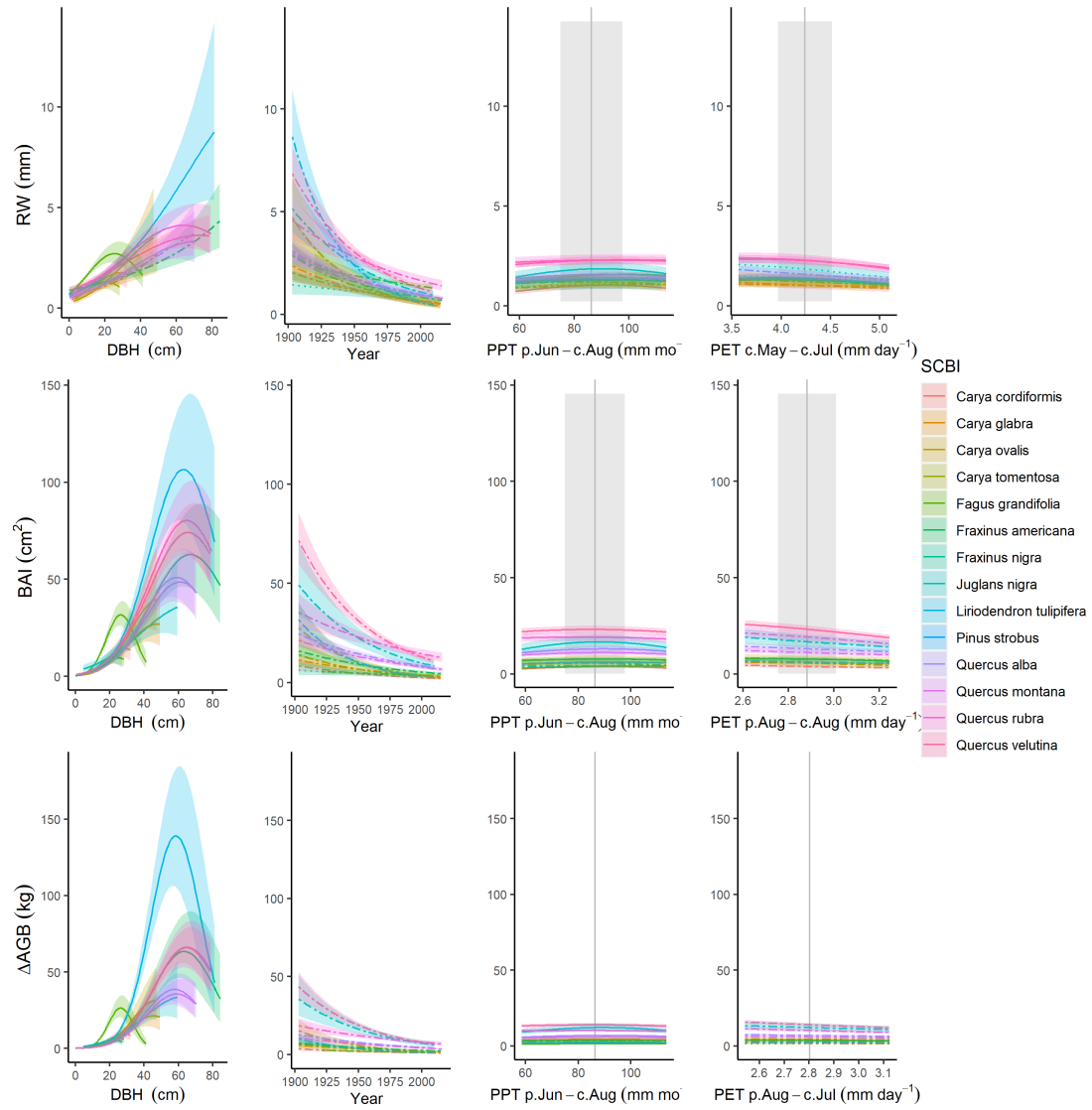


Figure S23. Best GLS models including climate, DBH, and year for the Smithsonian Conservation Biology Institute (Virginia, USA) for all three growth metrics examined here. Precipitation and temperature group variables are as selected by *climwin* (*p*=previous year, *c*=current year). For each species, relationships are plotted if included in top model, with best-fit polynomials plotted with solid lines when both first- and second-order terms are significant, dashed lines when only one term is significant, and dotted lines when neither is significant. Transparent ribbons indicate 95% confidence intervals. Vertical grey lines indicate the long-term mean for the climate variable, shading indicates 1 SD.

Figure S24. Best GLS models including climate and DBH for Lilley Dickey Woods (Indiana, USA)

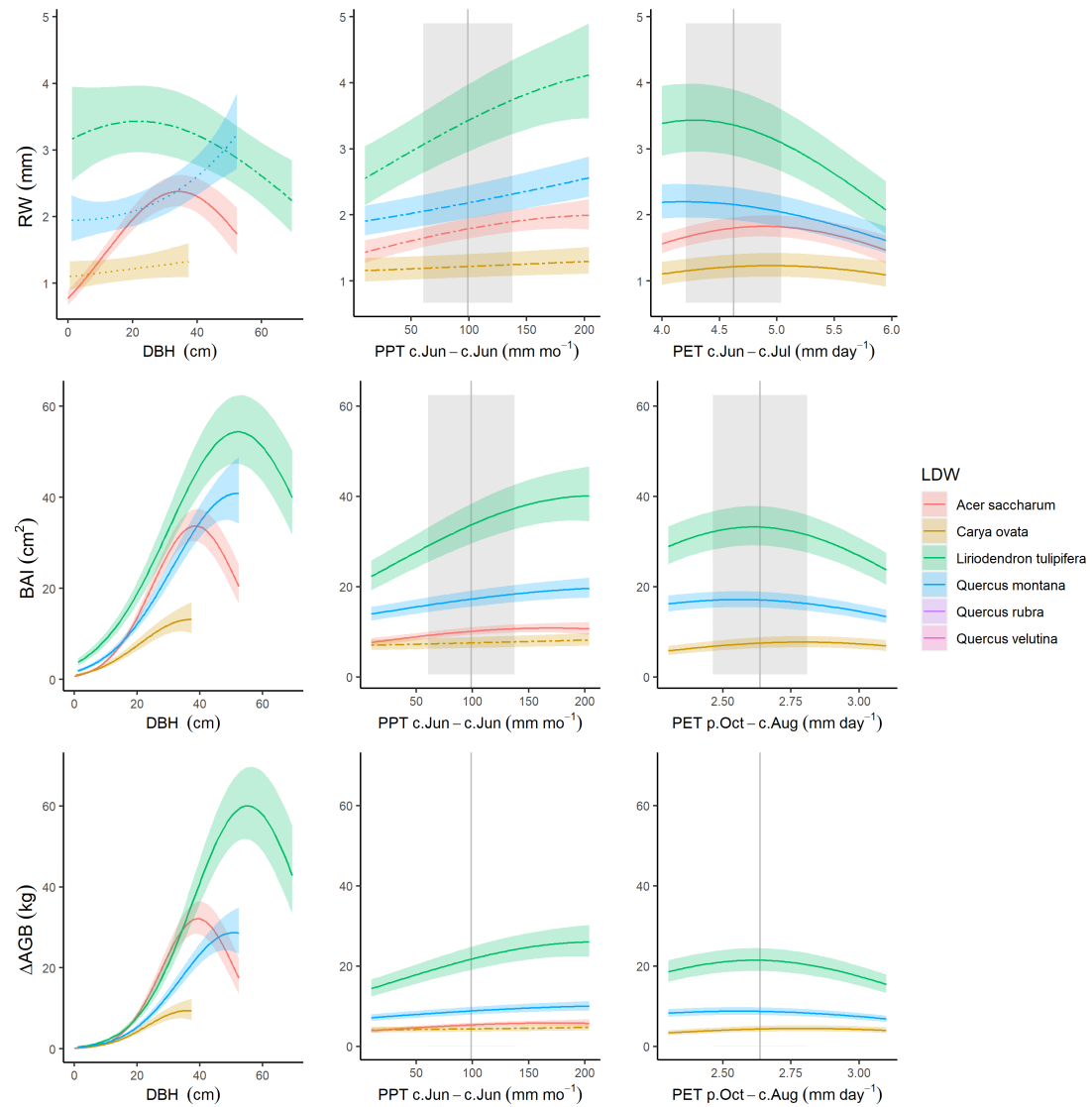


Figure S24. Best GLS models including climate and DBH for Lilley Dickey Woods (Indiana, USA) for all three growth metrics examined here. Precipitation and temperature group variables are as selected by *climwin* (*p*=previous year, *c*=current year). For each species, relationships are plotted if included in top model, with best-fit polynomials plotted with solid lines when both first- and second-order terms are significant, dashed lines when only one term is significant, and dotted lines when neither is significant. Transparent ribbons indicate 95% confidence intervals. Vertical grey lines indicate the long-term mean for the climate variable, shading indicates 1 SD.

Figure S25. Best GLS models including climate, DBH, and year for Lilley Dickey Woods (Indiana, USA)

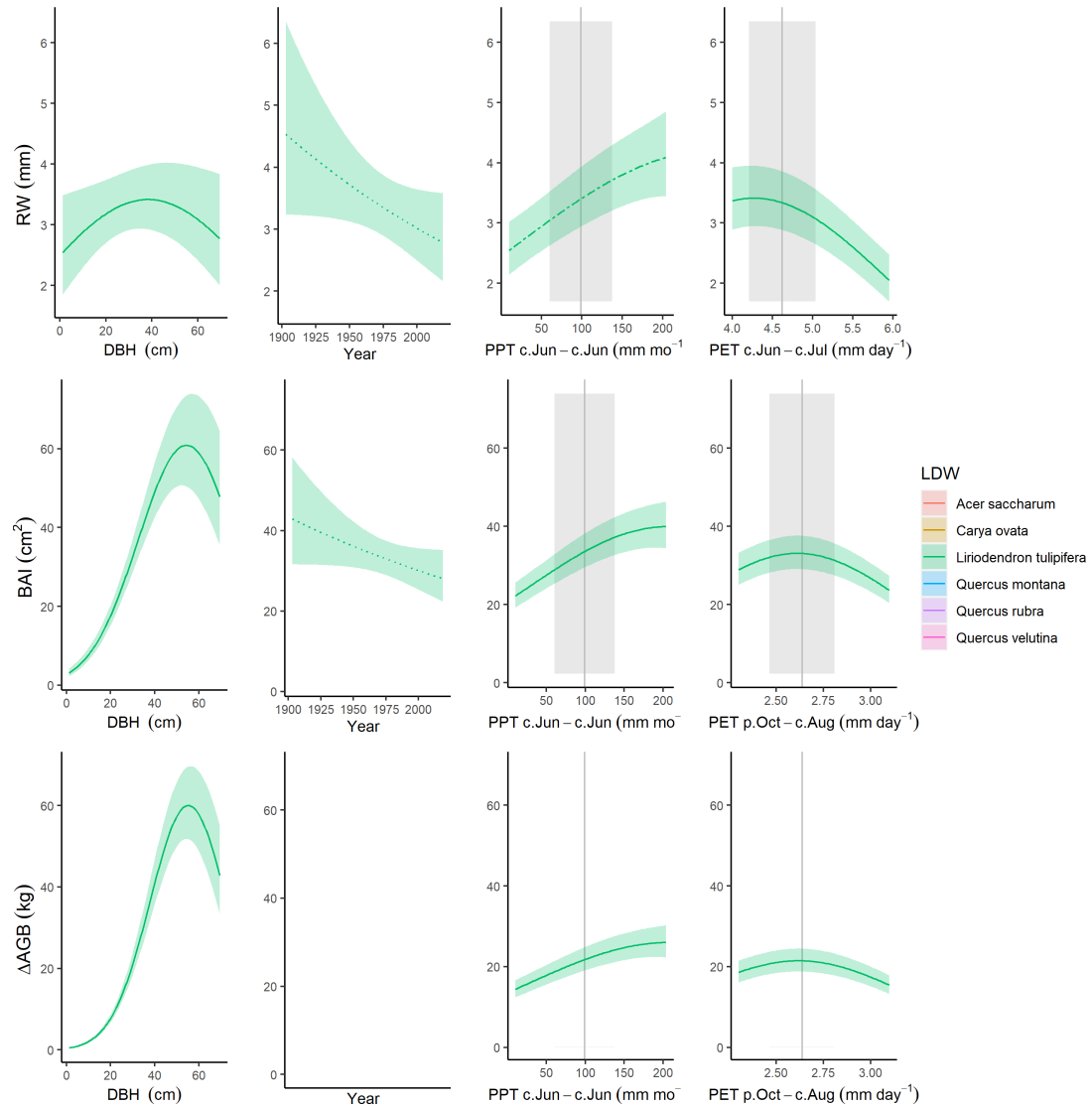


Figure S25. Best GLS models including climate, DBH, and year for Lilley Dickey Woods (Indiana, USA) for all three growth metrics examined here. Precipitation and temperature group variables are as selected by *climwin* (p=previous year, c=current year). For each species, relationships are plotted if included in top model, with best-fit polynomials plotted with solid lines when both first- and second-order terms are significant, dashed lines when only one term is significant, and dotted lines when neither is significant. Transparent ribbons indicate 95% confidence intervals. Vertical grey lines indicate the long-term mean for the climate variable, shading indicates 1 SD.

Figure S26. Best GLS models including climate and DBH for Harvard Forest (Massachusetts, USA)

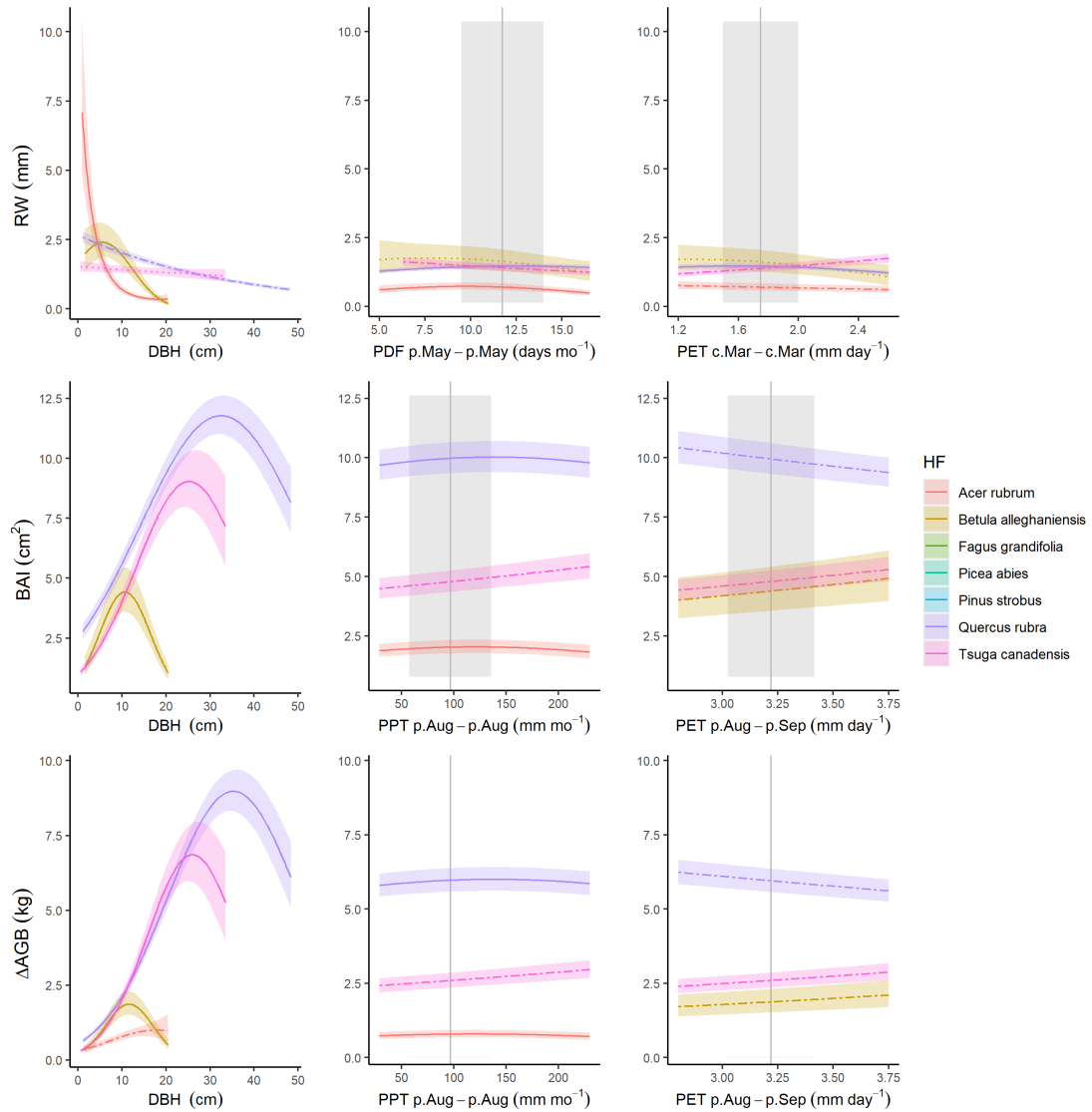


Figure S26. Best GLS models including climate and DBH for Harvard Forest (Massachusetts, USA) for all three growth metrics examined here. Precipitation and temperature group variables are as selected by *climwin* (p=previous year, c=current year). For each species, relationships are plotted if included in top model, with best-fit polynomials plotted with solid lines when both first- and second-order terms are significant, dashed lines when only one term is significant, and dotted lines when neither is significant. Transparent ribbons indicate 95% confidence intervals. Vertical grey lines indicate the long-term mean for the climate variable, shading indicates 1 SD.

Figure S27. Best GLS models including climate, DBH, and year for Harvard Forest (Massachusetts, USA)

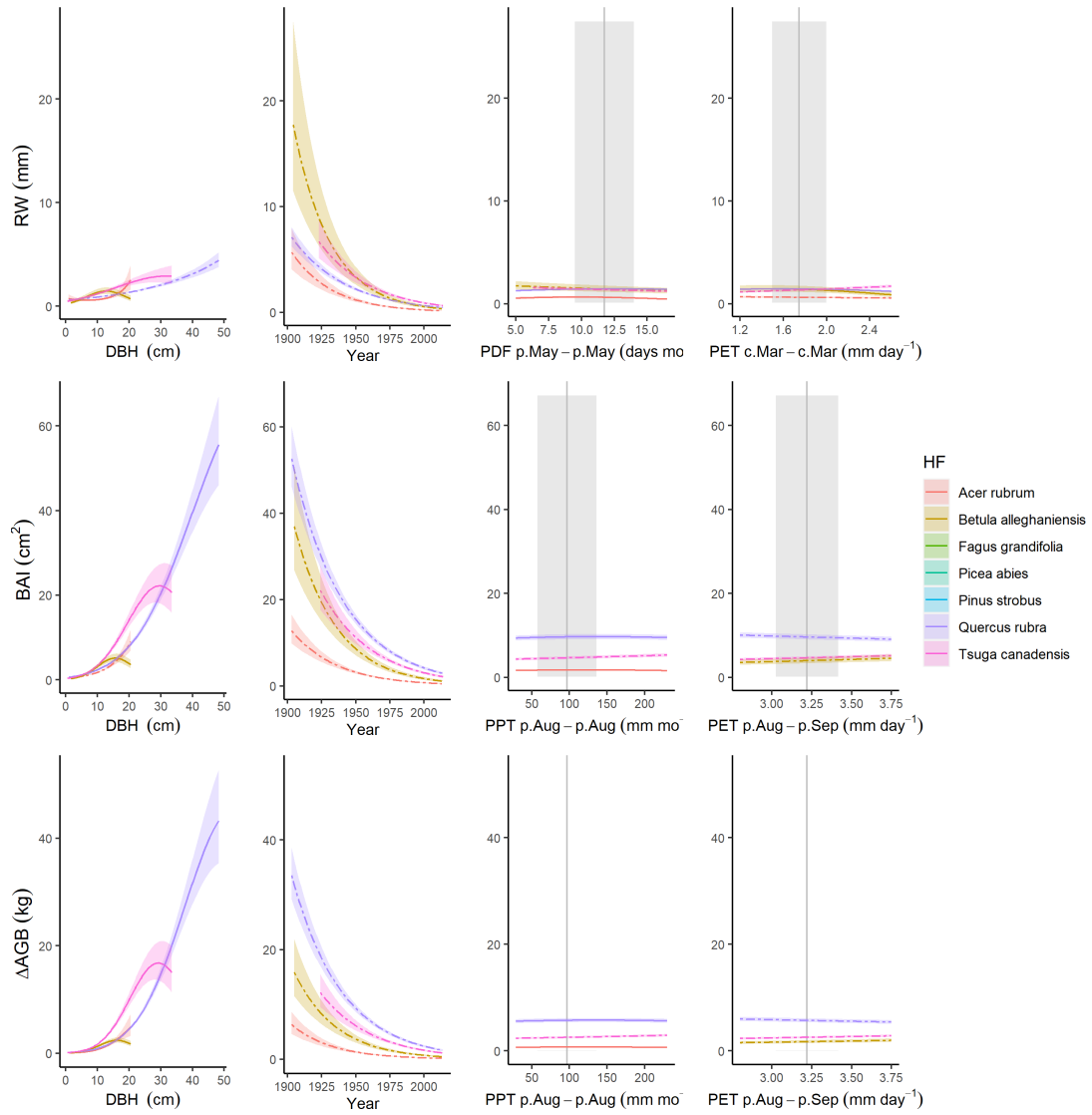


Figure S27. Best GLS models including climate, DBH, and year for Harvard Forest (Massachusetts, USA) for all three growth metrics examined here. Precipitation and temperature group variables are as selected by *climwin* (p=previous year, c=current year). For each species, relationships are plotted if included in top model, with best-fit polynomials plotted with solid lines when both first- and second-order terms are significant, dashed lines when only one term is significant, and dotted lines when neither is significant. Transparent ribbons indicate 95% confidence intervals. Vertical grey lines indicate the long-term mean for the climate variable, shading indicates 1 SD.

Figure S28. Best GLS models including climate and DBH for Zofin Forest (Czech Republic)

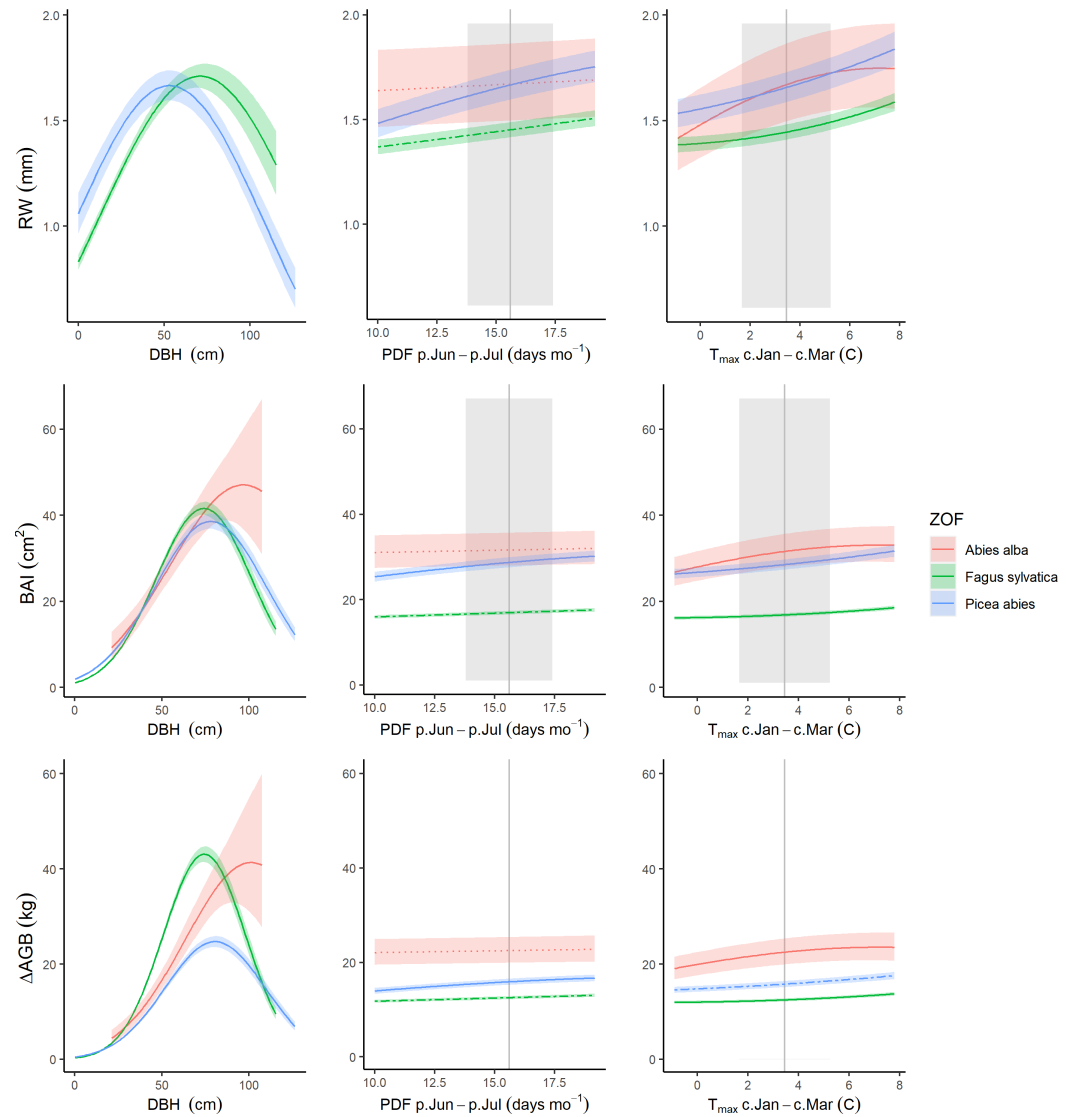


Figure S28. Best GLS models including climate and DBH for Zofin Forest (Czech Republic) for all three growth metrics examined here. Precipitation and temperature group variables are as selected by *climwin* (*p*=previous year, *c*=current year). For each species, relationships are plotted if included in top model, with best-fit polynomials plotted with solid lines when both first- and second-order terms are significant, dashed lines when only one term is significant, and dotted lines when neither is significant. Transparent ribbons indicate 95% confidence intervals. Vertical grey lines indicate the long-term mean for the climate variable, shading indicates 1 SD.

Figure S29. Best GLS models including climate, DBH, and year for Zofin Forest (Czech Republic)

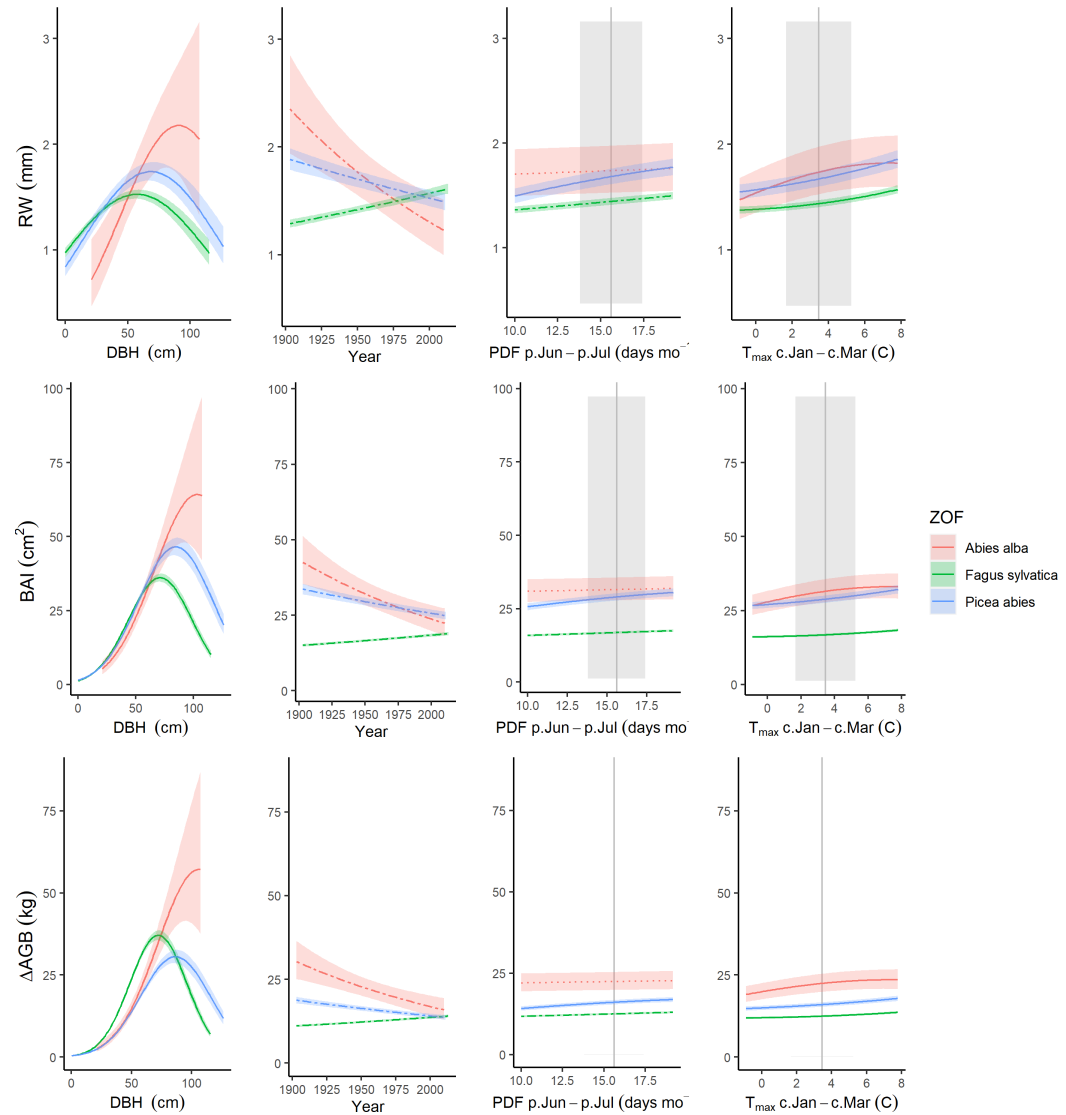


Figure S29. Best GLS models including climate, DBH, and year for Zofin Forest (Czech Republic) for all three growth metrics examined here. Precipitation and temperature group variables are as selected by *climwin* (p=previous year, c=current year). For each species, relationships are plotted if included in top model, with best-fit polynomials plotted with solid lines when both first- and second-order terms are significant, dashed lines when only one term is significant, and dotted lines when neither is significant. Transparent ribbons indicate 95% confidence intervals. Vertical grey lines indicate the long-term mean for the climate variable, shading indicates 1 SD.

Figure S30. Best GLS models including climate and DBH for Niobrara (Nebraska, USA)

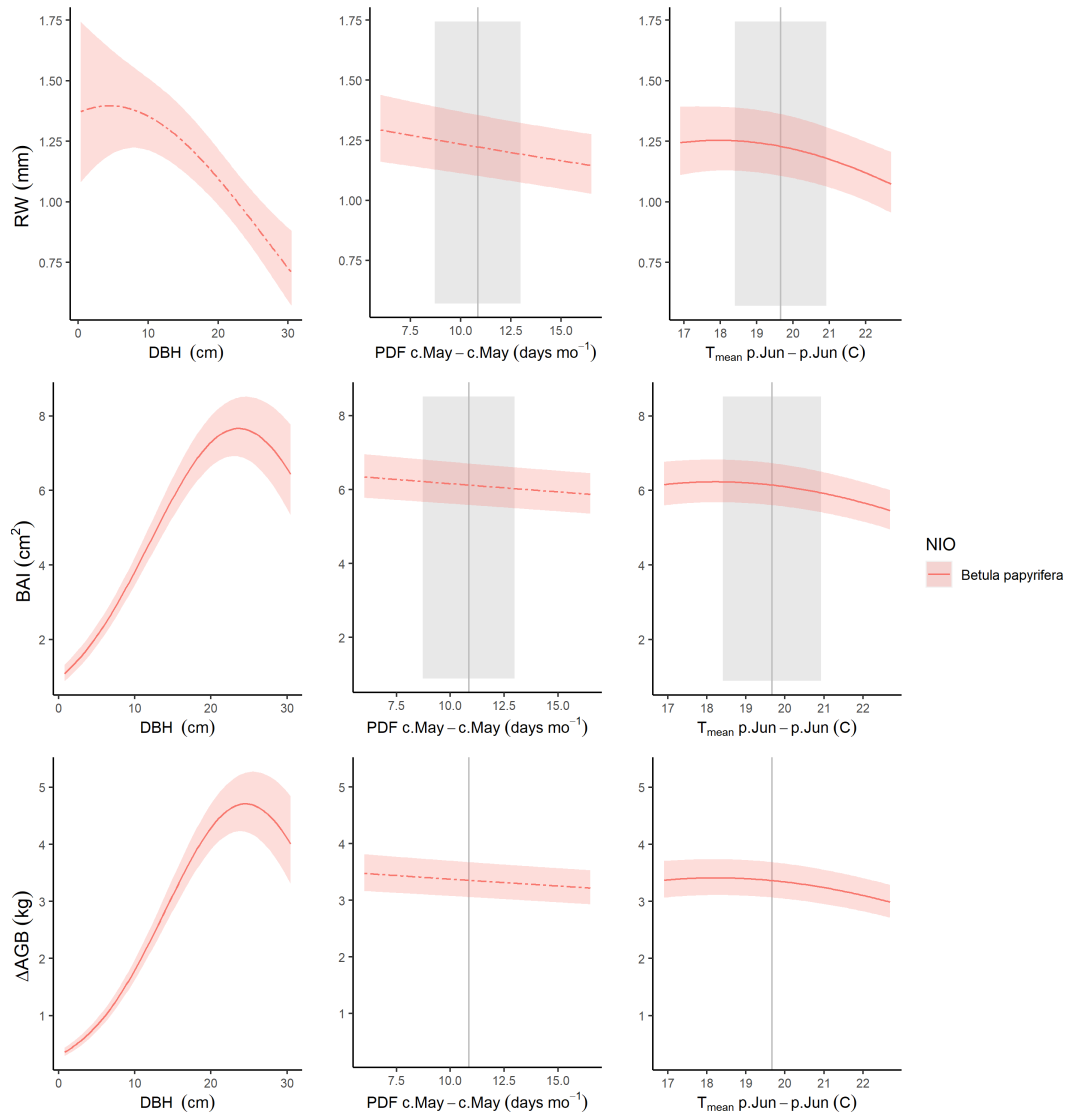


Figure S30. Best GLS models including climate and DBH for Niobrara (Nebraska, USA) for all three growth metrics examined here. Precipitation and temperature group variables are as selected by *climwin* (p=previous year, c=current year). For each species, relationships are plotted if included in top model, with best-fit polynomials plotted with solid lines when both first- and second-order terms are significant, dashed lines when only one term is significant, and dotted lines when neither is significant. Transparent ribbons indicate 95% confidence intervals. Vertical grey lines indicate the long-term mean for the climate variable, shading indicates 1 SD.

Figure S31. Best GLS models including climate, DBH, and year for Niobrara (Nebraska, USA)

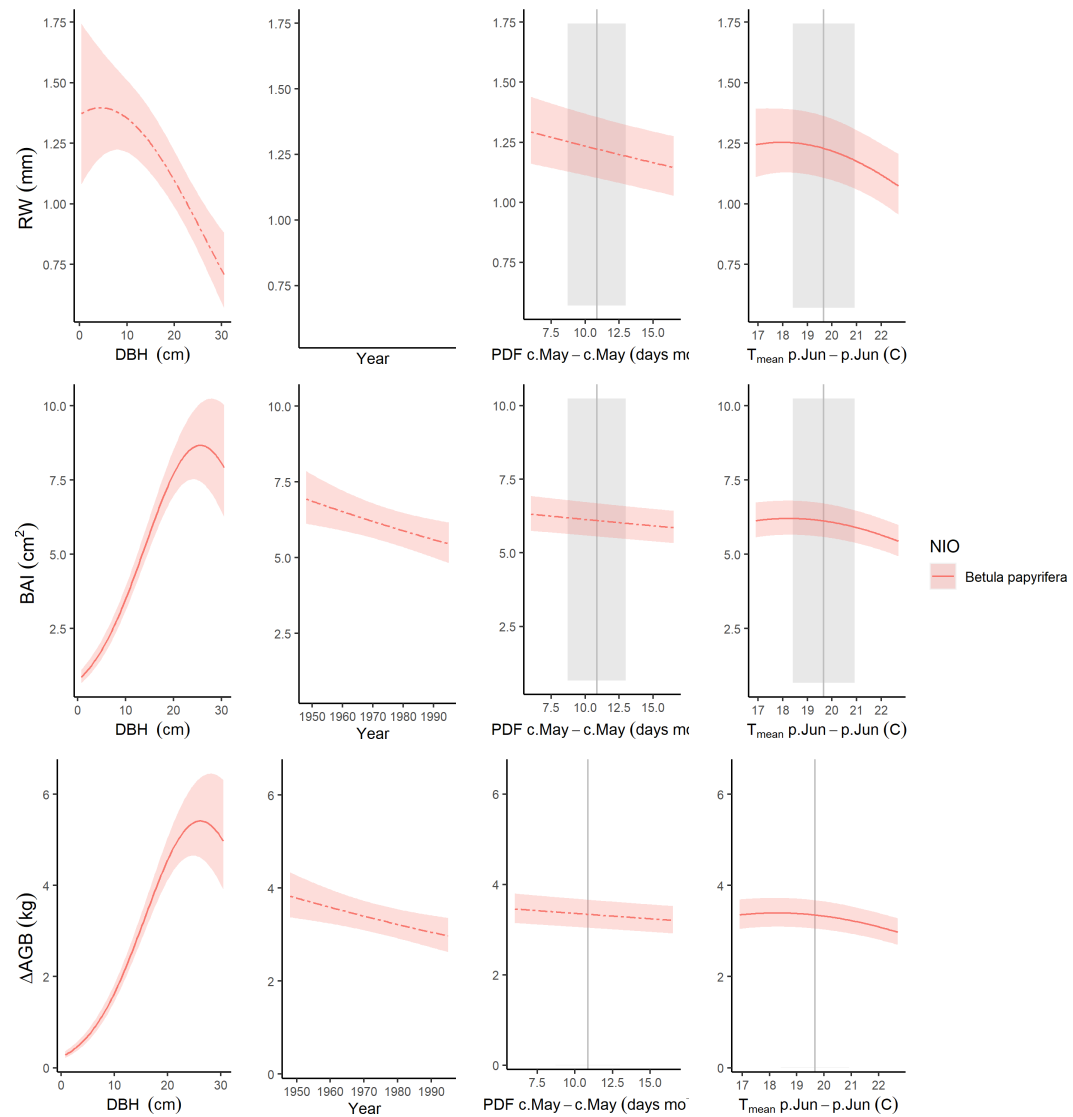


Figure S31. Best GLS models including climate, DBH, and year for Niobrara (Nebraska, USA) for all three growth metrics examined here. Precipitation and temperature group variables are as selected by *climwin* (p=previous year, c=current year). For each species, relationships are plotted if included in top model, with best-fit polynomials plotted with solid lines when both first- and second-order terms are significant, dashed lines when only one term is significant, and dotted lines when neither is significant. Transparent ribbons indicate 95% confidence intervals. Vertical grey lines indicate the long-term mean for the climate variable, shading indicates 1 SD.

Figure S32. Best GLS models including climate and DBH for Little Tesuque (New Mexico, USA)

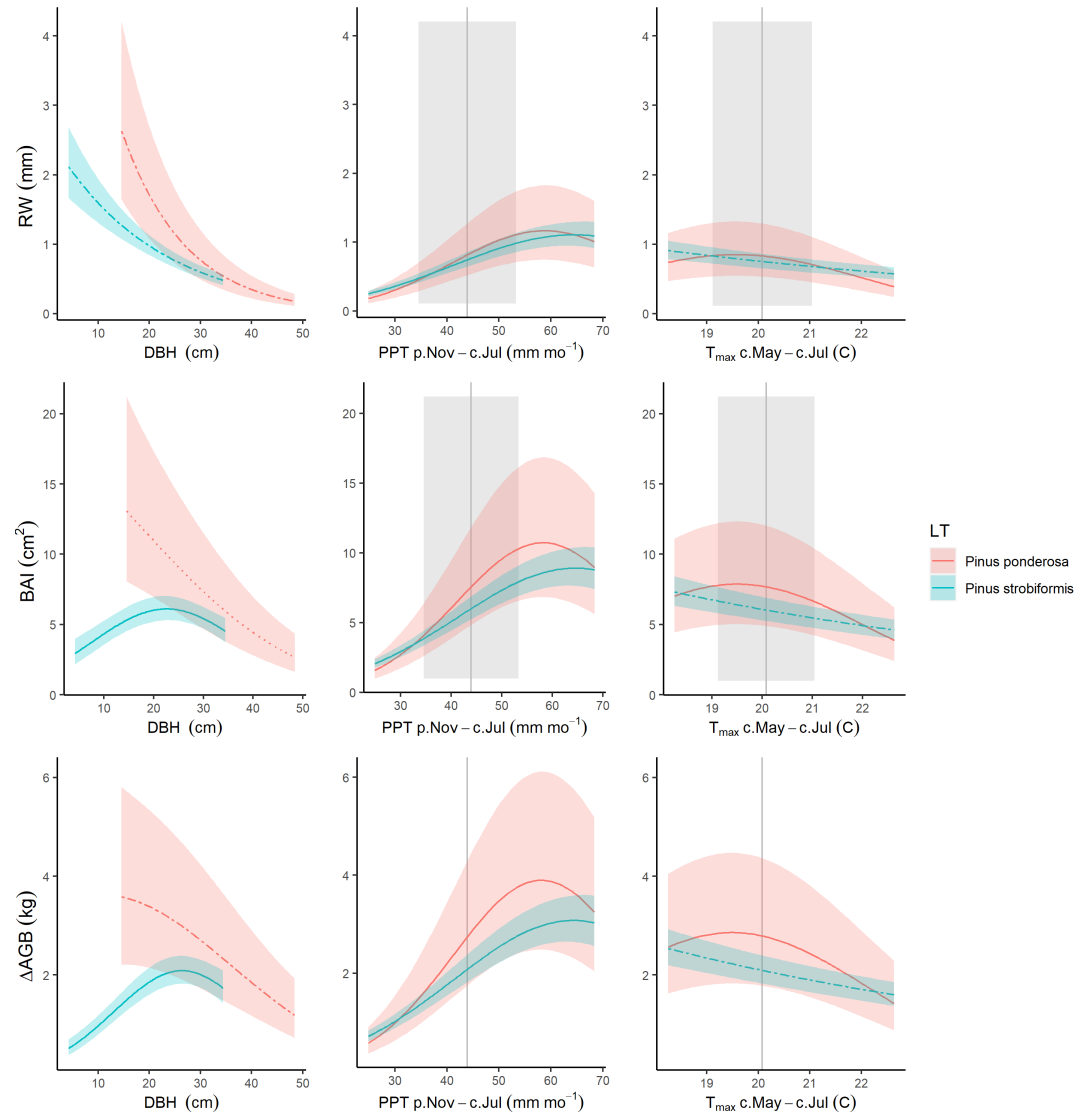


Figure S32. Best GLS models including climate and DBH for Little Tesuque (New Mexico, USA) for all three growth metrics examined here. Precipitation and temperature group variables are as selected by *climwin* (p=previous year, c=current year). For each species, relationships are plotted if included in top model, with best-fit polynomials plotted with solid lines when both first- and second-order terms are significant, dashed lines when only one term is significant, and dotted lines when neither is significant. Transparent ribbons indicate 95% confidence intervals. Vertical grey lines indicate the long-term mean for the climate variable, shading indicates 1 SD.

Figure S33. Best GLS models including climate, DBH, and year for Little Tesuque (New Mexico, USA)

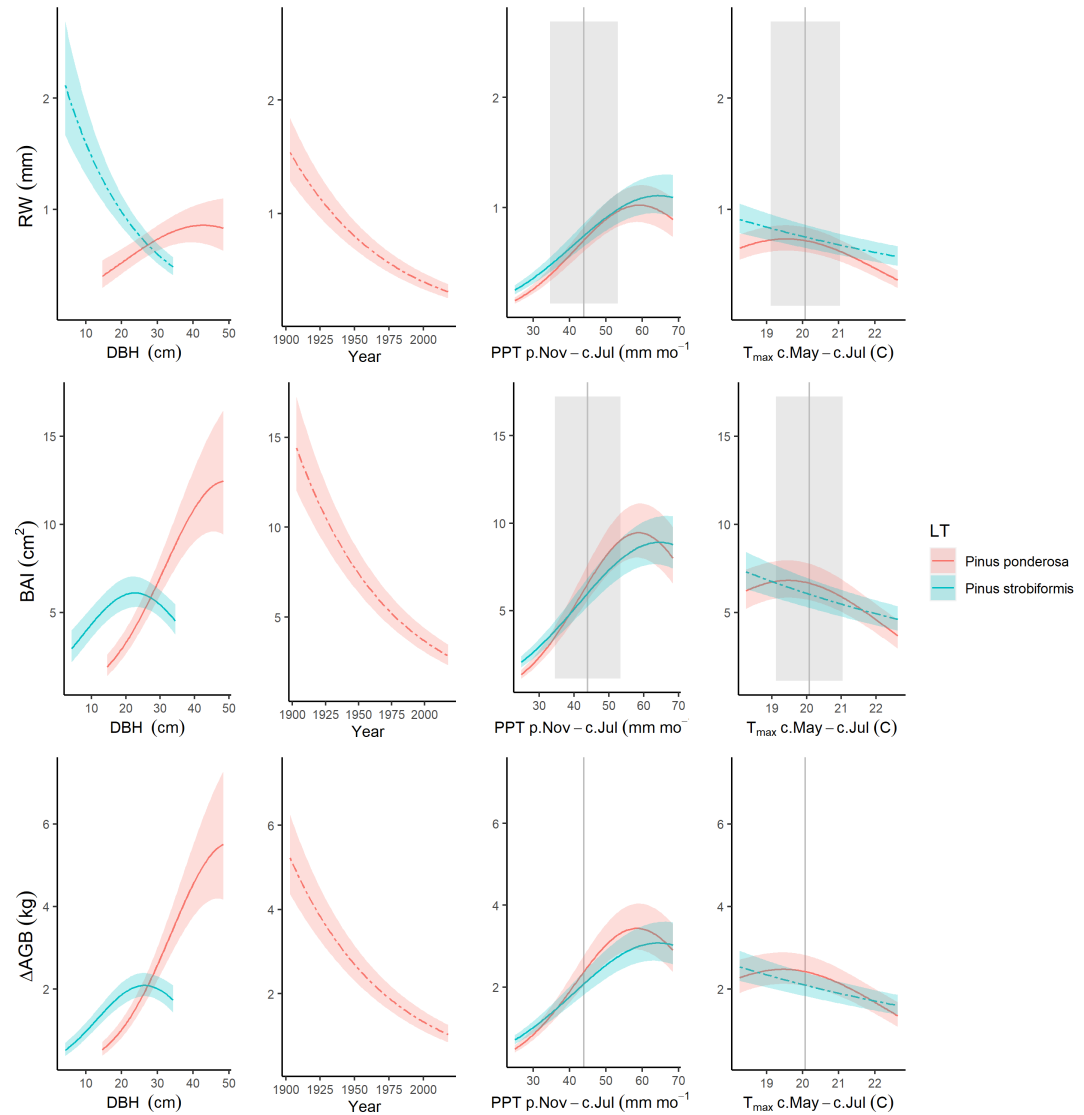


Figure S33. Best GLS models including climate, DBH, and year for Little Tesuque (New Mexico, USA) for all three growth metrics examined here. Precipitation and temperature group variables are as selected by *climwin* (*p*=previous year, *c*=current year). For each species, relationships are plotted if included in top model, with best-fit polynomials plotted with solid lines when both first- and second-order terms are significant, dashed lines when only one term is significant, and dotted lines when neither is significant. Transparent ribbons indicate 95% confidence intervals. Vertical grey lines indicate the long-term mean for the climate variable, shading indicates 1 SD.

Figure S34. Best GLS models including climate and DBH for Cedar Breaks (Utah, USA)

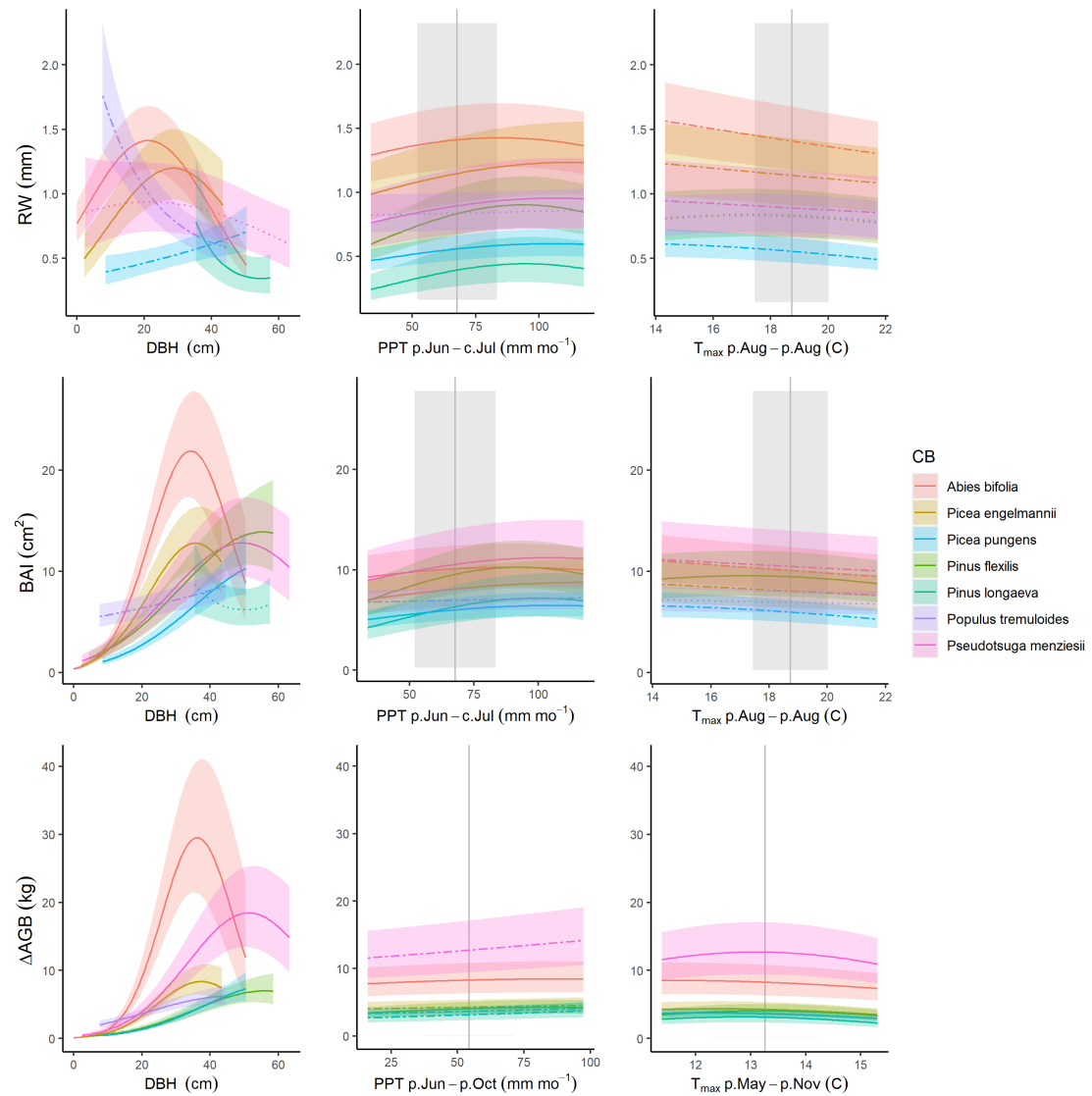


Figure S34. Best GLS models including climate and DBH for Cedar Breaks (Utah, USA) for all three growth metrics examined here. Precipitation and temperature group variables are as selected by *climwin* (p=previous year, c=current year). For each species, relationships are plotted if included in top model, with best-fit polynomials plotted with solid lines when both first- and second-order terms are significant, dashed lines when only one term is significant, and dotted lines when neither is significant. Transparent ribbons indicate 95% confidence intervals. Vertical grey lines indicate the long-term mean for the climate variable, shading indicates 1 SD.

Figure S35. Best GLS models including climate, DBH, and year for Cedar Breaks (Utah, USA)

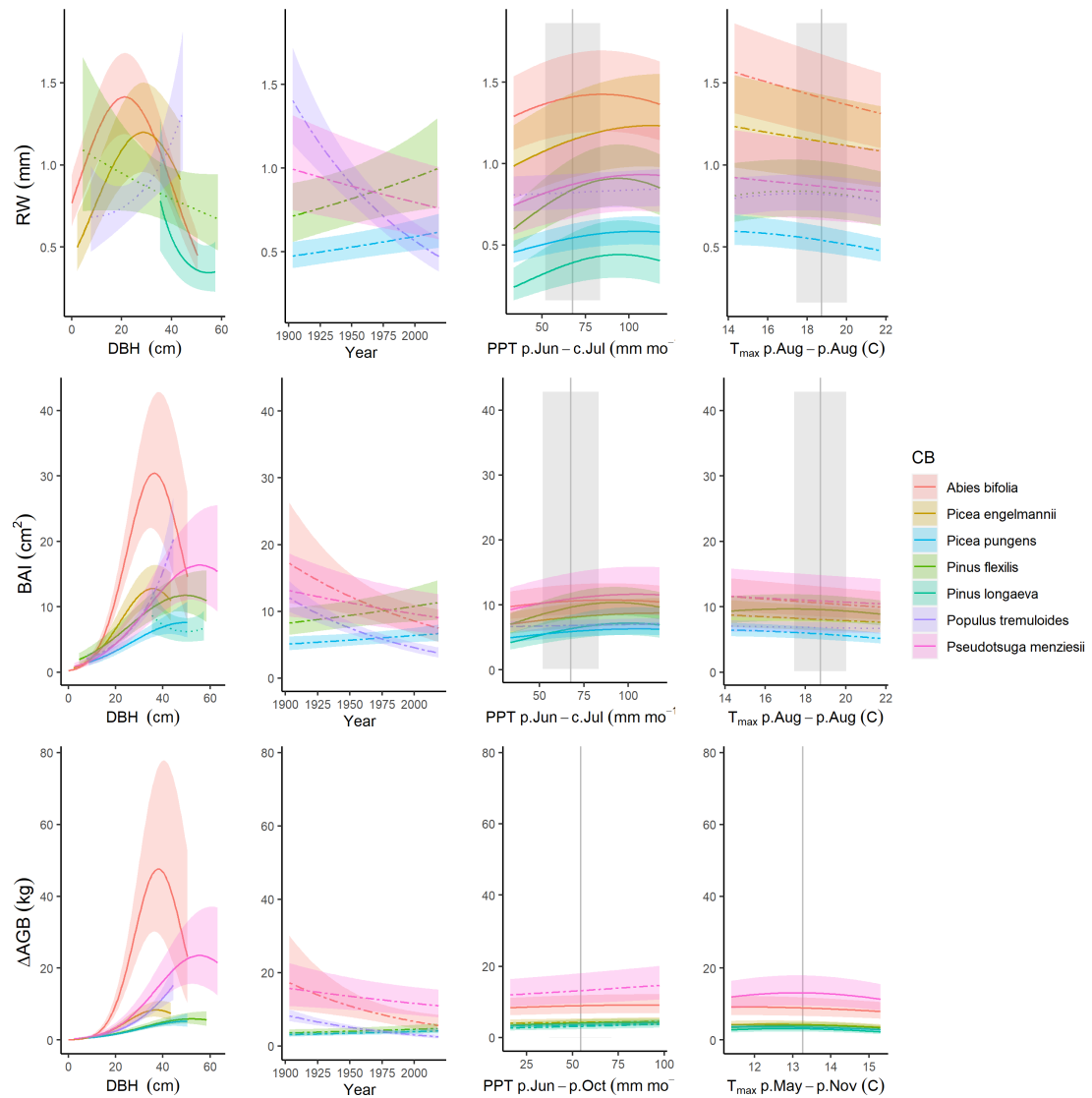


Figure S35. Best GLS models including climate, DBH, and year for Cedar Breaks (Utah, USA) for all three growth metrics examined here. Precipitation and temperature group variables are as selected by *climwin* (p=previous year, c=current year). For each species, relationships are plotted if included in top model, with best-fit polynomials plotted with solid lines when both first- and second-order terms are significant, dashed lines when only one term is significant, and dotted lines when neither is significant. Transparent ribbons indicate 95% confidence intervals. Vertical grey lines indicate the long-term mean for the climate variable, shading indicates 1 SD.

Figure S36. Best GLS models including climate and DBH for Scotty Creek (Northwest Territory, Canada)

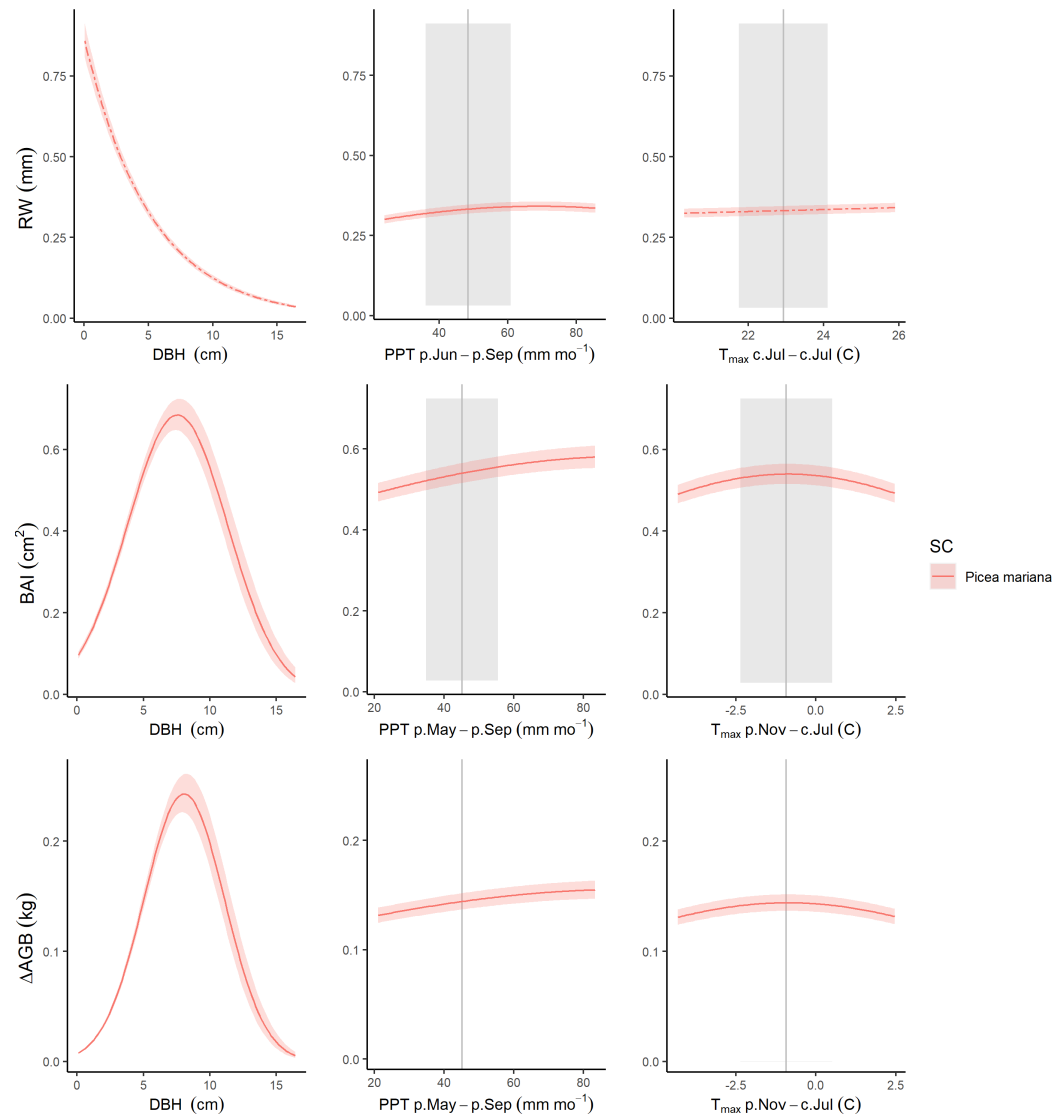


Figure S36. Best GLS models including climate and DBH for Scotty Creek (Northwest Territory, Canada) for all three growth metrics examined here. Precipitation and temperature group variables are as selected by *climwin* (p=previous year, c=current year). For each species, relationships are plotted if included in top model, with best-fit polynomials plotted with solid lines when both first- and second-order terms are significant, dashed lines when only one term is significant, and dotted lines when neither is significant. Transparent ribbons indicate 95% confidence intervals. Vertical grey lines indicate the long-term mean for the climate variable, shading indicates 1 SD.

Figure S37. Best GLS models including climate, DBH, and year for Scotty Creek (Northwest Territory, Canada)

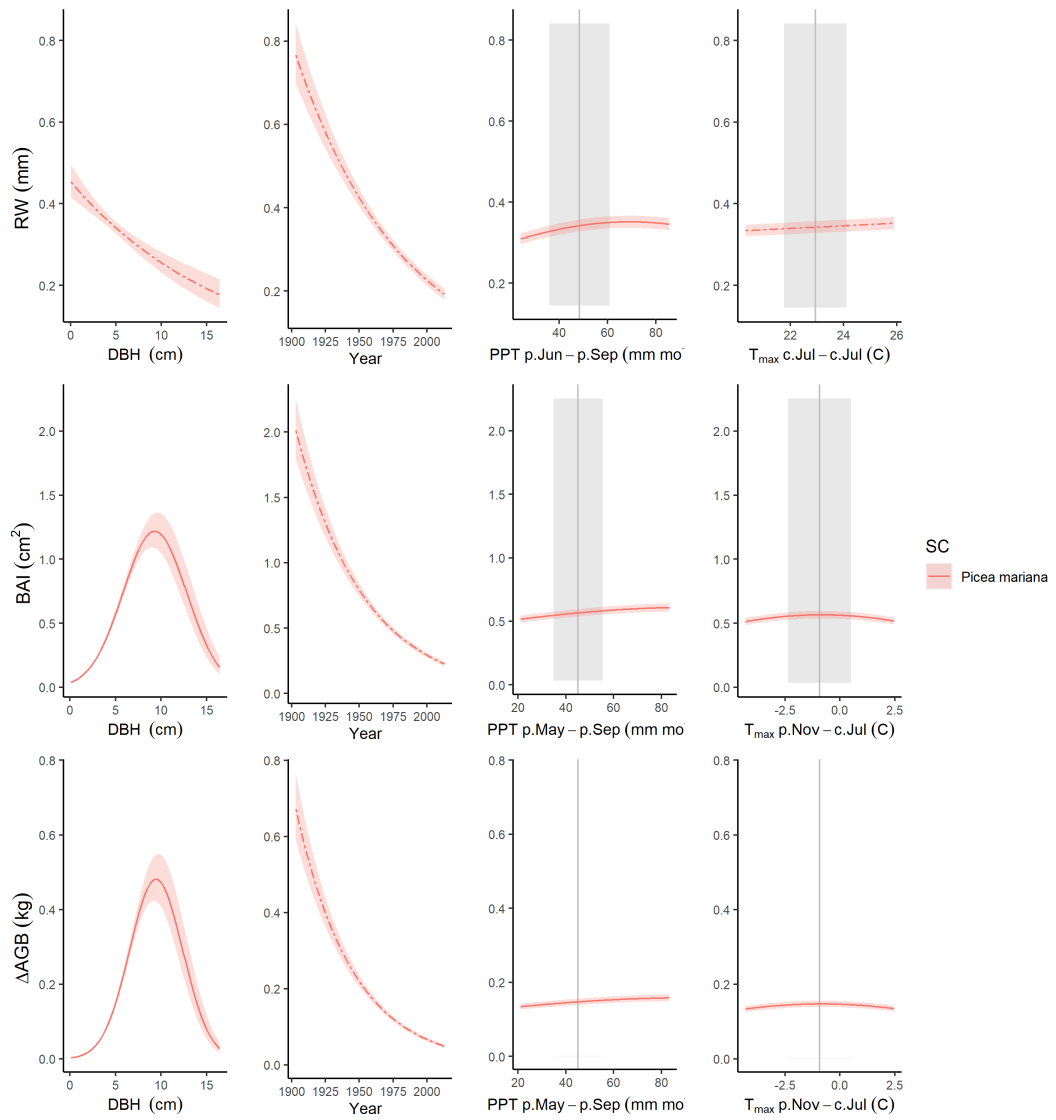
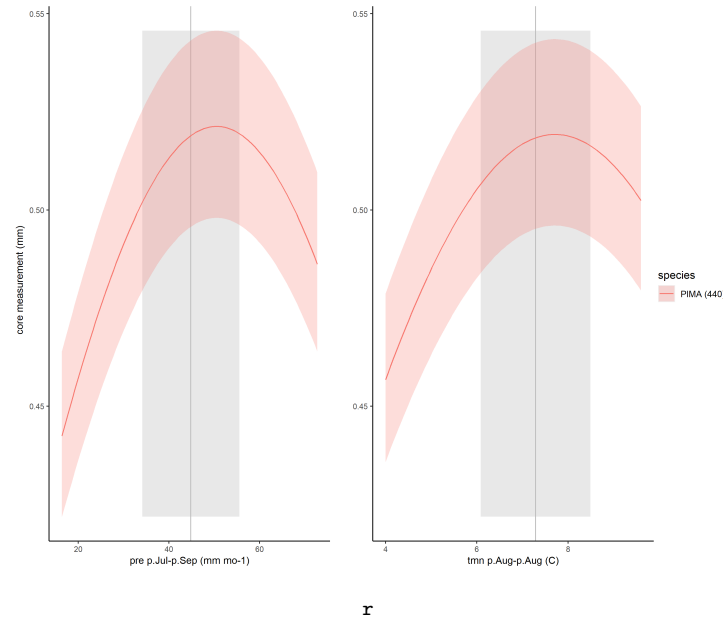


Figure S37. Best GLS models including climate, DBH, and year for Scotty Creek (Northwest Territory, Canada) for all three growth metrics examined here. Precipitation and temperature group variables are as selected by *climwin* (p=previous year, c=current year). For each species, relationships are plotted if included in top model, with best-fit polynomials plotted with solid lines when both first- and second-order terms are significant, dashed lines when only one term is significant, and dotted lines when neither is significant. Transparent ribbons indicate 95% confidence intervals. Vertical grey lines indicate the long-term mean for the climate variable, shading indicates 1 SD.

Figure S38. Climate responses at Scotty Creek (Northwest Territory, Canada) before and after 1970.

(a) pre-1970



r

(b) post-1970

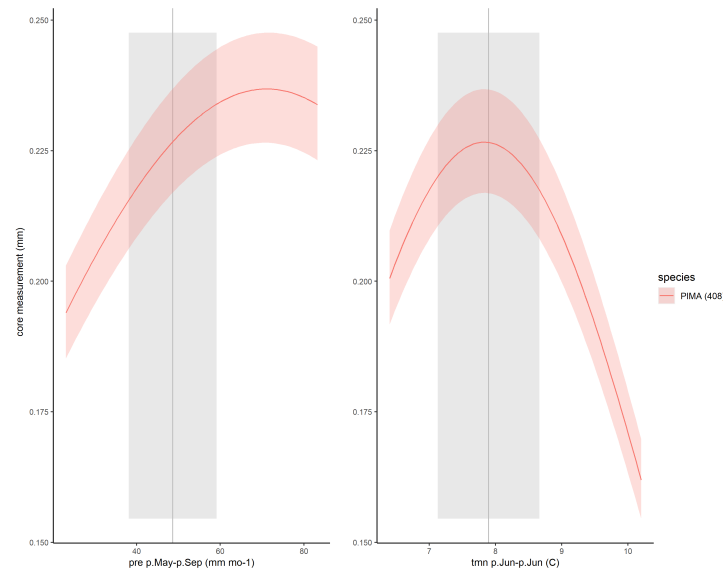


Figure S38. Climate responses at Scotty Creek (Northwest Territory, Canada) before and after 1970.

Figure S39. (RW_interactions_all)

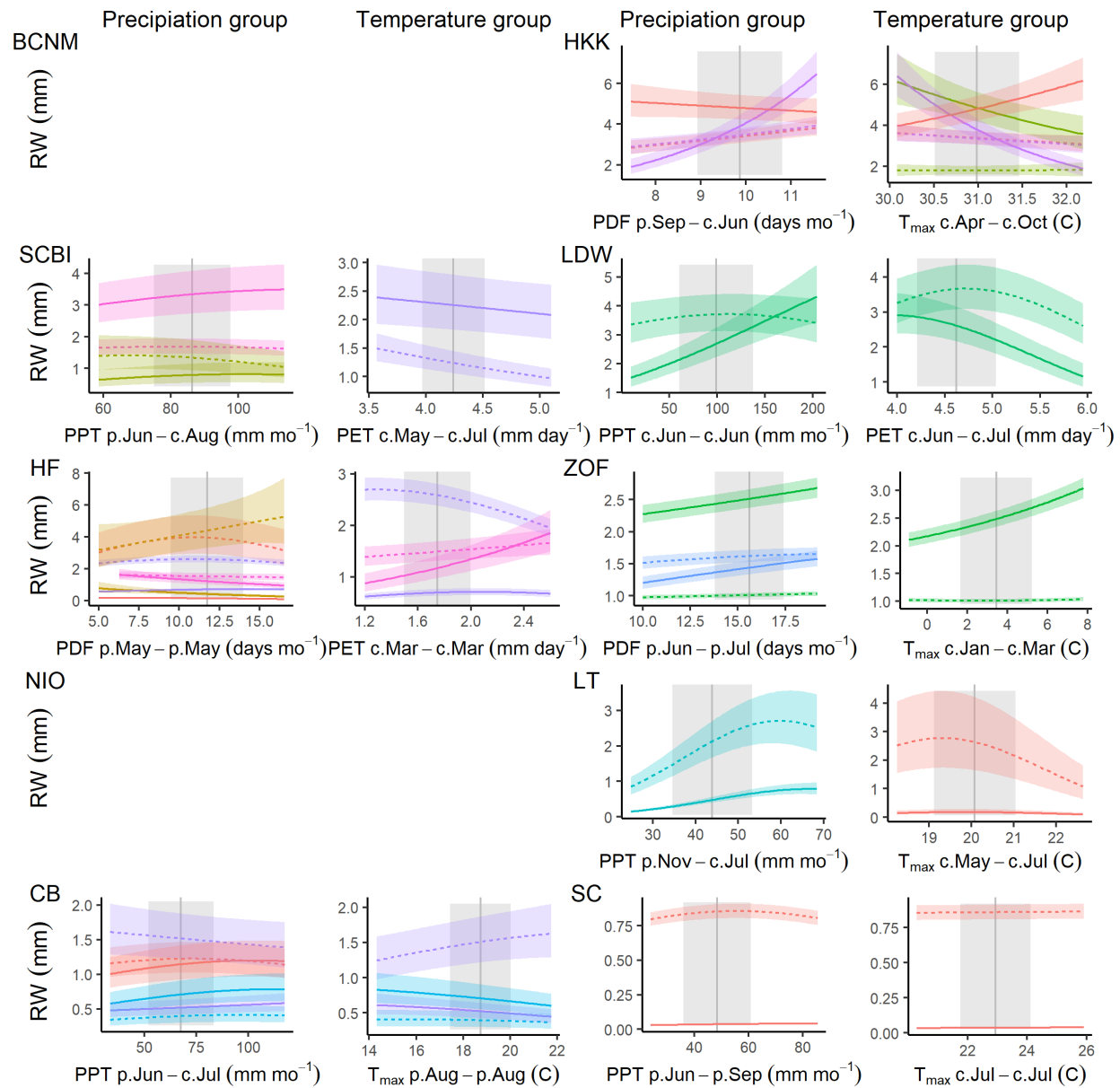


Figure S39. (RW_interactions_all)

Figure S40. (BAI_interactions_all)

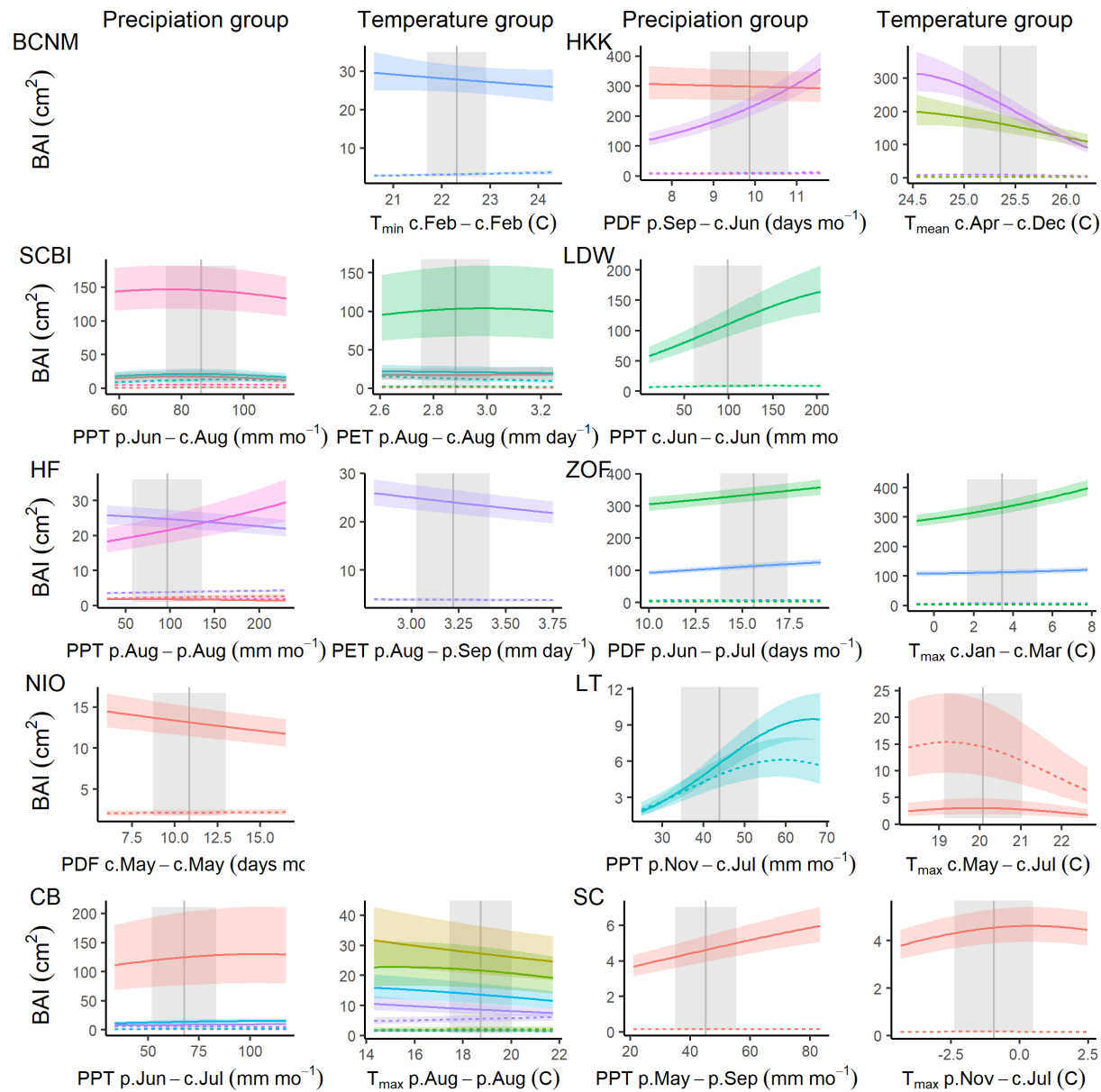


Figure S40. (BAI_interactions_all)

Figure S41. (Decadal BCNM)

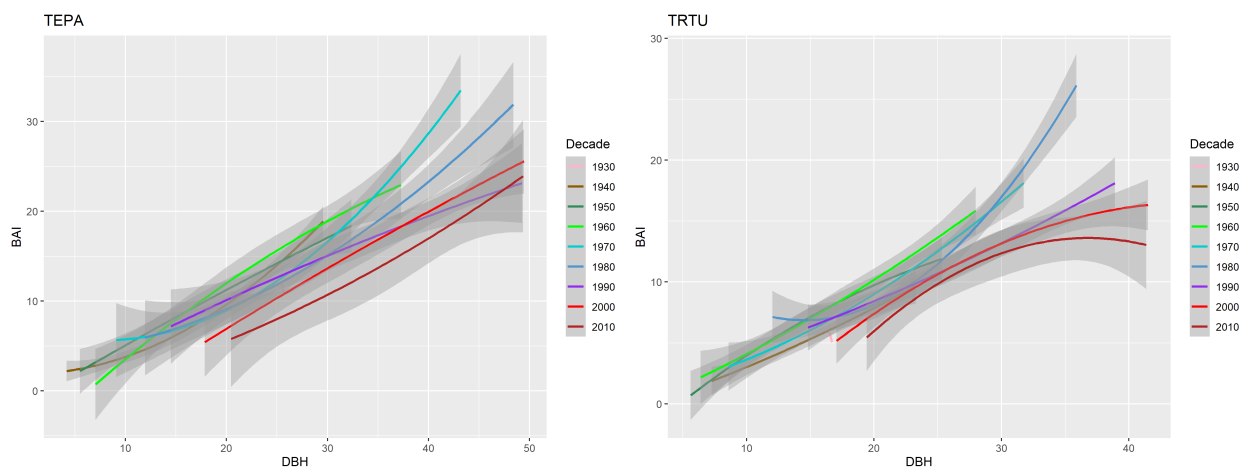


Figure S41. (Decadal BCNM) (generic legend)

Figure S42. (Decadal HKK)

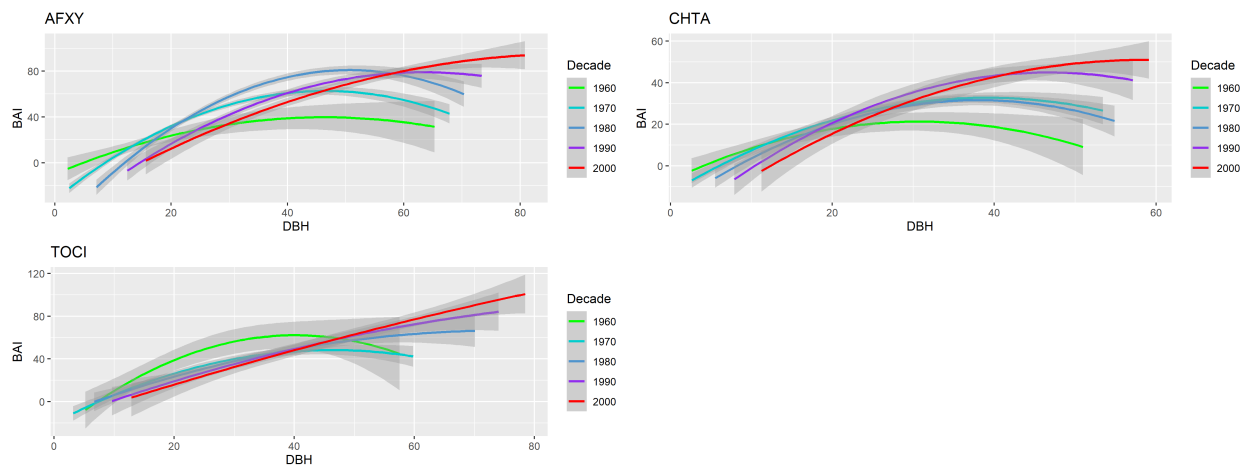


Figure S42. (Decadal HKK) (generic legend)

Figure S43. (Decadal SCBI)

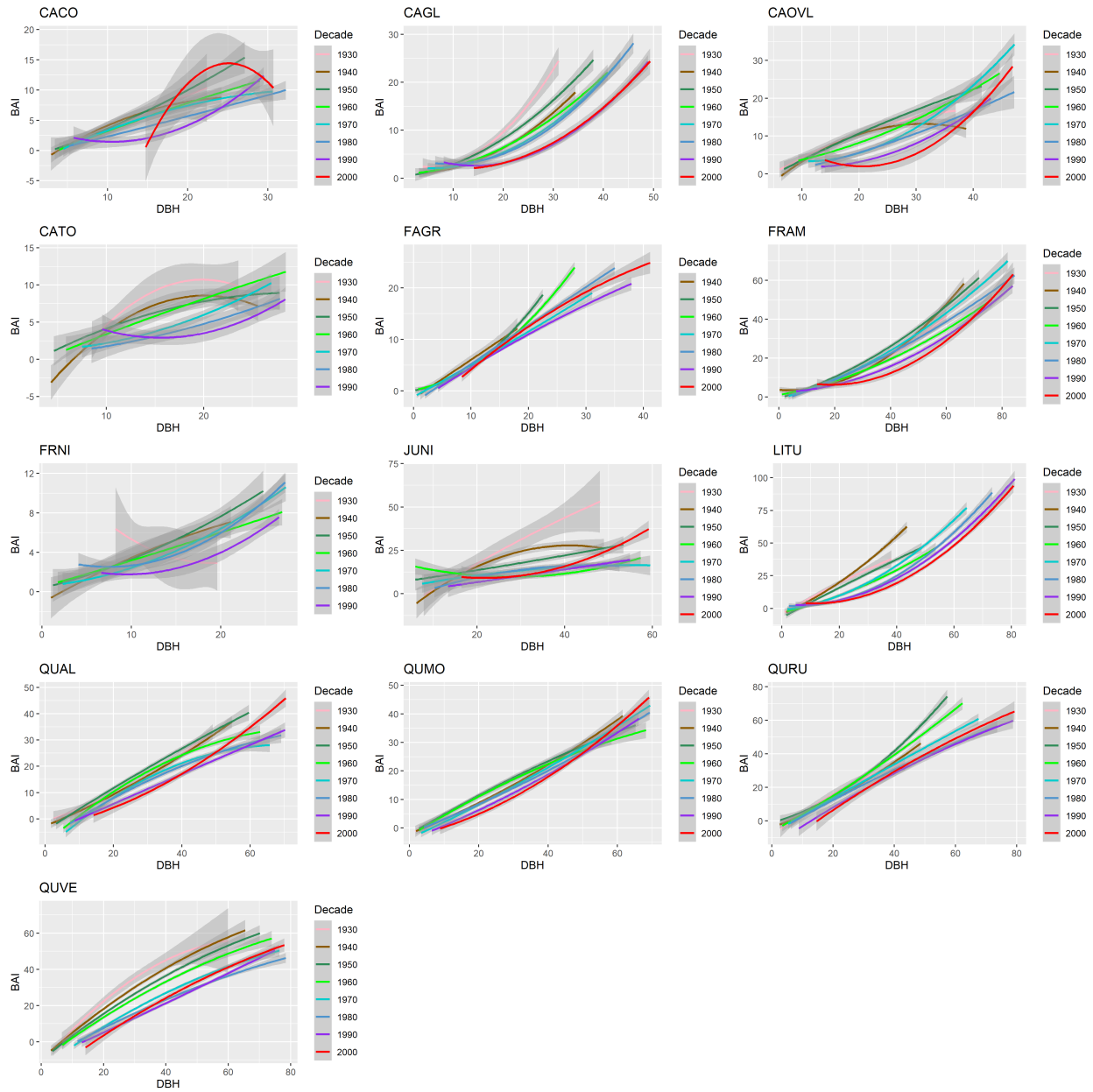


Figure S44. (Decadal LDW)

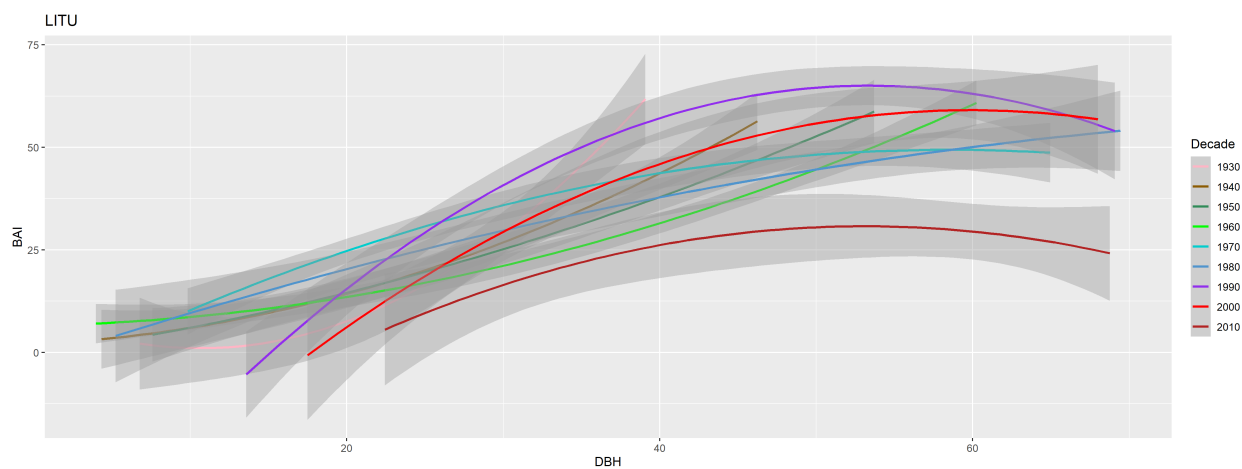


Figure S44. (Decadal LDW) (generic legend)

Figure S45. (Decadal HF)

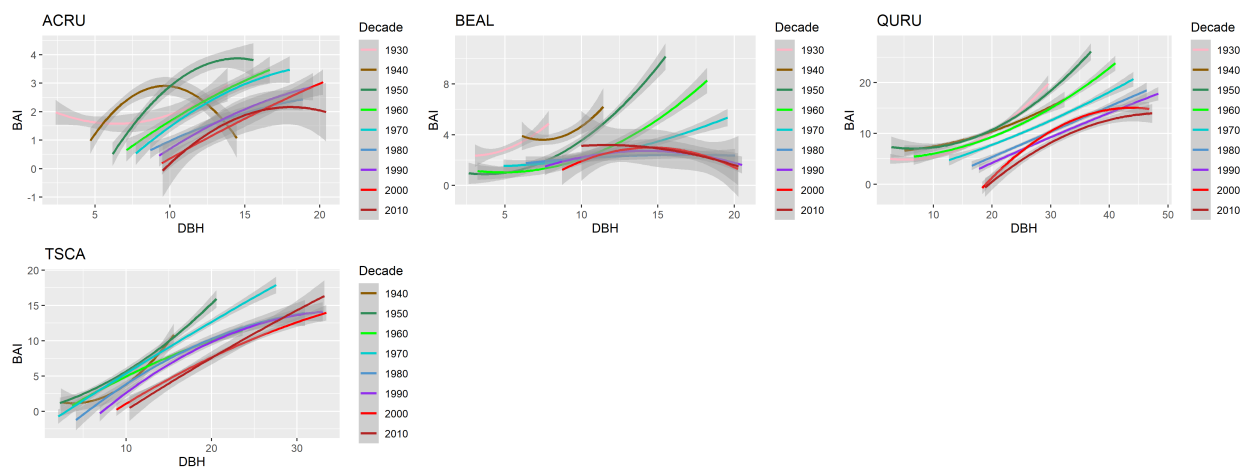


Figure S45. (Decadal HF) (generic legend)

Figure S46. (Decadal ZOF)

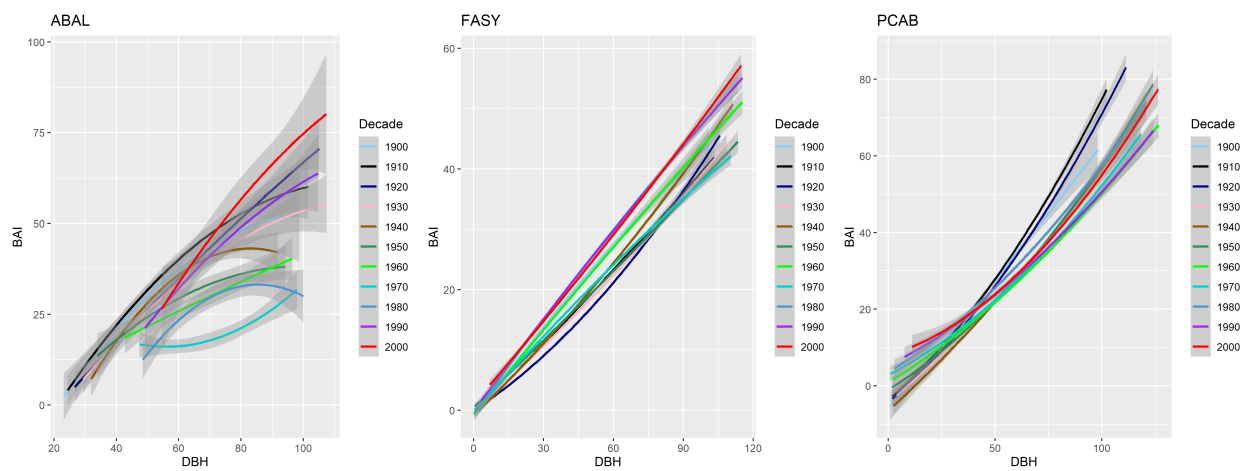


Figure S46. (Decadal ZOF) (generic legend)

Figure S47. (Decadal NIO)

```
!['r decadal_plot_NIO_legend` `r decadal_generic_legend`'](tables_figures/SI_figures/decadal_plots/NIO.p
```

Figure S48. (Decadal LT)

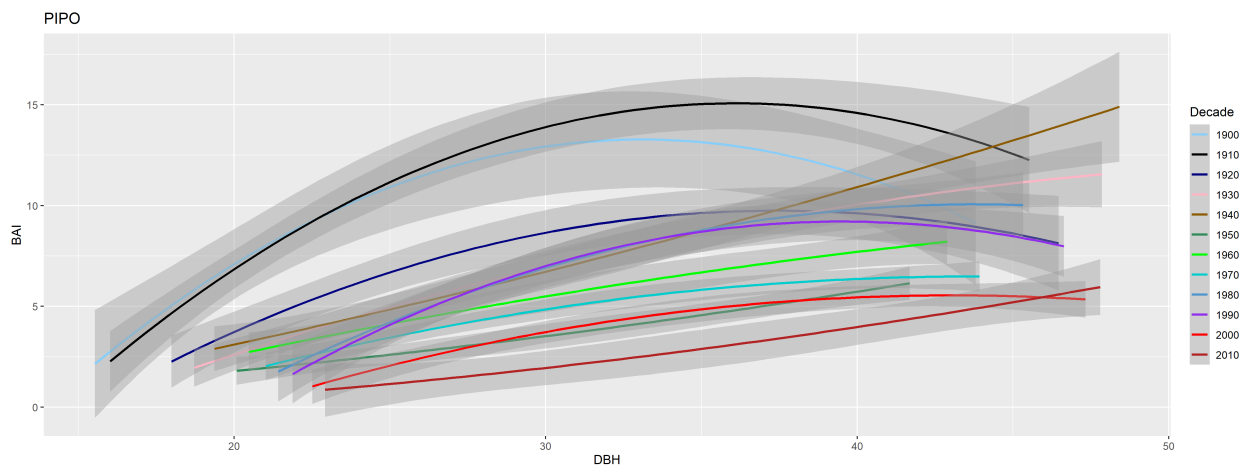


Figure S48. (Decadal LT) (generic legend)

Figure S49. (Decadal CB)

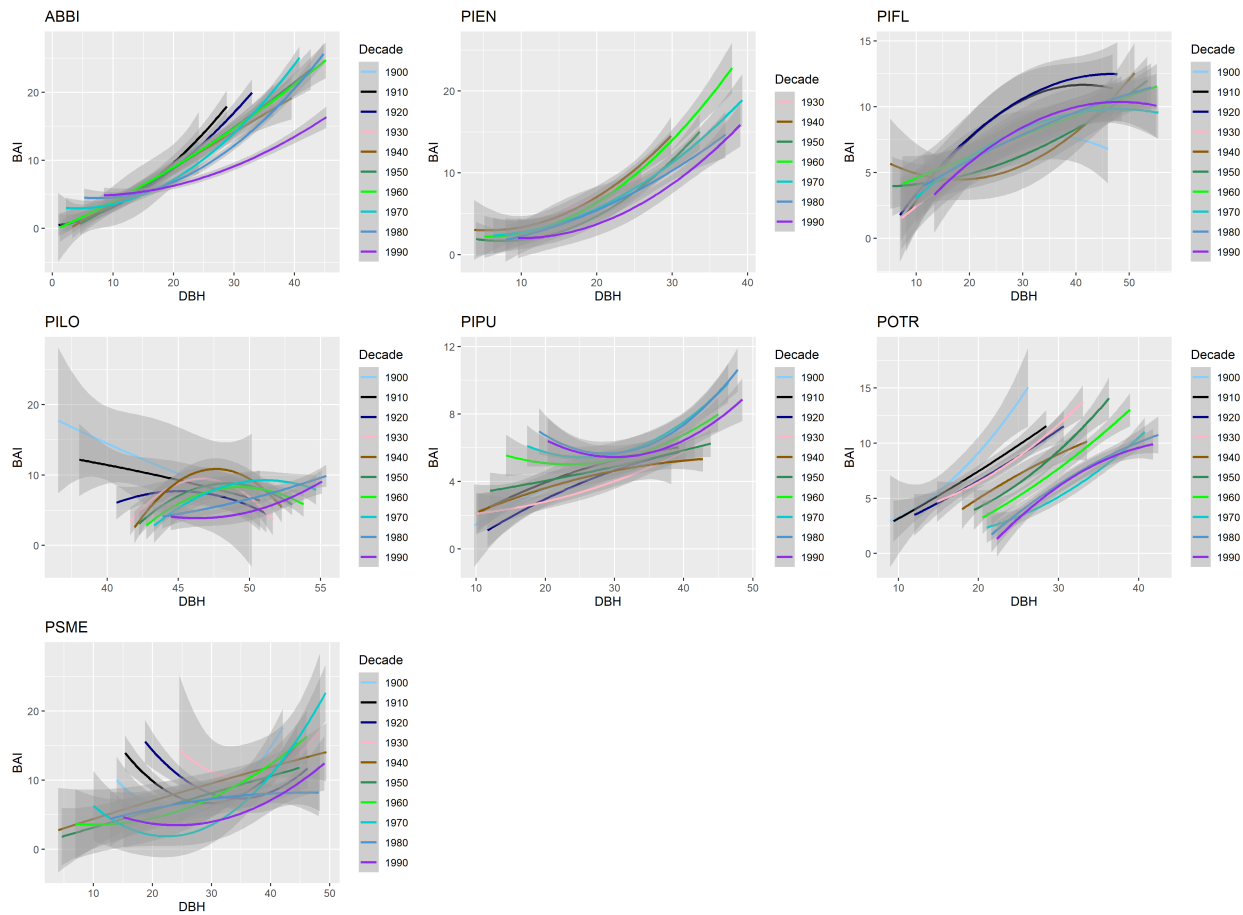


Figure S49. (Decadal CB) (generic legend)

Figure S50. (Decadal SC)

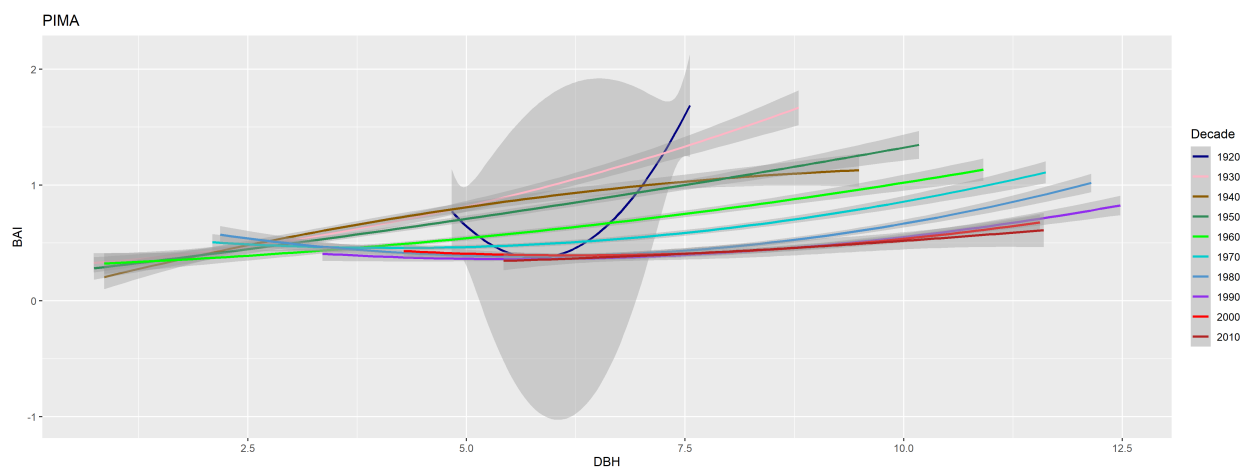


Figure S50. (Decadal SC) (generic legend)

SI References

- Alfaro-Sánchez, R., Muller-Landau, H. C., Wright, S. J., & Camarero, J. J. (2017). Growth and reproduction respond differently to climate in three Neotropical tree species. *Oecologia*. <https://doi.org/10.1007/s00442-017-3879-3>
- Applequist, M. (1958). A simple pith locator for use with off-center increment cores. *Journal of Forestry*.
- Baker, P. J., & Bunyavejchewin, S. (2006). Suppression, release and canopy recruitment in five tree species from a seasonal tropical forest in western Thailand. *Journal of Tropical Ecology*, 22(5), 521–529. <https://doi.org/10.1017/S0266467406003312>
- Baker, P. J., Bunyavejchewin, S., Oliver, C. D., & Ashton, P. S. (2005). Disturbance history and historical stand dynamics of a seasonal tropical forest in western Thailand. *Ecological Monographs*, 75(3), 317–343. <https://doi.org/10.1890/04-0488>
- Bumann, E., Awada, T., Wardlow, B., Hayes, M., Okalebo, J., Helzer, C., Mazis, A., Hiller, J., & Cherubini, P. (2019). Assessing responses of *Betula Papyrifera* to climate variability in a remnant population along the Niobrara River Valley in Nebraska, U.S.A., Through dendroecological and remote-sensing techniques. *Canadian Journal of Forest Research*, 49(5), 423–433. <https://doi.org/10.1139/cjfr-2018-0206>
- Charney, N. D., Babst, F., Poulter, B., Record, S., Trouet, V. M., Frank, D., Enquist, B. J., & Evans, M. E. K. (2016). Observed forest sensitivity to climate implies large changes in 21st century North American forest growth. *Ecology Letters*, 19(9), 1119–1128. <https://doi.org/10.1111/ele.12650>
- Cook, E. R. (1985). *A Time Series Analysis Approach to Tree Ring Standardization: Vol. Ph.D* [PhD thesis]. University of Arizona.
- Cook, E. R., & Kairiukstis, L. A. (Eds.). (1990). *Methods of Dendrochronology: Applications in the Environmental Sciences*. Springer Netherlands. <https://doi.org/10.1007/978-94-015-7879-0>
- Cook, E. R., & Peters, K. (1997). Calculating unbiased tree-ring indices for the study of climatic and environmental change. *The Holocene*, 7(3), 361–370. <https://doi.org/10.1177/095968369700700314>
- Duncan, R. P. (1989). An evaluation of errors in tree age estimates based on increment cores in kahikatea (*Dacrycarpus dacrydioides*). *New Zealand Natural Sciences*, 16, 31–37.
- Helcoski, R., Tepley, A. J., Pederson, N., McGarvey, J. C., Meakem, V., Herrmann, V., Thompson, J. R., & Anderson-Teixeira, K. J. (2019). Growing season moisture drives interannual variation in woody productivity of a temperate deciduous forest. *New Phytologist*, 223(3), 1204–1216. <https://doi.org/10.1111/nph.15906>
- Jones, P. D., Osborn, T. J., & Briffa, K. R. (1997). Estimating sampling errors in large-scale temperature averages. *Journal of Climate*, 10(10), 2548–2568.
- Kašpar, K., Tumajer, J., Vašíčková, I., & Šamonil, P. (n.d.). *Species-specific climate-growth interactions determine the future tree species dynamics of the mixed Central European mountain forests*.
- Maxwell, J. T., Harley, G. L., & Robeson, S. M. (2016). On the declining relationship between tree growth and climate in the Midwest United States: The fading drought signal. *Climatic Change*, 138(1-2), 127–142. <https://doi.org/10.1007/s10584-016-1720-3>
- Ninemets, Ü., & Valladares, F. (2006). Tolerance to shade, drought, and waterlogging of temperate northern hemisphere trees and shrubs. *Ecological Monographs*, 76(4), 521–547. <https://doi.org/10.1080/0012962060084/m9.figshare.e.c.3309258.v1>
- Paton, S. (2019). *Barro Colorado Island, Clearing_Precipitation, manual*. The Smithsonian Institution. <https://doi.org/10.25573/data.10042502.v3>
- Rutishauser, E., Wright, S. J., Condit, R., Hubbell, S. P., Davies, S. J., & Muller-Landau, H. C. (2020). Testing for changes in biomass dynamics in large-scale forest datasets. *Global Change Biology*, 26(3), 1485–1498. <https://doi.org/10.1111/gcb.14833>

- Sniderhan, A. E., & Baltzer, J. L. (2016). Growth dynamics of black spruce (*Picea Mariana*) in a rapidly thawing discontinuous permafrost peatland: Growth Dynamics Boreal Peatlands. *Journal of Geophysical Research: Biogeosciences*, 121(12), 2988–3000. <https://doi.org/10.1002/2016JG003528>
- Tumajer, J., Altman, J., Štěpánek, P., Treml, V., Doležal, J., & Cienciala, E. (2017). Increasing moisture limitation of Norway spruce in Central Europe revealed by forward modelling of tree growth in tree-ring network. *Agricultural and Forest Meteorology*, 247, 56–64. <https://doi.org/10.1016/j.agrformet.2017.07.015>
- Vlam, M., Baker, P. J., Bunyavejchewin, S., & Zuidema, P. A. (2014). Temperature and rainfall strongly drive temporal growth variation in Asian tropical forest trees. *Oecologia*, 174(4), 1449–1461. <https://doi.org/10.1007/s00442-013-2846-x>
- Williams, A. P., Allen, C. D., Macalady, A. K., Griffin, D., Woodhouse, C. A., Meko, D. M., Swetnam, T. W., Rauscher, S. A., Seager, R., Grissino-Mayer, H. D., Dean, J. S., Cook, E. R., Gangodagamage, C., Cai, M., & McDowell, N. G. (2013). Temperature as a potent driver of regional forest drought stress and tree mortality. *Nature Climate Change*, 3(3), 292–297. <https://doi.org/10.1038/nclimate1693>